TÉCNICO LISBOA

Metal Recovery from Spent Li-ion Batteries by Hydrometallurgy

Francisco José Mendes Veiga

Thesis to obtain the Master of Science Degree in

Materials Engineering

Supervisors: Prof. Fernanda Maria Ramos da Cruz Margarido
Dr. Carlos Alberto Gonçalves Nogueira

Examination Committee

Chairperson: Prof. Alberto Eduardo Morão Cabral Ferro
Supervisor: Dr. Carlos Alberto Gonçalves Nogueira
Member of the Committee: Dr. Rui Costa Neto

November 2021

Declaration

I declare that this document is an original work of my own authorship and that it fulfils all the requirements of the Code of Conduct and Good Practices of the Universidade de Lisboa.

Declaração

Declaro que o presente documento é um trabalho original da minha autoria e que cumpre todos os requisitos do Código de Conduta e Boas Práticas da Universidade de Lisboa.

Acknowledgments

First of all, I would like to thank my advisors Professor Fernanda Margarido and Dr. Carlos Nogueira for the opportunity, continuous support, guidance, and availability throughout this study. I would also like to thank Professor Rui Costa Neto and Professor Manuel Francisco for their willingness to help at any time.

Furthermore, I would like to acknowledge the financial support of the project Baterias 2030, ref POCI-01-0247-FEDER-046109, co-funded by COMPETE 2020/Portugal 2020/Lisboa 2020, through the European Regional Development Fund (FEDER), and extend my gratitude to Valorcar for providing the spent battery packs, Palmiresíduos and Ambigroup for cooperating in the discharging and dismantling, and Laboratório Nacional de Energia e Geologia (LNEG) for providing me with the space, materials, and equipment needed to perform this work.

A special thank you to my thesis partner Daniela Oliveira, for the companionship, exchanging of ideas, and giving thoughtful insight.

To all my IST colleagues especially Joana Brito, for all the encouraging conversations and honest reviews.

Last but not least, I would like to thank David Revés and my family, especially my parents and sisters, for their constant love and support throughout these years in Técnico. I can never thank you enough.

Resumo

O mercado de baterias, dada a atual transição energética, encontra-se em estado de rápido crescimento. Consequentemente, prevê-se, num futuro próximo, um exponencial aumento no número de baterias em fim de vida. Tendo em consideração os problemas ambientais decorrentes do fim de vida e da criticalidade dos recursos presentes nas mesmas, a reciclagem dos metais valiosos de baterias usadas é de extrema importância. Neste estudo, os processos de separação do pó da folha de elétrodo e lixiviação foram estudados com o objetivo de sugerir um processo que possa ser implementado industrialmente.

Dois métodos de separação foram testados: calcinação e dissolução por solvente com NMP. Conclui-se que a calcinação a 400ºC durante 5 horas será a opção mais eficiente, com 100% de desagregação. Tendo sido igualmente estudado o efeito da calcinação no rendimento de lixiviação, este corroborou o resultado anterior.

Analisou-se, ainda, o impacto da presença de redutor no comportamento de lixiviação, introduzindo, assim, a possibilidade de utilização de folhas de elétrodo como potenciais redutores, definindo $Na_2S_2O_5$ como o redutor mais eficiente.

As condições ótimas de lixiviação foram conseguidas com 3 M de H_2SO_4 como agente de lixiviação, 0,25 M de $Na_2S_2O_5$ como agente redutor, um rácio Liquido/Sólido de 5 L/kg, temperatura de 80ºC, durante 30 minutos. Para os parâmetros mencionados acima, a recuperação geral na solução de lixiviação para Li, Ni, Mn, Co, Cu e Al foi de aproximadamente 95%, 100%, 100%, 98%, 100% e 73%, respetivamente.

Adicionalmente, foi feita uma introdução ao processo de separação de metais.

Palavras-Chave: Bateria de iões de lítio, Hidrometalurgia, Lixiviação com Ácido Inorgânico, $Na_2S_2O_5$, Separação, Extração.

Abstract

The conversion to electric vehicles combined with the increase in demand for storage solutions for renewable energies is contributing to the rapid growth of the battery market and, consequently, the increase in end-of-life batteries in the near future. Bearing in mind the environmental problems after end-of-use and the criticality of resources, the recycling of metals from spent batteries is of the utmost importance. Herein, the processes of foil and powder separation and leaching are researched with the aim of suggesting a process that can be implemented industrially.

Two foil and powder separation methods were tested: calcination and solvent dissolution with NMP, which led to the conclusion that calcination at 400ºC for 5 hours was the most efficient option, with 100% disaggregation. Subsequently, the effect of calcination on the leaching yield was also studied, supporting the previous result.

Prior to the factorial design experiments, a study on the impact of the presence of reducer on the leaching behaviour was also conducted, introducing the possibility of electrode foils as potential reducing agents, and setting $Na_2S_2O_5$ as the leading reducer.

The optimal leaching conditions were found to be 3 M of H_2SO_4 as leaching agent, 0.25 M of $Na_2S_2O_5$ as reducing agent, a liquid/solid ratio of 5 L/kg, temperature of 80ºC, for 30 minutes. For the aforementioned parameters, the overall recovery in the leaching solution for Li, Ni, Mn, Co, Cu, and Al was 95.03%, 99.55%, 99.99%, 97.60%, 100%, and 72.47%, respectively.

Additionally, an introduction to the metal separation process was also made.

Keywords: Lithium-ion Battery, Hydrometallurgy, Inorganic Acid Leaching, $Na_2S_2O_5$, Separation, Extraction.

Table of Contents

List of Tables

List of Figures

List of Acronyms

AAS Atomic Absorption Spectrometry

BEV Battery Electric Vehicles

CE Circular Economy

DRC Democratic Republic of the Congo

EDS Energy Dispersive Spectroscopy

EoL End-of-life

EU European Union

EV Electric Vehicle

FDE Factorial Design Experiment

FEG-SEM Field Emission Gun Scanning Electron Microscope

GHG Greenhouse Gas

ICEs Internal Combustion Engines

ICP Inductively Coupled Plasma – Atomic Emission Spectrometry

IoT Internet of Things

IRP International Research Panel

L/S Liquid/Solid Ratio

LCO Lithium Cobalt Oxide

LFP Lithium Iron Phosphate

LIB Lithium-Ion Battery

LMO Lithium Manganese Oxide

LNEG Laboratório Nacional de Energia e Geologia

LTO Lithium Titanate Oxide

NCA Lithium Nickel Cobalt Aluminium

NMC Lithium Nickel Manganese Cobalt

NMP N-Methyl-2-pyrrolidone

O/A Organic/Aqueous Volume Ratio

PHEV Plug-in Hybrid Electric Vehicle

PVDF Polyvinylidene Fluoride

RES Renewable Energy Sources

RMI Raw Material Initiative

SEI Solid Electrolyte Interphase

SEM Scanning Electron Microscopy

XRPD X-Ray Powder Diffraction

Chapter 1

Introduction

1.1. Context and Problematic

The world is currently facing a massive migration from fossil fuel to electric energy, a transition to a low-carbon economy, due to global warming, and the upcoming energy crisis. And so, as stated by the European Technology and Innovation Platform on Batteries, "(…) within this decade, where it is technologically and economically viable, everything that can be electrified will be electrified" [1].

Jointly, the energy and transport sectors are responsible for approximately two-thirds of total global Greenhouse Gas (GHG) emissions, with the energy sector having the biggest potential for cutting emissions. CO_2 emissions can be eliminated if energy continues to be generated through various Renewable Energy Sources (RES) like solar, wind, geothermal, and so forth. But most of these power generating systems, due to their intermittence, always need an energy storage system for their efficient use [2–4].

The transport sector alone contributes with more than 28% of global GHG emissions and represents a major source of airborne emissions in cities, endangering human health and ecosystem quality within city borders. Therefore, the decarbonization of the transport sector is also essential to achieve the 2ºC average temperature target set during the 2015 Paris Agreement [2,5,6].

The European Commission has established the objective of reducing GHG emissions by 80% to 95% by 2050 when compared to 1990. With road transport accounting for about 73% of all GHG, this means a reduction of 54 to 67% of transport sector GHG emissions. This low-emission mobility strategy has resulted in a growing switch from the traditional Internal Combustion Engines (ICEs) to Electrical Vehicles (EVs), including Battery Electric Vehicles (BEVs) and Plug-in Hybrid Electric Vehicles (PHEVs) [5,7,8].

BEVs have seen an accelerated, and welcomed, introduction in the market, not only due to their better environmental performance, comprising zero emissions in use and lower net carbon emissions per kilometre, but also due to their improvement in battery durability over the past years, and the decrease in cost per kWh of charge capacity [9].

This continuous conversion of ICEs into EVs has been increasing the need for electrochemical energy storage devices, i.e. batteries, with Lithium-ion Batteries (LIBs) being recognised as the preferred choice, due to their advantages of zero memory effect, large capacity, small self-discharge, good capacity retention, wide operating temperature range, long-life cycle, small size, and safety [3–5].

In Europe, at least 80% of the vehicle fleet is expected to be fossil-free or fully electrified by 2050. The total global battery demand is expected to exceed 2600 GWh by 2030, representing an increment of fourteen times, comparatively to 2018, as can be seen in Figure 1, with the main contributor for the rising demand of LIBs being the EV market [1,5].

When the LIB reaches the design lifetime, generally 8-10 years for EVs, the battery must be replaced, and to create a true Circular Economy (CE) for LIBs, disposal must be avoided, reducing dependence from countries with geopolitical conflicts and tackling the issue of availability of critical raw materials, e.g. cobalt, lithium, and graphite. Also, landfilling can constitute threats to human health and the environment in terms of explosions, leakages of hazardous elements, especially with the expected end-of-life (EoL) LIB quantity increase in the upcoming future. European Union (EU) legislation in 2016 set a minimum collection rate of 45% for batteries in member states and a 50% minimum recycling rate. In 2020 a new directive was released, setting a 65% collection target and recycling efficiency for 2025, and 70% for 2030. However, it is estimated that, globally, 95% of all LIBs are still landfilled. And, with the increase in demand, an increase of LIBs in the waste stream will follow [3,6,9–13].

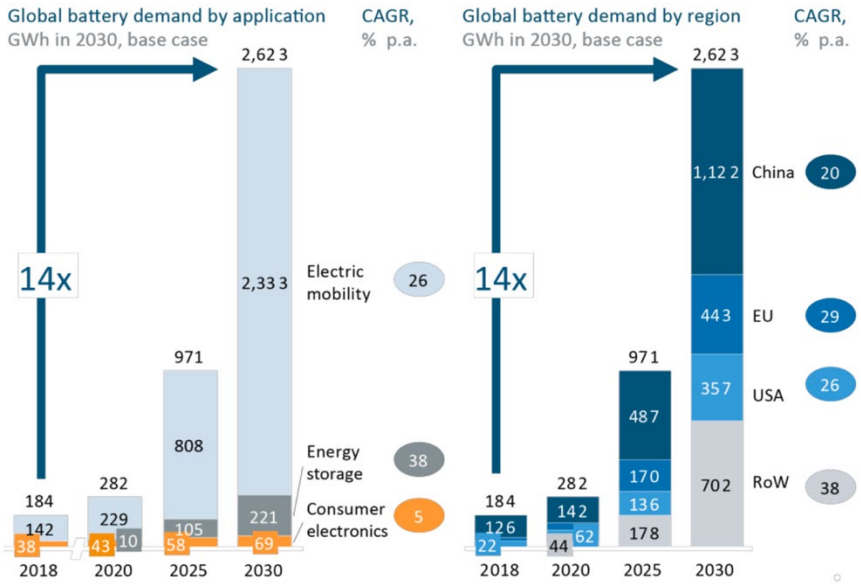

Figure 1 - Current and predicted global battery demand [1].

After reflecting on the information mentioned above, it is obvious that efforts to improve the recyclability of spent batteries are necessary. This work intents to make a contribution for that need. At present, the two main methods applied for recycling of spent LIBs are hydrometallurgy and pyrometallurgy, with the main difference between them being on the metal-extraction process. This work, integrated into the project Baterias 2030 – Batteries as a Central Element for Urban Sustainability, focuses on recovering elements from two Nickel Manganese Cobalt (NMC) spent LIBs from an EV by hydrometallurgy, since this is a simpler and environmentally friendlier process, with lower energy requirements and higher purity [4].

1.2. Research Questions

This work was developed with the following research questions in mind:

1. Does the pre-treatment (for removing the binder) affect the composition of a LIB cell, and what is the relation between the pre-treatment and the chemical and metallurgical processing?
2. Can electrode foils be used as (or combined with) reducing agents? How does it affect the leaching yield?
3. Can there be an alternative Industrial Process that includes both pre-treatment and hydrometallurgy?

1.3. Research Strategy

In an effort to provide answers for the questions that catalysed this thesis, the following strategy was followed:

- Question 1: Perform a visual inspection, XRPD, SEM, and EDS analysis in a sample of each pre-treated electrode, carry out a series of leaching tests in samples of each efficiently pre-treated electrode, and perform ICP analysis in order to obtain the leaching yield.
- Question 2: Test different leaching conditions, alternating the presence of reducing agent (chemical reagent or electrode foil), and perform ICP analysis to calculate the leaching yields.
- Question 3: Bearing in mind the data obtained, propose an alternative industrial process including all the operations required to recycle an EoL LIB.

1.4. Thesis Outline

From here on, this thesis is divided in five more chapters.

Chapter 2 and 3 consist of an extensive literature review. In Chapter 2 an introduction to the Lithium-Ion battery is given, explaining its working principle, structure, and different types. Additionally, its composing raw materials and their criticality are discussed to emphasize the importance of a new approach on handling Lithium-Ion batteries towards circular economy.

In Chapter 3 a complete description of the industrial techniques currently used to recycle end-of-life lithium-ion batteries is available, along with a collection of research made recently about the hydrometallurgical technique.

Chapter 4 accommodates the experimental approach described in detail, and Chapter 5 presents the results and their discussion regarding their meaning and possible impact.

In closing, Chapter 6 reviews the conclusions of this work, its most significant achievements, and sets out some recommendations for future developments.

Chapter 2

Li-ion Battery

2.1. Introduction

LIBs were developed in the 70s and appeared on the market for the first time in 1991 through SONY. Since then, due to their distinct characteristics, like high energy capacity and long-life cycle, LIBs have become an integral part of our daily life, especially in the field of portable electronic goods. Additionally, LIBs are currently on the verge of transforming both the transportation and energy sectors, providing a helping hand in securing the goals established in the Paris Agreement [4,14,15].

Batteries are distinguished by their different type of redox mechanisms and electrochemistry, but their working principle is analogous: the movement of ions from a negative electrode to a positive one during discharge, and vice versa during charging. Consequently, the ionic chemical reactions occurring in a conventional LIB are the following:

At the anode:

$$C + yLi^+ + ye^- \leftrightarrow Li_yC \quad (1)$$

At the cathode:

$$LiMO_2 \leftrightarrow Li_{(1-x)}MO_2 + xLi^+ + xe^- \quad (2)$$

Net cell reaction:

$$Li_{(1-x)}MO_2 + {}^{x}/_{y}\, Li_yC \leftrightarrow LiMO_2 + {}^{x}/_{y}\, C \quad (3)$$

with the onward direction representing the charging process, the reverse, the discharging process. M symbolizes the metal oxide in the cathode, and C the carbonaceous material, e.g. graphite. As it is possible to follow from (1), (2) , and (3) when a Li-ion cell is charged, the cathode electrode material oxidizes, and the anode material is reduced. In other words, the Li-ions deintercalate from the cathode electrode material, and intercalate into the anode material, remaining stored until discharge. In Figure 2, a representation of the electrochemical process is portrayed [16].

When compared with other types of batteries (such as lead acid, nickel cadmium, and nickel metal hydride), LIBs present superior properties. Their predominant use is linked some properties like lower reactiveness, security, and longer life cycles, a consequence of the absence of metallic lithium in the cell. Lower environmental risks, compact design, better resistance to self-discharge, higher voltage output, no memory effect, better resistance to elevated temperatures, and a continuously decreasing cost, are some additional singularities of the LIBs [4,14,17–20].

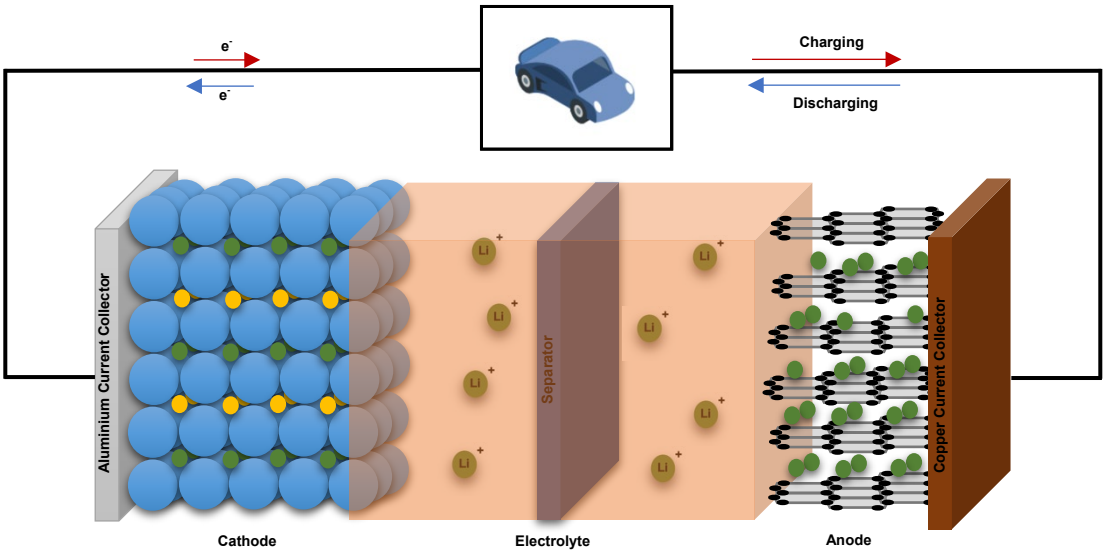

Figure 2 - Representation of the electrochemical process in a LIB.

2.2. Structure

The four basic components of the battery are the cathode, positive electrode, the anode, negative electrode, the separator, and the electrolyte, a substance used for the transfer of ions between the electrodes. The exact mass and chemical compositions of each component vary, and most of the valuable metals within a LIB can be found in the cathode [4,17,21].

2.2.1. Cathode

Typically, the cathode comprises 25-30% of the battery cell's total weight and entails a thin aluminium current collector sheet, usually layered with metal oxides. These materials are classified according to their crystal structure: layered oxides containing lithium and one or more other metals, e.g. Lithium Cobalt Oxide (LCO), Lithium Nickel Cobalt Aluminium Oxide (NCA), and Lithium Nickel Manganese Cobalt Oxide (NMC); spinels, e.g. Lithium Manganese Oxide (LMO); or olivine, e.g. Lithium Iron Phosphate (LFP). In Figure 3, three different examples of crystal structures are provided. Manufacturers might use different combinations to achieve different performance results. Under other conditions, combinations of different chemistries can also be made in order to get the different benefits of each chemistry into one battery. The metal oxide powder represents 80-85% of the cathode material, with the remaining 20% and 15% corresponding to polyvinylidene fluoride (PVDF) binder and acetylene black, respectively. LFP and LMO cathodes cost significantly less to produce than LCO cathodes because of the lower value metal used, and the recycling of LCO batteries is the highest, mainly due to the same reason, the valuable cobalt. Other valuable metals, like niobium in LFP, can also be found within the cathodes in trace amounts as an added component to improve some characteristics [17,20–24].

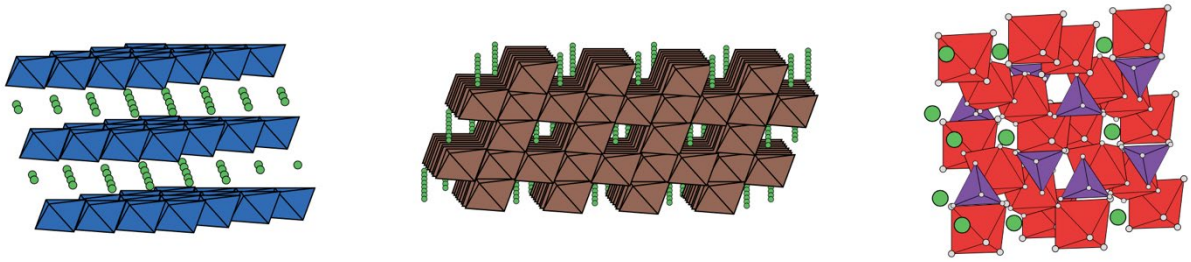

Layered Oxides $LiCoO_2$ | *Spinel* $LiMn_2O_4$ | *Olivine* $LiFePO_4$

Figure 3 - Example of the different crystal structures used in LIBs, with the green spheres representing the Li ions (Adapted from: [25]).

The ideal cathode material must fulfil the following six requirements: [26]

1. The negative Gibbs free energy related to the discharge reaction must be large – high discharge voltage.
2. The host structure needs to have low molecular weight and enough capacity to intercalate large amounts of Li-ions – high energy capacity.
3. The lithium chemical diffusion coefficient of the host structure ought to be high – high power density.
4. Intercalation and deintercalation should produce as few structural modifications as possible – long life cycle.
5. The materials required for production should be non-toxic, inexpensive, and chemically stable.
6. The employment of the materials should be easy.

LFP not only has high power capability, which means that it can accept a regenerative braking charge and can provide an acceleration discharge very quickly but also is of relatively low cost because iron phosphate is quite common and low cost. Safety-wise, it has been deemed as safer, due to its tolerance of abusive conditions, such as cell overcharging or high temperatures, and lower energy density, meaning that there is less energy to discharge in the event of a failure. However, its lower energy density also presents itself as a disadvantage [24,27].

LCO is the original Li-ion chemistry and is most commonly used in small electronics, e.g. cell phones or laptops. Although it offers high energy density, long life cycle, on the other hand, it's less stable at higher temperatures and more reactive than other chemistries – the reason for which it has not seen wide use in large applications. Pricewise, due to the high amount of cobalt, it has a somewhat higher cost [24,27].

NMC, or NCM, depending if it has a higher percentage of Cobalt or Manganese, is known for its higher energy density, higher voltage, and acceptable level of safety. All of these characteristics are responsible for the stronger prevalence of this type of battery chemistry [24,27].

NCA cells are known due to their appearance in the traction battery of Tesla's cars, and for having an even higher energy density. Despite that, they're somewhat unsafe, and, also due to the presence of cobalt, their price is higher [24,27].

Finally, LMO, are a lower-cost chemistry with high energy and high power. At the same time, their life cycles are relatively shorter. Inevitably, their use is limited to applications where you want long run time but not necessarily in automotive applications, where you want a long life. For the latter, a combination between NMC and LMO is made to achieve a compromise between both [24,27].

The biggest market share for EV, approximately 45% of the total LIBs on the market, is attributed to LMO cathodes. Having said this, by 2025, with the increase in use of NMC, NCA, and LFP cathodes, their market share is predicted to go up to 28%, 23%, and 32%, respectively, leaving LMO with a 17% market share [22].

New cathode chemistries continue to appear, with the objective of decreasing the costs of production and extending battery capacity and performance.

2.2.2. Anode

An ideal anode material has to accomplish five basic requirements: [26]

1. The anode material must enable the accommodation of large fractions of Li-ions.
2. Its electrode potential needs to be as close as possible to that of Li metal.
3. It must possess suitable electronic and Li conductivity.
4. The material should not react with the electrolyte and must remain stable in the solvents of the electrolyte.
5. The material must be cheap and environmentally friendly.

The capacity of a battery is determined by how many lithium ions can be stored in a determined amount of anode material. The typical anode active material is graphite, hexagonally bonded carbon atoms arranged in sheets, coated on copper foil. Lithium ions are stored within the graphite during charging, interposing between the sheets. Here, it is crucial that the material provides an efficient flow of Li-ions, without excessive structural and volume changes, while at the same time conducting electrons [14,17,20–22].

Since the theoretical storage capacity of graphite is fairly low, approximately 372 mAh/g, replacement technologies are still being developed, with the aim of improving the anode performance, e.g. silicon composites, carbon nanotubes, tin compounds, and metallic nanoparticles. On top of that, metal nitrides, sulphides, and phosphides can also be used as potential candidates for anodic material. Lithium Titanate Oxide (LTO), although scarcely, can also appear, but their applications are only suitable for stationary cases due to its low specific energy, caused by the increase in safety [17,18,20–22,28,29].

2.2.3. Separator

The separator is placed between the electrodes and behaves like a non-conductor, allowing the passage of lithium ions during the cycling process, and avoiding direct contact and short-circuiting. The usual material of choice is micro-porous polypropylene or polyethylene. Ongoing research aims at the development of separators with better durability and safety, e.g. nonwoven aluminium oxide composites [4,14,20–23,30].

2.2.4. Electrolyte

Another component is the electrolyte, a liquid or gel-based solution that the anode and cathodes are emerged in, used for the transfer of ions between the electrode, acting as a medium through which ions are moved from one electrode to the other, converting the chemical energy into electrical energy. Electrolytes are composed of solvents and solutes. Solutes are usually Li salts, e.g. $LiBF_4$, $LiPF_6$, and $LiClO_4$. Among these, $LiPF_6$ has exhibited adequate performance, but, at the same time, has the lowest thermal stability and can easily adsorb water and hydrolyse, creating safety risks. Most of the solvent solutions used, so as to meet the required physical and chemical properties for the respective LIB type, use mixtures of various organic solvents. Usually, 20-50% of ethylene carbonate is mixed with carbonates, e.g. dimethyl, diethyl, and ethyl methyl carbonate, or esters, e.g. ethyl acetate and methyl butyrate. With an eye towards safety improvements, efforts are being channelled into the substitution of lithium salt, the introduction of flame retardants, and the development of polymer and solid-state electrolytes. Additives are commonly found but are often highly specific and confidential. These additives provide different benefits, but their main function is to facilitate the formation of the solid electrolyte interphase (SEI) layer, to reduce the irreversible capacity and gas generation of the SEI formation and long-term cycling, and to amplify the cell's thermal stability [3,14,20,21,23,24].

At the moment of the first electrochemical reaction, the electrolyte begins to react with the graphite or carbon anodes, and some of the lithium starts to form a passivation layer on the anode's surface (SEI), resulting in an irreversible loss of capacity. This said, this nonactive layer of lithium also protects the graphite or carbon surface from further chemical reactions with the electrolyte [24].

2.2.5. Binder

The last component is the binder, commonly PVDF, which is used to connect the electrode material to the respective electrode foil. PVDF is the usual choice not only due to its good electrochemical stability and binding capability but also due to its ability to adsorb electrolyte for facile transport of the Li-ions to the active material surface or cathode [22,23,28].

2.3. Raw Materials

The demand for EV, thanks to government encouragements and increase in social awareness, is growing rapidly, replacing sales of ICEs. For instance, in 2020, about 3.24 million EVs were sold, a substantial increase when compared to the 2.26 million from the previous year. Such hasty transformation is creating a considerable growth in demand, which will lead to pressure on natural resources needed for the production of EV, and, at the same time, raise questions concerning their availability and cost. An example is the case of Volkswagen that, in 2017, could not place a contract to secure its need for cobalt for its EVs [31–34].

Several initiatives such as the International Research Panel (IRP) of the United Nations, the Raw Materials Initiative (RMI) of the EU, the Critical Materials Strategy of the USA, the Critical Minerals Strategy of Australia, and the Resource Securement Strategies of Japan, have been launched in

different parts of the world aiming at the building of knowledge around this problematic, addressing aspects like supply, demand, resource efficiency, and recycling [32].

One of the top priorities of the RMI was to establish a list of critical non-energy raw materials at the EU level, materials that have high economic importance and high supply risk. As result, in 2011 the first list was established, and it is updated every three years to maintain a regular assessment of the criticality of raw materials for the EU. The identification of the critical raw materials is done using two important parameters. One is the Economic Importance, which states the importance of a given material in the EU regarding end-use applications and the performance of its substitutes in these applications. The other factor is the Supply Risk, studied bearing in mind the possibility of disturbance in the supply of a given material, considering certain aspects such as government stability, supply concentration, trading constraints and agreements, import dependence, and existence and criticality of a substitute. If the economic importance is higher than 2.8 and the supply risk higher than 1, then the raw material is classified as critical. In Figure 4 the overall results of the 2020 assessment are portrayed [35].

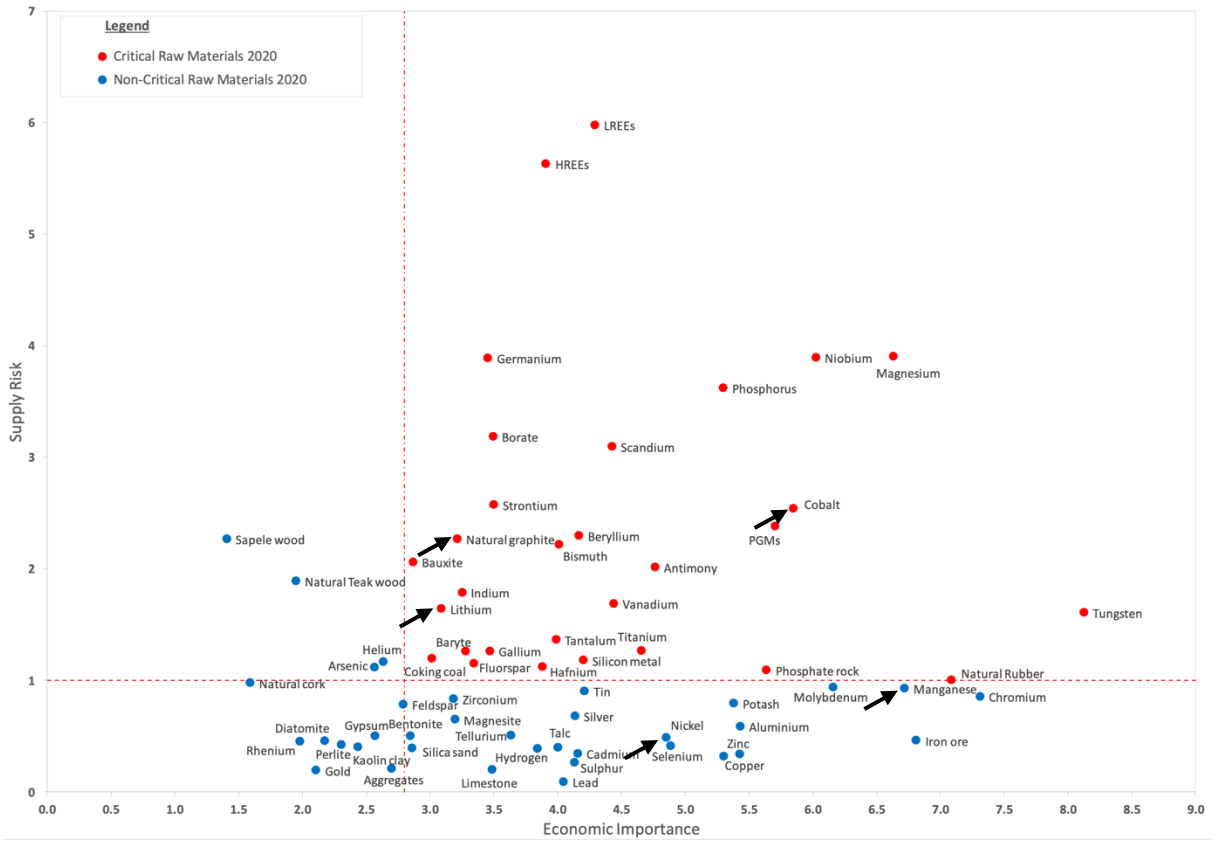

Figure 4 - Results of the critical assessment of 2020. The arrows indicate the position of the LIB elements (Adapted from: [35]).

The batteries, a fundamental part of all EVs, are composed of materials such as cobalt, lithium, nickel, manganese, and graphite. All of the stated materials, with the exception of manganese and nickel, are included in the EU's Critical Raw Materials List of 2020 [31,35].

Additionally, there is copper, the most frequently used heavy non-ferrous metal, in its pure form or in two common alloys: brass and bronze. Despite having a low supply risk, copper is of high economic

importance. It is an essential element in the low-carbon transition, having a significant impact in areas such as transport (energy infrastructures, EVs and their associated charging infrastructures), wind power (cabling and temperature control within the wind turbines), solar power (photovoltaic panels), and tidal power. Because the EU is highly dependent on refining and smelting imported concentrates, as well as on recycling production scrap and EoL products, due to European mined copper being insufficient to meet the demand, focus has started to be driven to this material [36].

In the coming pages, a more detailed description of each metal is given, providing an extended view of their value chain and criticality. The parameters used on each assessment were geographic location, end uses, and substitutability.

2.3.1. Cobalt

Cobalt is a shiny, silver-grey, transition metal with many diverse applications. It is known for retaining its strength at high temperatures, for having a high melting point, for being ferromagnetic, and keeping its magnetic properties at the high temperatures, highest of any other metal. In addition, it is multivalent, produces intense blue colours, and can form alloys with other metals imparting their high-temperature strength and increasing wear resistance [37].

Global mined and refined production of cobalt has been growing over the last couple of decades at an annual rate of over 7% and is projected to increase to 13% in the following decade, due to the increase in demand for cobalt inflicted by the expansion of the EV market. Cobalt appears as a by-product of nickel and copper production. The Central African Copper Belt, which spans across the Democratic Republic of the Congo (DRC) and Zambia, is the world's most important cobalt resource area [37].

The DRC is its dominant producer and exporter, for both cobalt ores and concentrates, with a share of 97% of global exports in terms of value in 2017. The EU consumption of cobalt ores is majorly sourced by DRC, around 68%, and from domestic production in Finland, around 14%. Concerning refined cobalt, the production comes mainly from domestic production, Finland and Belgium, 54% and 7% of EU sourcing, respectively. In Figure 5, the EU sources for cobalt are portrayed. On the other side, China, another country with a critical political situation, is the world's largest importer of both cobalt ores and concentrates, reaching 61% of total imports by value, and intermediates and refined cobalt, with 39% of total imports by value, which translates in less availability for other countries [37].

EoL products, e.g. cobalt-bearing alloys or batteries, can also represent a source of cobalt by collecting and recycling them. And, although lifespans of EV batteries delay the batteries' availability to the near future, their recycling will mean a significant amount of secondary cobalt [37].

Over the past five years, cobalt prices have been inconstant, mostly due to concerns over the supply and demand balance, but also by the political environment of its principal producer, DRC. An example of its volatility is the 273% rise from March 2016 to March 2018, which meant an increase from 20,000€ to 76,700€ per tonne, followed by a 66% decrease in June 2019, to 25,800€ per tonne. These variations were the consequence of excitement regarding an eventual scarcity of cobalt due to the electrification of the transport sector. Having said this, the result was a market surplus, creating a decline in its price.

Currently, even though the price suffered a downfall due to the current pandemic situation, COVID-19, it continues to increase stoutly [37,38].

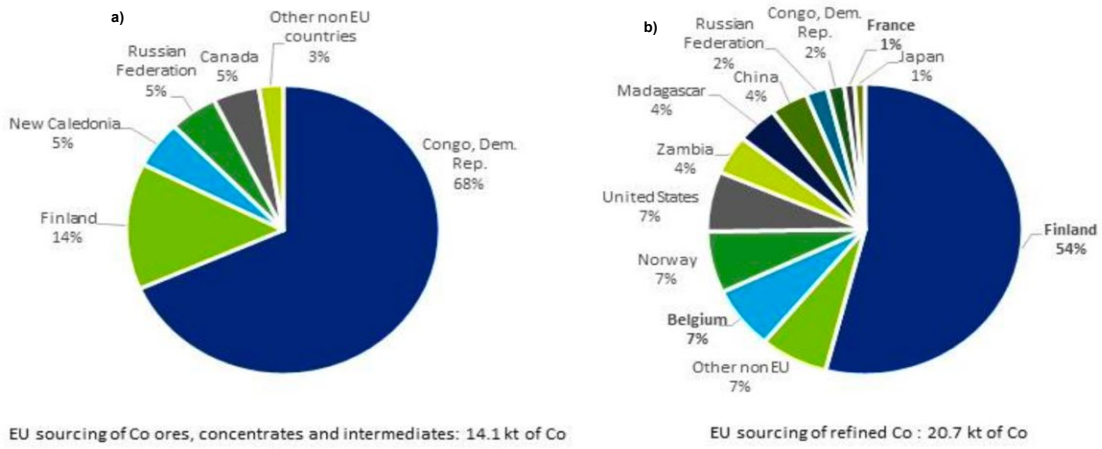

Figure 5 - EU sources of cobalt between 2012 and 2016: a) ores, concentrates, and intermediates; b) refined cobalt (Adapted from [37]).

Cobalt is a crucial raw material for the transition to a climate-neutral economy as it is fundamental in the manufacture of rechargeable batteries for EV and energy storage systems. Globally, the rechargeable battery market is responsible for the largest and fastest-growing demand for cobalt. Only in 2016, rechargeable batteries consumed half of the cobalt worldwide. In the EU, superalloys, used to make parts for gas turbine engines, are the major application for cobalt, accounting for 36% of the consumed cobalt. Figure 6 portrays all of the major end uses for cobalt in the EU, in cobalt content, in 2015. The low value for battery applications in EU reveals the considerable gap in the battery manufacturing industry [37].

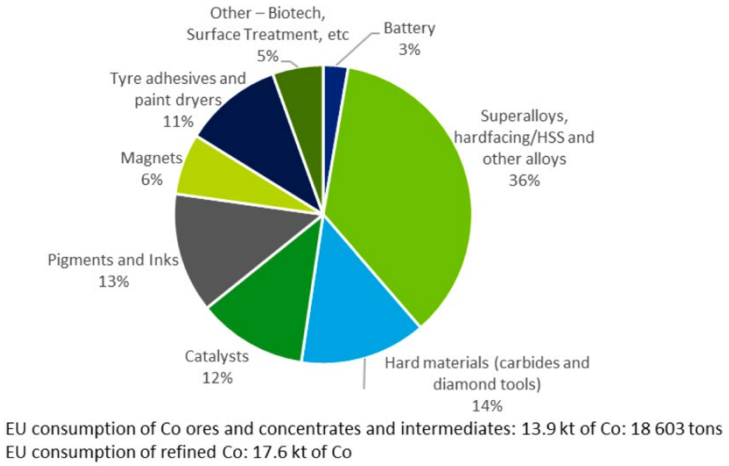

Figure 6 - End uses for cobalt in the EU industry, in cobalt content, in 2015 [37].

Substitution is attainable in battery chemicals using chemistries without cobalt, or through managing the cobalt content, adopting configurations with less cobalt loading. Nevertheless, cobalt substitution is

limited in many of its applications because of its remarkable properties. In superalloys and hard materials, for example, functional cobalt substitution is severely restricted due to loss of performance [37].

Overall, the criticality of cobalt can be attributed to the lack of substitutes in most applications and its provenance from politically unstable countries.

2.3.2. Natural Graphite

Natural Graphite, or simply Graphite, is a grey-black mineral, more specifically, carbon allotrope that carries both metallic and non-metallic properties. It is composed of planar, weakly bonded, sheets formed from three-coordinated carbon atoms, with powerful intra-planar bonding. As a result of the weak bonds holding the sheets together, the layers can slide over each other easily. It is known for having good thermal and electrical conductivity, as a consequence of the free electrons between the layers, and has a high melting point, 3,650 ºC. In addition to these, graphite is also renowned for its high thermal and corrosion resistance, non-toxicity, chemical inertness, and lubricity [37].

Classification of graphite is done using two parameters: purity and particle size. In commercial use, there is flake, amorphous, and vein graphite. Flake graphite is known for having a distinct flake structure, whereas amorphous graphite, holds no flake structure and is typically of lower carbon grade. Vein graphite is a speciality product only produced in Sri Lanka [37].

Half of the world's graphite reserves are situated in China. Other significant reserves can be found in Mozambique and Tanzania, with 15% share each of the world's total graphite. In the EU, Sweden, Czechia, and Finland compose the largest natural graphite deposits. China is responsible for the majority of graphite production and exportation worldwide, having, in 2017, 71% and 59% market shares, respectively. Prospects for graphite supply are positive as supply increases from Africa, more specifically Mozambique, as a number of large-scale natural flake graphite projects are expected to reach production by 2025. In the EU, only 2% of its natural graphite consumption is sourced domestically, with China being its principal supplier, providing 47% of EU's demand, followed by Brazil, with 12%, Norway, with 8%, and Zimbabwe, with 7%. These and other sources are disclosed in Figure 7 [37].

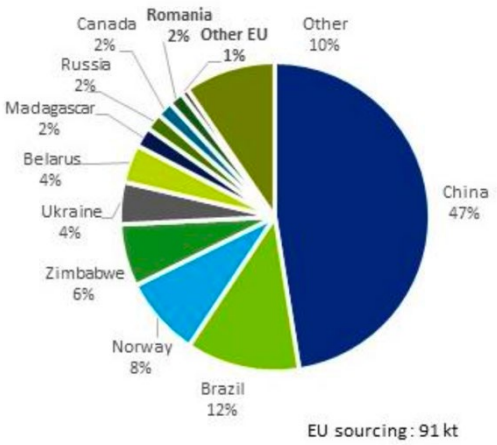

Figure 7 - Average of the European Union's sourcing of natural graphite from 2012-2016 [37].

Consumption of natural graphite is immediately associated with the production of steel, its leading consumer, due to its use in refractories. Examples of other uses, as portrayed in Figure 8, are lubricants, batteries, friction materials, refractories, and others. Some applications such as batteries, brake lining, lubricants, or carbon brushes may substitute graphite for its synthetic version. That being so, in refractory applications, natural graphite cannot be substituted [37].

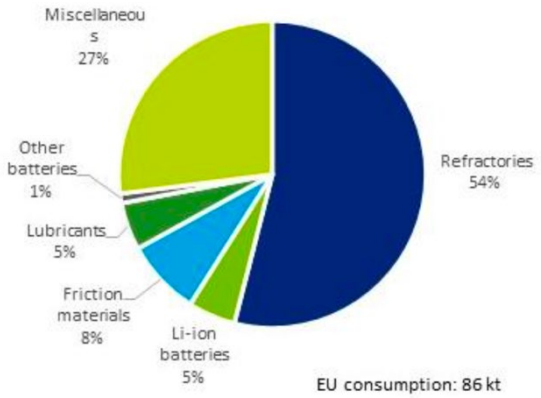

Figure 8 - Average end uses of natural graphite in the EU industry between 2012 and 2016 [37].

Flake graphite, being of higher purity and size, is set at higher prices, whilst amorphous prices are much lower. In 2011, due to China's huge steel needs (an increase in demand), the prices of flake graphite suffered a big increase. With excess production and weak demand from the steel industry, prices returned to low levels. In 2018 prices began to increase, caused by a short supply and increase demand for Li-ion batteries, but since then have been suppressed again as supply. From new projects in Africa began to appear [37].

To achieve the EU targets for a carbon-free economy, graphite is essential, as it is present in EV and energy storage systems. This allied to the fact that EU import reliance is 98% and its input recycling rate is only 3%, make up the reasons to why graphite is classified as a critical raw material [37].

2.3.3. Lithium

Lithium is a silver-white alkali metal. It is the lightest metal known, the least dense at room temperature, and has a low melting point, 180ºC. More than that, lithium is known for its excellent electrical conductivity and having the highest electrochemical potential of all metals [37].

Being highly reactive, lithium only appears in nature as inert mineral compounds, e.g. silicate. As consequence of its high solubility, it can also appear as chloride in brines and seawater. When considering hard-rock lithium minerals, Australia, the world's most abundant hard-rock minerals resource, is the main producer and exporter. On the other hand, Chile dominates the market for lithium carbonate from brines. The "Lithium Triangle", composed by Chile, Argentina, and Bolivia, contains half of the world's lithium resources and 70% of global reserves. China is the main importer of both lithium concentrates and carbonates. Additionally, China monopolizes most of the global lithium refined

production and three-quarters of the global installed manufacturing capacity for LIBs, dominating lithium's midstream and downstream segments of the value chain for LIBs [37].

Since 2015, lithium's price has been fluctuating, rising 250% from 2015 to mid-2018, caused by the expected rise in demand for EV batteries. An oversupply caused a decrease in price, until December 2020, when lithium's price skyrocketed, again due to an expected increase in EV sales [37,39].

EU's demand for lithium concentrates is met primarily by imports from Australia. For this case, import reliance is 87%. Regarding lithium compounds, because there is no domestic refining, import reliance is 100%, with Chile being the largest supplier. In Figure 9, EU sourcing for both refined lithium and concentrates is portrayed. Having said this, Portugal, Czechia, Finland, Germany, Spain, and Austria have important hard-rock mineral deposits. Considerable brine resources can also be found in Germany [37].

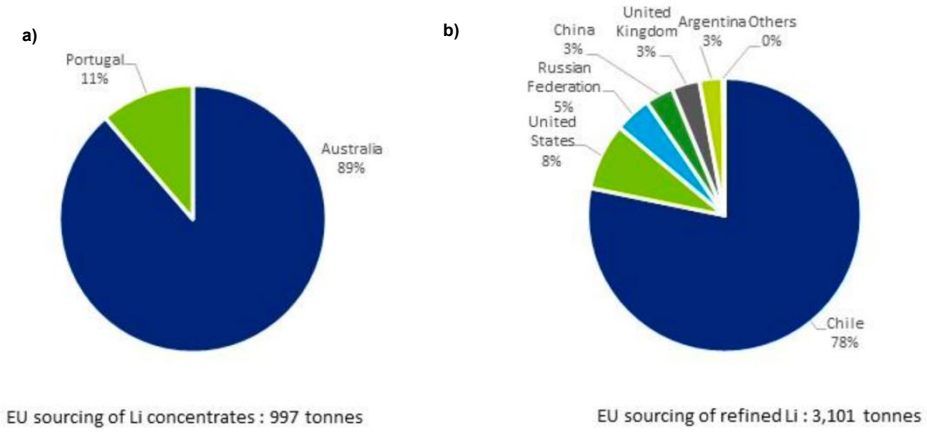

Figure 9 - Average EU sourcing between 2012 and 2016 for a) lithium concentrates b) refined lithium (Adapted from: [37]).

Lithium and its compounds have a wide range of applications such as batteries, grease lubricants, pharmaceutical products, or glassware and ceramics, with the latter composing 66% of the EU's total consumption. This said batteries constitute the highest consumption of lithium, 39%. In Figure 10, applications in EU industry are shown. Moreover, substitutes for batteries, lubricant greases, glass, and ceramics do exist, but, for rechargeable batteries used in EV and energy storage systems, a substitute that can replace the role of lithium has yet to be found [37].

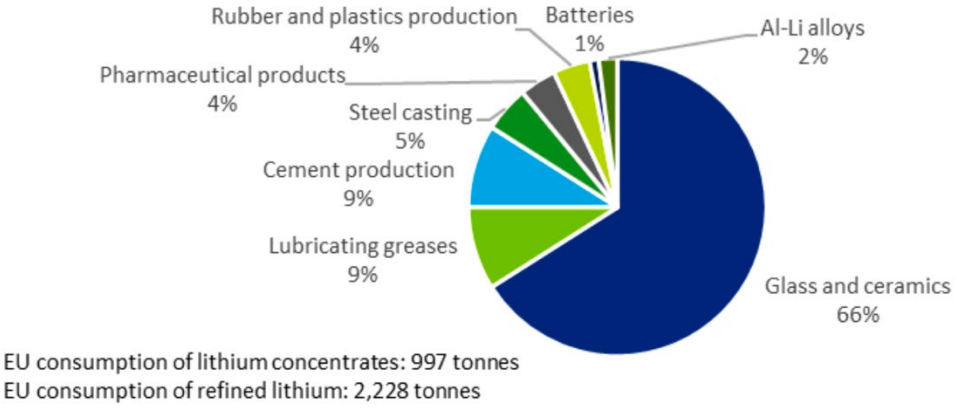

Figure 10 - Average EU industry end uses for lithium and its compounds between 2012 and 2016 [37].

To sum up, lithium is a critical raw material due to its important role in the implementation of the EU measures to achieve climate neutrality by 2050, and even though LIBs are currently being recycled in the EU, industrial-scale recycling is still far from achieving a significant role in decreasing the alarming values for import reliance.

2.3.4. Manganese

Manganese, the 12th most abundant element in the earth's upper crust, is a relatively hard yet brittle paramagnetic metal with a high melting point, 1246 ºC. It is found in several deposit types such as sedimentary, sedimentary-hydrothermal, and supergene, and its principal ore mineral is pyrolusite (MnO_2), with braunite ($Mn^{2+}Mn^{3+}{}_6SiO_{12}$), psilomelane ($Ba•(H_2O)Mn^{3+}{}_5O_{10}$)), and rhodochrosite ($MnCO_3$) also having some local importance.

Asia supplies approximately half of the global supply of manganese, dominating the global manganese market, followed by Africa with one-third of the global supply. Furthermore, Asia also prevails in global demand, constituting 80% of global demand.

EU domestic production corresponds to 3% of global production and comes from Spain, with 46%, and France, with 39%. Apart from this, Norway, South Africa, and India are the most important non-EU suppliers. This said Spain and France are still the most import sources for the EU, as is shown in Figure 11.

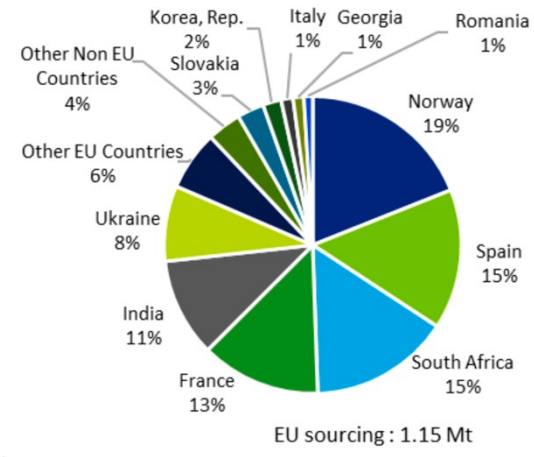

Figure 11 - Average EU sourcing of manganese between 2012 and 2016 [36].

Manganese applications are mainly associated with steel production, which accounts for over 90% of global manganese consumption, due to its efficiency at fixing sulphur and powerful deoxidiser. Additionally, it is used in the production of non-steel alloys (e.g. aluminium alloys), dry cell batteries, where it is used as depolariser, and pigments. Average EU industry end uses, obtained between 2012 and 2016, are portrayed in Figure 12. Substitutes for manganese in its major application, i.e. iron and steel production, are currently unavailable.

Generally, global manganese prices have been declining since 2012, due to the decline in global steel production in many parts of the world, with the exception of China.

The Kalahari manganese district in South Africa represents 70% of the global manganese resources and about 25% of the global reserves. Together with Brazil and Ukraine, South Africa represents nearly 65% of the global reserves.

EoL recycling of manganese comes mainly from ferrous and non-ferrous scrap, such as iron or aluminium packaging, respectively. In addition to this, slag generated during the production of steel can also represent a source for manganese, along with iron. This said, in 2020, the end-of-life recycling input rate for manganese was 9%.

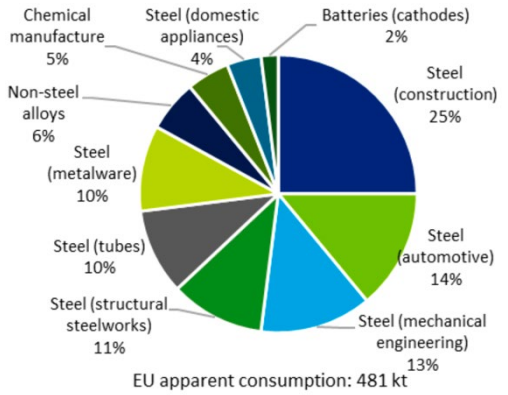

Figure 12 - Average EU industry end uses, obtained between 2012 to 2016 [36].

Currently, there is no concern about manganese shortage, as reserves are estimated to meet global demand for several decades. Having said this, because manganese has a relevant role in meeting the future low carbon technology requirements, it is still advisable to be attentive to this material's market behaviour.

2.3.5. Nickel

Nickel is a shiny white metal with average metallic properties that occurs in combined form and has a relatively high melting point, 1,455 ºC. Its main use is in alloy production, e.g. stainless steel. Within the EU, more than half of nickel consumption is related to the manufacturing of various types of machinery and equipment, 35%, and basic metals, 22%. In Figure 13, the different end uses for nickel at a mine stage are portrayed.

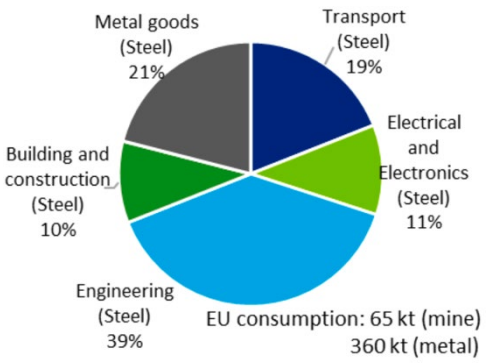

Figure 13 - Average EU industry end uses for nickel between 2012 and 2016 [36].

In metal and leisure goods, building and construction material, machinery, or medical equipment, the substitution of nickel by other steel alloy material is possible, e.g. titanium, chromium, manganese, and cobalt. Be that as it may, these alternative steel alloys are usually pricier or have adverse impacts on performance. An example would be the batteries where currently the objective is to decrease the quantity of cobalt use and substitute it with nickel, due to concerns regarding cobalt prices and availability, as formerly explained.

From 2011 to 2019, nickel price has suffered a decrease. Since January 2019, nickel price has been rising, probably due to the expected rise in refined nickel-metal usage for the next twenty years.

In the EU, almost half of the consumption of nickel ore is produced domestically by Greece, 45%, and by Finland, 40%. On the other hand, the consumption of refined nickel is mostly supplied by the Russian Federation, 36%. Greece and France are the two main suppliers of refined nickel within the EU. In Figure 14 a) and b), EU sourcing of both nickel in mine and metal stage is portrayed in detail.

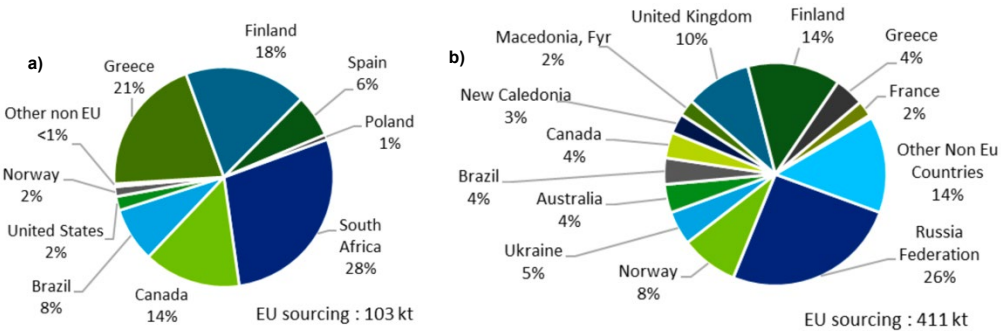

Figure 14 - Average EU sourcing between 2012 and 2016 of nickel in a) mine stage; b) metal stage (Adapted from:[36]).

For refined nickel metal, China and the Russian Federation are the world-leading suppliers with 29% and 12% of the global production, respectively. EU production accounted for 4% of the global production, with Finland representing 66% of that value. For nickel concentrates, Indonesia leads the production, with 18% of the total production, followed by the Philippines, with 17%, Australia and the Russian Federation, both with 11%, and Canada, with 10%. Europe only represents 2% of the global production, with 85% taking place in Greece and Finland.

Due to the widespread of nickel as an alloying element in several non-ferrous alloys, e.g. stainless steel, its collection and recycling is facilitated, with the economic value of nickel also providing a significant incentive to this. The recycling efficiency for nickel metal is estimated to be around 68%.

In view of nickel having a significant part in renewable energy technologies, e.g. solar panels, and batteries, nickel became a significant key raw material for the decarbonization of the EU, and even though at the moment nickel is classified as a non-critical raw material, supply can still overtake demand.

2.4. Circular Economy Approach

CE strategies may represent countermeasures to achieve a more sustainable use of global resources while meeting climate and sustainable development goals and guaranteeing the eco-sustainability of post-use products. In recent years, the adoption of such measures has proven to be effective in the reduction of primary extraction and the promotion of a more resilient and green supply chain for EV batteries. When LIBs reach their EoL, in other words when capacity falls to 80% of its original capacity, they can no longer fulfil their original role in EV. In certain conditions those batteries can have a second-life use in stationary storage applications, but at the end all of them must be sent for recycling [40–42].

Recycling creates an opportunity to secure raw materials supply for EV batteries, reduce the high amount of energy use and emissions from EV battery life cycle. Currently, three different methodologies, used alone or in pairing, are employed for recycling LIBs: pyrometallurgy, hydrometallurgy, and direct recycling [43–45].

Recycling to recover raw materials has been the main focus in traditional recycling, but since the battery still has 80% of its original capacity, the introduction of a more inclusive CE approach allows for an extension of its lifespan by giving new purposes: reusing, refurbishing and repairing, re-manufacturing, and only then reclaiming the raw materials, as portrayed in Figure 15, closing production loops to minimize the generation of waste and the demand for natural resources. To put it in another way, instead of immediately recycling, the remaining capacity can be repurposed, giving batteries a second life in less demanding applications, and, at the same time, increasing the product's value chain and enabling the retention of the value and quality for as long as possible [40,41,45,46].

These new applications can be sorted according to their energetic demand: [40]

(i) Residence related application (3-4 kWh)
(ii) Commercial applications (25 kWh to 4 MWh): telecommunication towers, light commercial, uninterruptible power supply.
(iii) Energy-related/industrial applications (up to 50 MWh): renewable energy storage, grid stabilization.

Considering there are a variety of second life applications, to ensure efficient and safe use of the battery, the right choice of application at the right time must be made. When repurposing batteries, i.e. re-using packs, modules or cells, accurate assessments of both state of health (the degree to which a battery meets its initial design specifications) and the state of charge (the degree to which a battery is

charged or discharged) are essential. A proper analysis of the state of health allows for a better understanding of whether the battery is suited for re-use, and if so, for which application, remanufacture or recycling. The state of charge acts as a safety precaution [40,45].

To implement these strategies, recovery of EoL products must be done, i.e. the recovered materials must return to their respective original manufacturers or to external parties, that will re-introduce them into the supply chain. This said, the supply chain is already complex, and the introduction of reverse logistics is something that most companies are not yet ready to deal with [46].

Traditional waste management strategies are complex and time-consuming because of the diverse nature of waste materials. The Internet of Things (IoT) has to do with the interconnection of physical objects, through the Internet, sharing information, and coordinating decisions based on data. This is a very good example of an information technology tool that can play a key role in supply chain management, creating a faster and more sustainable collection of waste, leading to lower costs and increased added value associated with the recovery process [46].

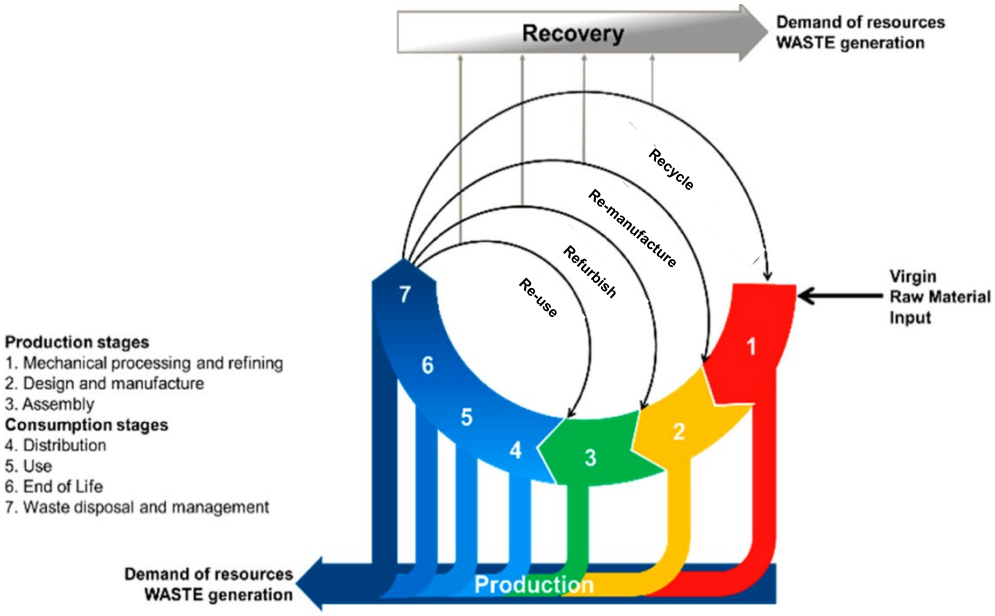

Figure 15 - Circular Economy model (Adapted from:[14]).

One thing is certain, in the future, high cost and unreliable supply of raw materials, environmental and safety concerns regarding the disposal of spent LIBS, among other factors, will establish recycling of LIBs as a necessity rather than an option.

2.5. Future Outlooks

Research to find alternative materials with the objective of decreasing the costs of production, increasing safety, and extending battery capacity and performance. Currently, the principal concern is to reduce or eliminate the presence of cobalt from the current LIB cathode chemistries. Furthermore, economic and ethical considerations aside, the energy density of cobalt-containing LIB chemistries,

namely NCA and NMC, do not meet the advised threshold necessary to penetrate the mass consumer market. And so, cobalt-free chemistry substitutions, e.g. LFP, are bound to take over the market, as seen in Figure 16. Additionally, replacement technologies are also being developed with the aim of improving the anode performance, i.e. allow faster charging. To improve the safety of electrolytes, efforts are being channelled into the substitution of lithium salt, the introduction of flame retardants, and the development of polymer and solid-state electrolytes [22,47].

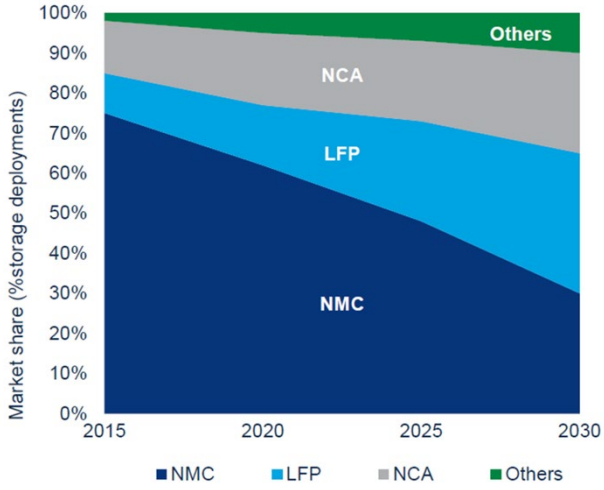

Figure 16 - Battery chemistry market share forecast for energy storage systems [48].

Chapter 3

Recycling of LIBs

The recycling process can be divided into two parts: pre-treatment and metal extraction. In large scale recycling, the metal extraction part can be done using hydrometallurgy, pyrometallurgy, direct recycling, or a combination of pyrometallurgy, physical separation techniques and hydrometallurgy. The outputs from the recycling process range from metal alloys, high purity metals, intermediates or feed materials for further processing, active battery materials or their precursors. In Figure 17 a generalized recycling loop scheme is presented. This scheme is an optimized loop considering as hypothesis that all the recovered metals from recycling would be used to manufacture new batteries, which is not necessarily so. In the following sub-chapters, descriptions of different alternatives for each step can be found [6,17,44].

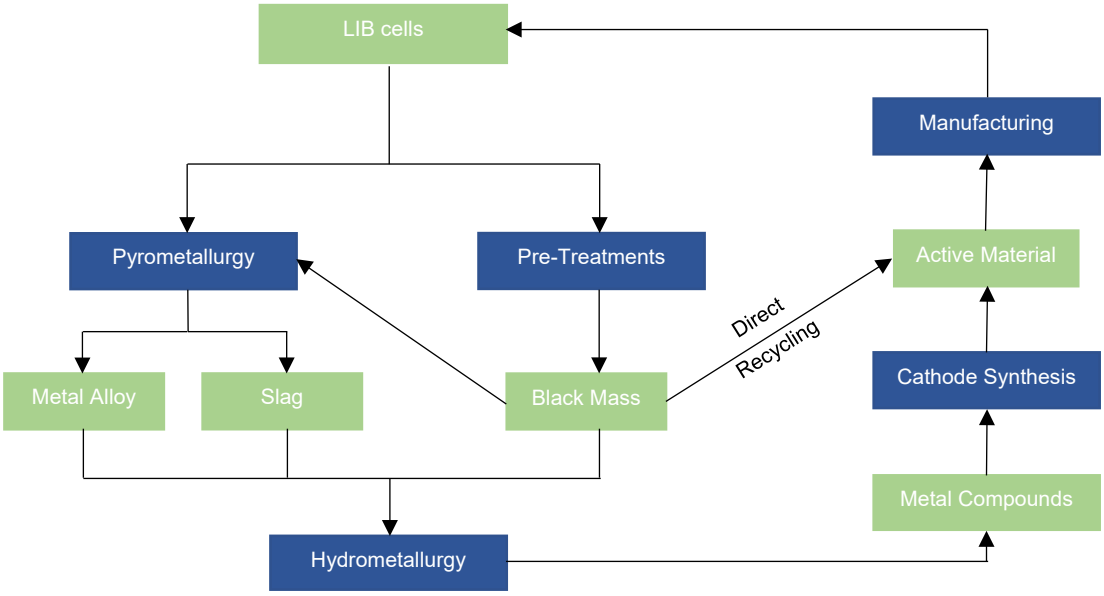

Figure 17 - Generalized LIB recycling loop.

3.1. Pre-treatment

The complete pre-treatment procedure includes mechanical separation processes, heat treatment processes, and dissolution processes. The use of a pre-treatment step in the recovery process is advantageous, as it leads to a decrease in the acid consumption, increase in the leaching efficiency, decrease in the impurities in further steps, and, consequently, a decrease in the number of purification steps, which results in fewer operation costs [3,23].

As spent LIBs have a small amount of remaining charge, they can detonate during the recycling process. And so, the first step is the discharge of the LIB, preventing short circuits and self-igniting. Two common methods used to neutralize the LIB's charge are either heating up to 300 ºC, which also leads to the removal and evaporation of the electrolyte, or soaking the spent LIBs in NaCl or Na_2SO_4 saturated solution for 24 – 48 hours. The operating times are highly influenced by the specific solution conductivity,

operating temperatures and by the LIBs state of charge. Other alternatives are covering LIBS with stainless steel chips, stimulating the controlled short circuit, connecting them to a resistors to collect and reuse the residual energy, or stabilizing the battery by spraying it with liquid nitrogen, until the battery reaches -100 ºC [3,23,42,49,50].

LIBs possess a wide variety of physical configurations, cell types and cell chemistries, depending on the manufacturer. This diversity represents a challenge for battery recycling. Figure 18 displays three different types of battery cell designs with their respective packs. It is evident that these three different designs, require different approaches when disassembling. The prismatic and pouch cells have planar electrodes, the cylindrical cells are tightly coiled. Their format and relative size differ, creating a constraint for automation. And so, vehicle design has to make a concession between safety, centre of gravity, space optimization and recyclability [45].

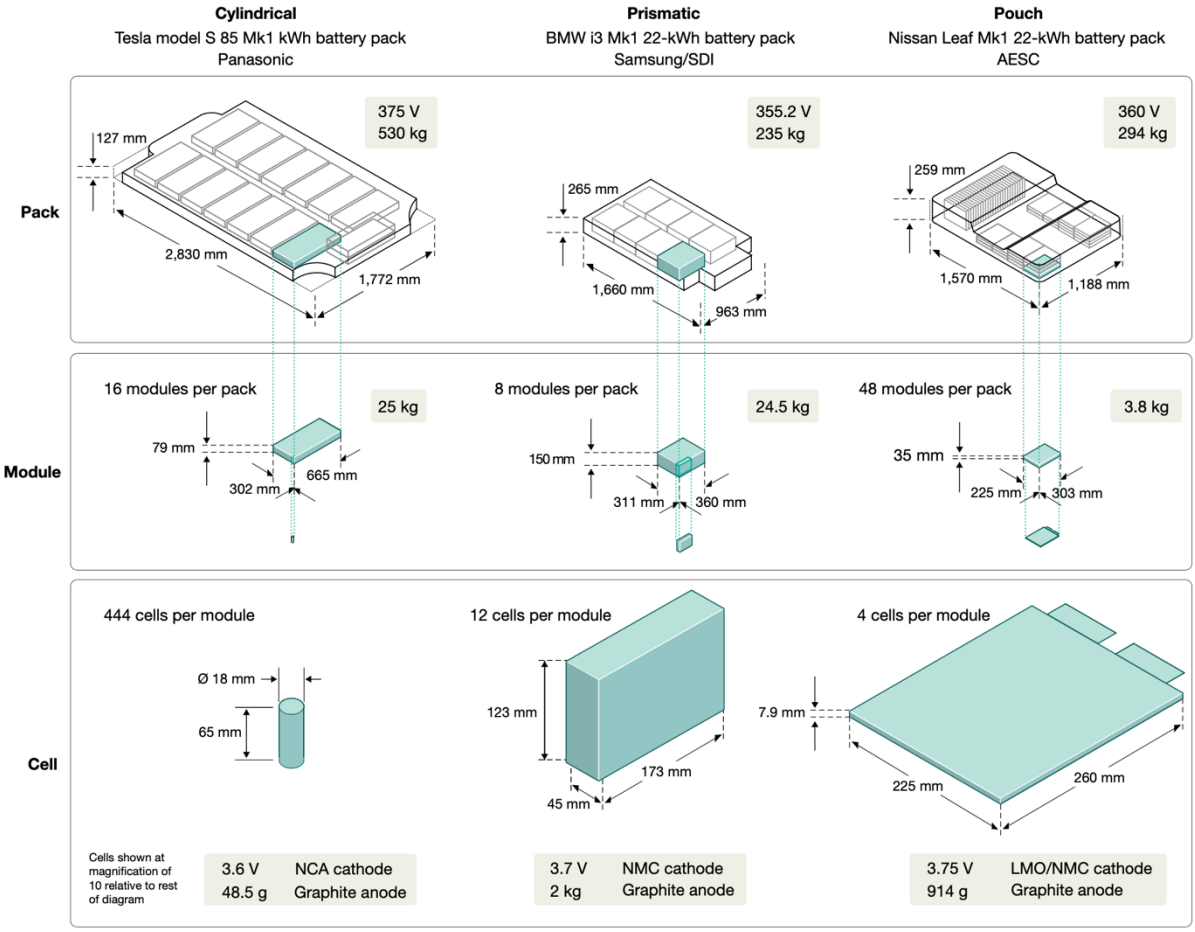

Figure 18 - Example of three battery packs and their respective cells [45].

After discharging, the spent battery packs are dismantled, often manually, allowing the separation and recovering the metal casings, electronic devices, cables, and other components. Following dismantling, there is mechanical separation, the most used technique at industrial level, which has the sole function of removing the outer case, to segregate valuable materials, and reduce scrap volume. This technique includes crushing, magnetic separation, sieving, and other physical separation

operations. On top of this, grinding by milling in the last stage of pre-treatment can also be done, leading to a higher free surface and, as a result, the leaching efficiency increases. Mechanical pre-treatment is either applied by a company specified only on this step, while all recovered components are further distributed to other recycling plants and metal producers, e.g. Akkuser, in Finland, or separated components are processed within the same company. In the case of Akkuser, the mechanical pre-treatment is followed by mechanical separation of black mass (common designation of the mixture of cathode and anode active powder material) from current collectors, foils, and other battery components, e.g printed circuit boards or casing. The latter are then sold to specialised recyclers or metal producers [3,23,42,51].

The next, and last step, on the pre-treatment procedure chain, is the separation of the cathode materials from the foil. Some of the most common methods are thermal treatment, ultrasonic separation, and solvent dissolution method. Solvent dissolution methods use organic solvents with good solubility, e.g. NMP, DMF, DMAC, DMSO, to weaken the adhesion force between the foils and activate materials. Nevertheless, the solvent is usually costly and toxic, which is very likely to threaten the ecological environment. The ultrasonic operation, due to the effect of cavitation, is recognized as an effective method for separating cathode materials from foil substrates. This said, the procedure is considerably noisy, and its investment costs are high. Finally, the thermal methods eliminate the adhesive force between the binder and the cathode active material using high temperatures (400 – 700 ºC), causing the active cathode material to be separated from the foil. In addition, the high temperatures induce metals phase transformation, increasing the subsequent leaching efficiency. This process is simple to operate and easy to apply in practice. Yet, bonding agents and additives in the process generate harmful gases, so a waste gas treatment step is needed. Plus, the energy consumption of the process is high [3,23,42,52,53].

Many researchers through the years have proposed a lot of different pre-treatment methods. Unfortunately, finding an environmentally and economically sustainable one is still a major challenge.

3.2. Metal Recovery Processes

The objective of the metal extraction process, as the name suggests, is to convert the metals, usually in the cathode materials, into an alloy form or a solution state to promote separation. As stated in the previous chapter, the main methods currently employed are pyrometallurgical or hydrometallurgical processes, direct regeneration, or a combined pyro/hydrometallurgical process [3,6,44].

3.2.1. Direct Recycling

Direct recycling, in contrast to the other processes here presented, only uses physical processes to separate the different components present in the active material from the cells. Additionally, attempts can be made to refresh or reactivate the active material, recovering any capacity or properties lost during cycling. Steps included in this process range from physical separation of the active material, washing of binder, thermal treatment, lithium replenishment, and a final thermal treatment. Currently under development at the lab scale, this process aims to attain an extensive and efficient re-use of all major

battery components, avoiding chemical processing as much as possible. Despite the short recycling route, the disuse of chemicals and the possibility of the recovery of almost all battery materials, the material may not perform as well as virgin material, and the mixing cathode materials could reduce the value of the recycled product. Furthermore, the variability of battery designs and chemistries, and the ever-evolving cathode metal oxides formulations, constitute the main drawbacks for direct recycling deployment, that is, direct recycling processes are tailored to specific cathode formulations [4,43,45,54,55].

Throughout the years, several methods have been developed. Retriev, a company based in Lancaster, Ohio, with plants placed across North America, patented a process that consists of cryogenic crushing and screening, followed by a thermal treatment at 500 ºC, that destroys the binder (PVDF) and modifies the carbon surface. After, through selective flotation, the carbon is removed, and the sink fraction containing the cathode powder is mixed with an appropriate amount of lithium hydroxide before calcination at 500-800 ºC, creating new lithium-ion cathode materials. In Figure 19, a schematic of the process is shown [6,55,56].

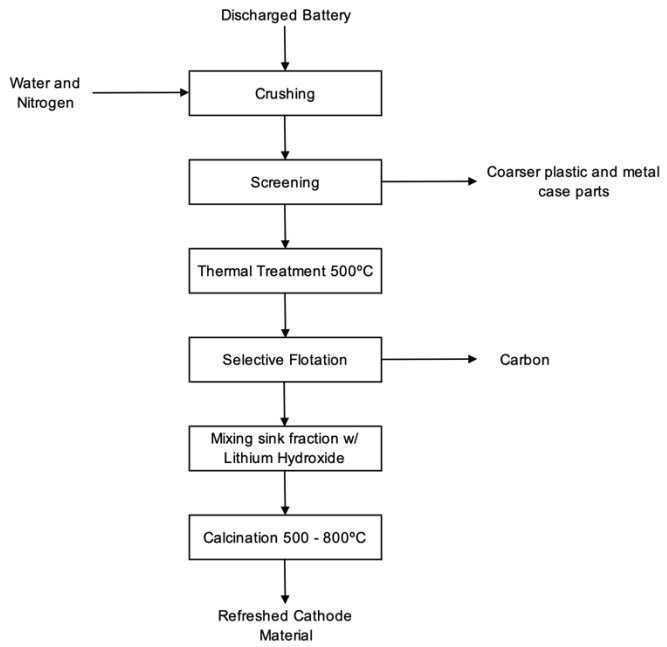

Figure 19 - Schematic representation of Retriev's recycling process (based on [56]).

3.2.2. Pyrometallurgy

In pyrometallurgy, a single method is used to decompose the constituents of LIBs by heating at high temperatures promoting the melting of the materials. The most commonly recovered materials are Ni, Co, Fe, and Cu, with the remaining, e.g. Li, Al, and Mn lost in slag. To produce separate products further hydrometallurgical methods are needed and introducing slag formers, adjusting the chemistry of the slag, can improve the recovery of the valuable metals [3,4,18,44,54].

Pyrometallurgy is usually used in combination with hydrometallurgical processes and other pre- or post-treatment processes. In such cases, spent LIBs start by being discharged, after which they are dismantled through a series of steps. Next, the electrolyte is recovered and the LIBs are crushed and screened, separating plastics, graphite, and metals. Lastly, the metals are recycled through high-temperature smelting, i.e. pyrometallurgy. Alternatively, the spent LIBs can be sent directly to the smelting furnace, after being discharged, without any pre-processing steps. In both cases, as mentioned before, to separate the metal in their respective salt or metal forms, further hydrometallurgical processing is needed [6,43,45].

The main advantages of this process are the elimination of the need for mechanical pre-treatment, the possibility of handling large volumes of waste at the same time, the possibility of decomposing organic materials (with eventual energy recovery), and its universal effect on various EoL batteries. Advantages like this have made several companies such as Sumitomo-Sony, Accurec, Akkuser, and Umicore, to investigate, and in some cases employ pyrometallurgy as their go-to process. However, factors such as high energy consumption (mainly deriving from fossil-based fuels), emission of hazardous gases, and material losses, may turn the typical pyrometallurgical approach useless in the near future, since these factors contribute to the carbon footprint of the recycled materials [3,4,6,18,43,44,54].

Currently, pyrometallurgy is the most ubiquitous metal recycling technique used. The German company Accurec started by developing a process designed to treat Ni-Cd batteries, which, since then, has broadened its scope to process various types of batteries, including LIBs. Figure 20 reveals how the process employs a combination of mechanical, pyrometallurgical, and hydrometallurgical processes [14,57].

The process starts by manual dismantling the spent LIBs and removing the organic components (electrolytes, plastics, and binders) by pyrolysis under vacuum, using a temperature of 250 ºC. The cells then undergo comminution in a hammer mill, and four separate size fractions are obtained by mechanical classification (magnetic separation, air separation, zig-zag classier, or vibrating screen). Next, a binder material is added to the fraction containing the target metals, i.e. Co, Mn, Li, to agglomerate the particles to the pellets, which are then smelted at a temperature of 800 ºC, producing a Co alloy, and Li is lost in the flue dust and slag. Subsequently, the Li-rich slag is treated by hydrometallurgical processes, precipitating Li in the form of Li_2CO_3. Accurec claims that the process achieves a Li_2CO_3 recovery of 90% [14,57].

In order to handle, sustainably, a large number of spent LIBs in the future, the best possible recovery approach is required to have lower energy consumption, fewer environmental hazards, and higher recycling rates.

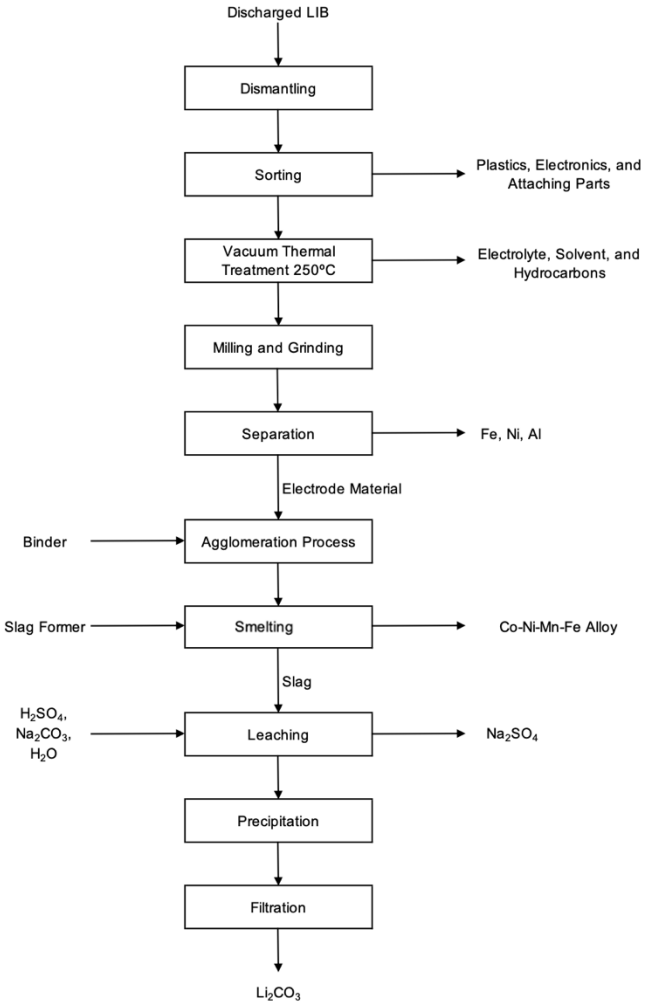

Figure 20 - Schematic representation of Accurec's recycling process (based on [14]).

3.2.3. Hydrometallurgy

Hydrometallurgical processes involve dissolving the cathode materials with proper chemical reagents, i.e. leachants, and separating the metals in the leaching solution. Contrary to pyrometallurgical processes, hydrometallurgical processes require processing after discharging and dismantling to maximize the recovery rate. Low energy dissipation, high extraction effectiveness, minimum capital cost, and less hazardous gas emission, make this one of the major and most powerful technologies applied for the recovery of metals from spent LIBs. The core operation is the leaching where the electrode fraction of the spent LIB batteries is reacted to form aqueous soluble metal. Depending on the employed solution, the leaching operation can be classified as acid leaching (inorganic or organic), alkaline or ammonia leaching, electrochemical leaching, and bioleaching [3,4,18,44,45].

Leaching is a fundamental procedure for the recycling of useful metals from LIBs. In inorganic acid leaching, strong acids such as hydrochloric acid (HCl), sulfuric acid (H_2SO_4), nitric acid (HNO_3), and phosphoric acid (H_3PO_4) are the most commonly used. Additionally, hydrogen peroxide (H_2O_2), sodium sulphite ($NaHSO_3$), grape seed, tea waste, or glucose, are used as reducing agents to reduce the transition metal oxides to lower oxidation states, facilitating their dissolution in the acid solution, and,

therefore, improving the leaching efficiency. Recovery effectiveness for expensive metals such as Li, Ni, and Co, when using inorganic acids is over 95%. This said, challenges in the recovery of Al, Cu, and Fe or low pH leachates, and the fact that this process can potentially generate detrimental by-products such as Cl_2, SOx, and NOx, raise some uncertainties about the environmental friendliness of this process. In alternative, there is alkaline or ammonia leaching, where through the use of inorganic bases such as sodium hydroxide (NaOH) and ammonium hydroxide (NH_4OH), metal can be recovered from pre-treated materials or metal slags from spent LIBs [4,18,42,44].

Temperature, acid and reducing agent concentration, reaction time, and pulp density are the main parameters of this process. A diverse number of studies have been published throughout the years, exploring different combinations of acids and reducing agents, concentrations, and processing conditions. In Table 1, an overview of some of those works is displayed, revealing the pair H_2SO_4 and H_2O_2, as the most commonly used leaching and reducing agent, respectively.

Table 1 - Summary of some published studies on leaching valuable metals from spent LIBs.

Leachant	*Reducer*	*Leaching Efficiency / %*						*T*	*L/S*	*t*	*Ref.*
		Al	Cu	Li	Ni	Mn	Co	*ºC*	*L/kg*	*min.*	
H_2SO_4	H_2O_2	-	-	96	93	98	91	60	50	60	[58]
H_3PO_4	H_2O_2	-	-	100	99	99	96	60	20	60	[53]
H_2SO_4	Electrode Foils	98	99	98	96	99	98	60	200	360	[59]
H_2SO_4	C_2H_5OH	-	-	99	-	-	99	90	20	160	[60]
HCl	-	-	-	100	99	99	99	70	20	50	[61]
H_3PO_4	H_2O_2	-	-	100	-	80	-	85	30	180	[50]
H_2SO_4	H_2O_2	-	-	98	98	97	97	80	20	60	[62]
H_2SO_4	$Na_2S_2O_5$	-	-	>90	>90	>90	>90	60	10	60	[63]
H_2SO_4	$Na_2S_2O_5$	-	-	86	90	78	85	50	50	60	[64]

The procedure is usually carried out at a temperature below 100 ºC, reducing energy costs. The valuable metals present in spent LIBs are dissolved in the leaching solution and therefore separated from the undissolved residues by filtration. From this leaching liquor metals are reclaimed by several approaches, including: chemical precipitation, solvent extraction, ion exchange, electrochemical deposition, and membrane separation, etc. Because impurities such as aluminium, magnesium, calcium, and iron are also leached, additional purification and separation processes are required [3,4,42,44,65,66].

Chemical precipitation, one of the most traditional, simple, and practicable separation technologies, uses a variety of chemical reagents, i.e. precipitants, and depends on the different solubilities of metal compounds at defined pH values. Here, precipitants are added into the leaching solution and their anions will attract the metal cations, forming insoluble precipitants. NaOH is the most widely used precipitant. Under different pHs, selective precipitation can occur allowing the purification of the solution, e.g. Al can be removed as aluminium hydroxide above pH 3, while efficient precipitation of Ni, Co, and Mn occurs at pH above 8. For the determination of operating conditions for chemical precipitation, a trial-and-error method is commonly used. Unfortunately, even though the precipitation approach is useful and has been extensively used owing to its low cost and simple operation, with the growing demand for NCA and NMC cathodes, a leaching solution containing multiple metals ions became more complicated. Thus, precise control is needed to obtain the desired products with high yield and purity [66–68].

For solvent extraction, the process is done using a specific immiscible solvent that selectively extracts a given metal from the aqueous phase. The extraction system is formed by extractants, one or more types of organic chemicals with specific function groups, mixed with specific diluent and modification reagents. The process consists of two operations: extraction and stripping. In extraction, the metals in the aqueous phase, i.e. leaching liquor, are transferred to the organic phase, where the metals are more soluble into. Following extraction, the extracted metals are recovered from the organic phase to the stripping solution. This technology has been extensively used in the industry for many decades, such as in the metallurgies of copper, rare-earths, and uranium, in cobalt-nickel separation and platinum-group metals refining, for the separation of valuable metals from spent LIBs. For cases where the solution contains multiple metal ions, more than one extractant is commonly employed in order to secure a higher selectivity. Occasionally, to avoid multiple extraction stages due to similar chemical characteristics of metal ions, coextraction and coprecipitation processes are adopted simultaneously. Despite its low power dissipation, high extractant selectivity, quality extraction effect, and easy working conditions, the expensive extractant values make the application in industry costly [66,67,69].

Despite being a very promising technology, implemented hydrometallurgical processes are still scarce amongst recycling plants. Duesenfeld, a Germany based company, developed a recycling process aiming for the recovery of nearly all valuable materials of a battery system. Figure 21 displays a scheme of its process.

The process begins with the discharging of large battery packs followed by disassembling, where components such as screws, cables, tray, housing, battery management system, etc, are manually separated and fed to established recycling routes. Afterwards, there are two comminution steps. After the first one, there is a separation of any heavy parts and a drying step to remove the remaining components of the electrolyte. Here, all the vaporized solvents can be recovered by condensation or combusted via thermal post-combustion process which regains the thermal energy. The second comminution stage aids the following separation of plastics, Al, Cu, or separators from the black mass. Next, the black mass undergoes a leaching process, where graphite can be filtered and separated. Graphite aside, the leaching liquor undergoes either a precipitation step or a cementation step, to get

rid of any Cu contamination. This is followed by another purifying operation, oxidation and precipitation, resulting in the precipitation of any Al, Fe, or Ti. Finally, Ni and Co are removed through solvent extraction. Mn is obtained either by solvent extraction or precipitation, and, lastly, Li by precipitation. [6,70,71].

The main advantage of the hydrometallurgical process is the possibility of producing new battery precursors from the waste with sufficient purity. It is also more versatile regarding the variation of the feed materials resulting from the evolution of the cathode chemistries. Despite the large demand for chemical reagents, the possibility of extended use for several years of the chemical reagents and the possibility of re-utilization of several by-products within the same technology, make it possible for minimization of the overall secondary waste generation. Nevertheless, the wastewater produced has negative environmental impacts, if not treated. Having said this, hydrometallurgy seems to be one of the most promising approaches to meet the requirements, but also to create a path to a circular economy in the battery market [3,4].

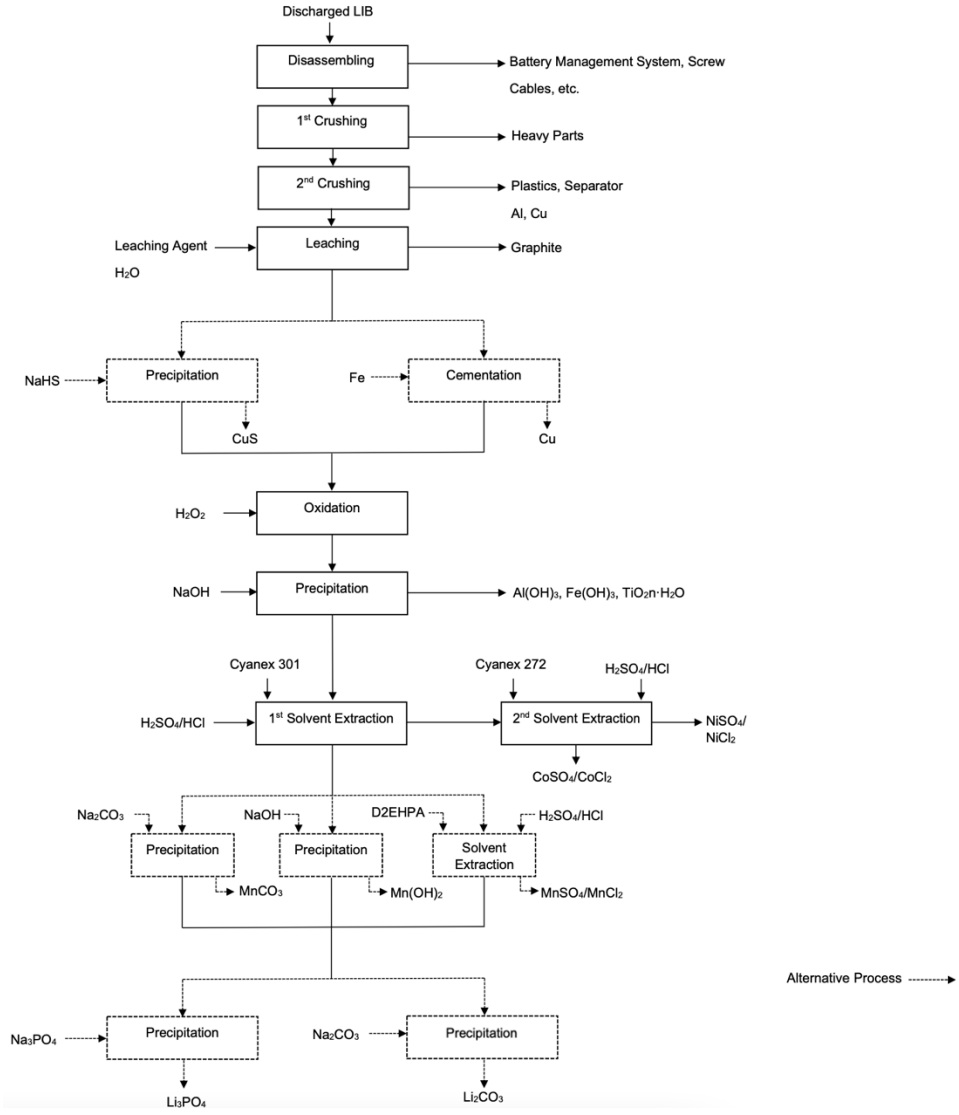

Figure 21 - Schematic representation of Duesenfeld's recycling process.

Chapter 4

Experimental Methodology

In this chapter, the experimental procedures of pre-treating and leaching of LIB waste are disclosed.

After a comprehensive literature review to gather the theoretical background, each operation was developed meticulously, with the overall goal of optimizing the whole process. Figure 22 illustrates all the steps present in the developed process. Discharging, dismantling, and removal of the electrolyte were not objects of study, however, being fundamental operations for the recycling process, it is important to represent them. In order to preserve confidentiality, all car models and battery manufacturers cannot be disclosed.

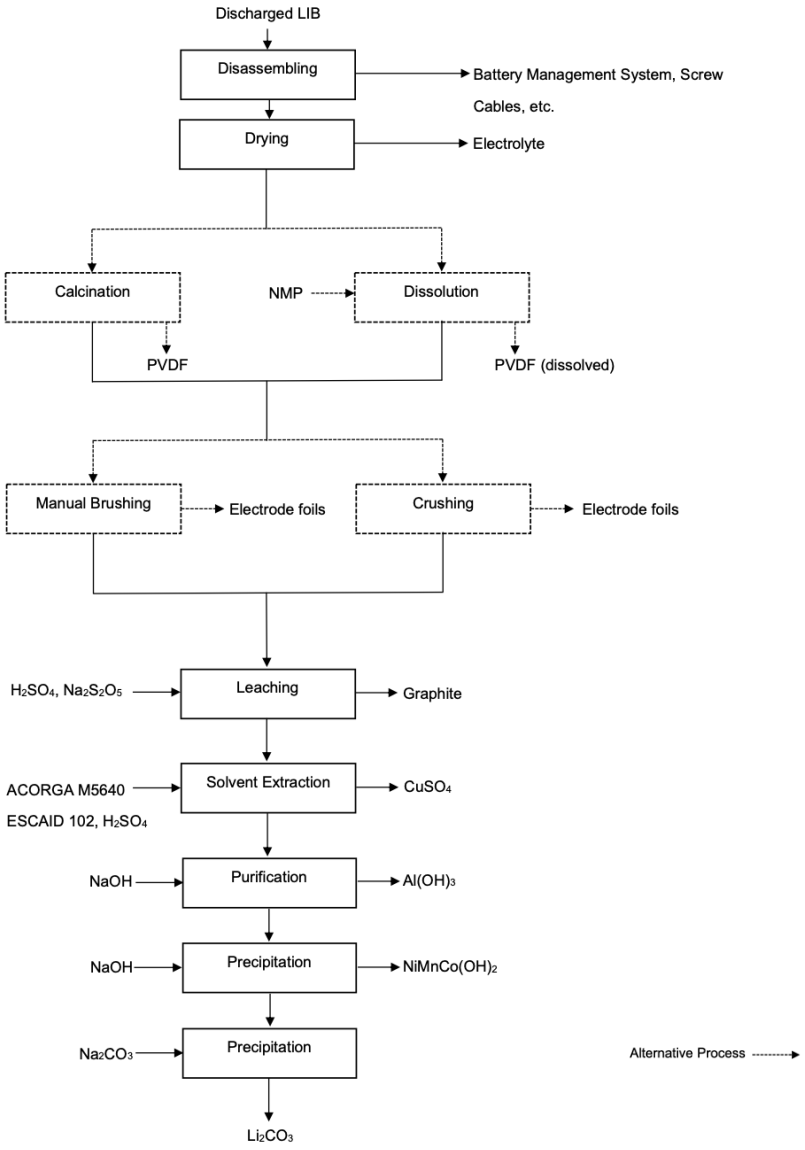

Figure 22 - Schematic representation of the overall experimental methodology.

The process began with two different NMC LIB cells already discharged, dismantled, and dried, i.e. free of electrolyte, designated as Cell 5 and Cell 7. To start this operation, two starting scenarios were tested: one where the separation of the electrode from the foil was done via heat treatment, and another where the separation was done using a dissolution process, each one tested at two different temperatures during two time steps. The most successful operation was chosen, and the process proceeded to the mechanical treatment. Here, two methods were analysed. Following mechanical treatment, the resulting black mass was chemically processed. The leaching was conducted using an inorganic acid, H_2SO_4, as the leaching agent and sodium metabisulfite ($Na_2S_2O_5$) as the reducing agent. Time, temperature, liquid/solid ratio, reducer, and acid concentration were the test parameters used to achieve the main goal, optimizing the whole process. Lastly, all the metals were extracted from the leaching liquor via solvent extraction and precipitation.

4.1. Material

The spent LIB packs were provided by Valorcar and discharged and dismantled in Ambigroup and Palmiresíduos, two recycling plants in Portugal, in light of the project a Study Strategy for Treating Lithium-ion Batteries.

All of the chemicals used in this work were of p.a. purity and were kindly supported by Laboratório Nacional de Energia e Geologia (LNEG), where all of the experimental procedures were developed.

4.2. Pre-treatment

4.2.1. Thermal Treatment

Separating the electrode active material from the foil is seen as a crucial step in order to maximize efficiency in the leaching process.

This stage starts by cutting small squares from the cathode and anode (with approximate dimensions of 3.5 x 3.5 cm, which are then weighed and placed in crucibles to be thermally treated in a *Carbolite* muffle. During calcination, in the temperature range of 400-500 ºC, carbon and organic materials are removed, together with the PVDF binder, which evaporates at temperatures between 250-350 ºC [72], reducing the adherence of the active materials from the foils. With the above values in mind, two temperatures were studied, namely 400 ºC and 500 ºC, for 1 and 5 hours. Here, the cathodes and anodes from each cell were tested separately. Figure 23 displays each step in the thermal treatment procedure.

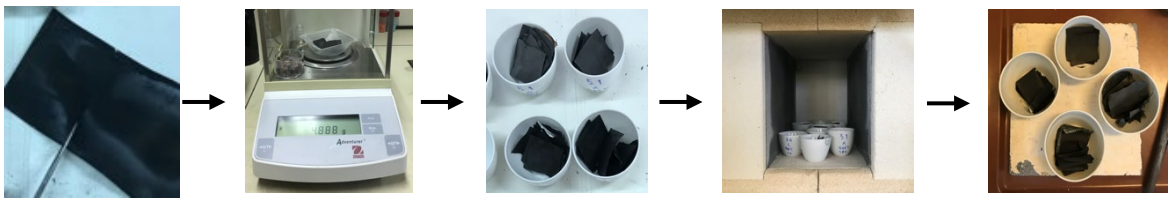

Figure 23 - Schematic representation of the thermal treatment procedure.

4.2.2. Dissolution Process

As explained in the previous chapter, there are various methods for separating the electrode active material from the foil. Dissolution is one alternative where an organic solvent is used to dissolve the binder.

Similar to the beginning of the thermal treatment, the electrodes are cut into small squares and weighed. After that, a certain volume of N-methyl-2-pyrrolidone (NMP) was measured and mixed with the cut electrode squares in a round glass reactor with cover. As in He's work [73], the solid/liquid ratio used was 1:10 g/mL. The glass reactor was inserted in a temperature-controlled oven from *Cassel* with orbital agitation (120 rpm) for a specific amount of time. The temperatures studied were 25 and 90 ºC, for 1 and 2 hours. Afterwards, the solution was filtered, and the filtered solids (active material) were dried in an oven at 55 ºC. Along with these studies, another dissolution process was done using an ultrasonic bath from *Fritsch Laborette* at room temperature for 1 hour. Figure 24 summarizes the dissolution process.

In every experiment, the cathodes and anodes from each cell were treated separately.

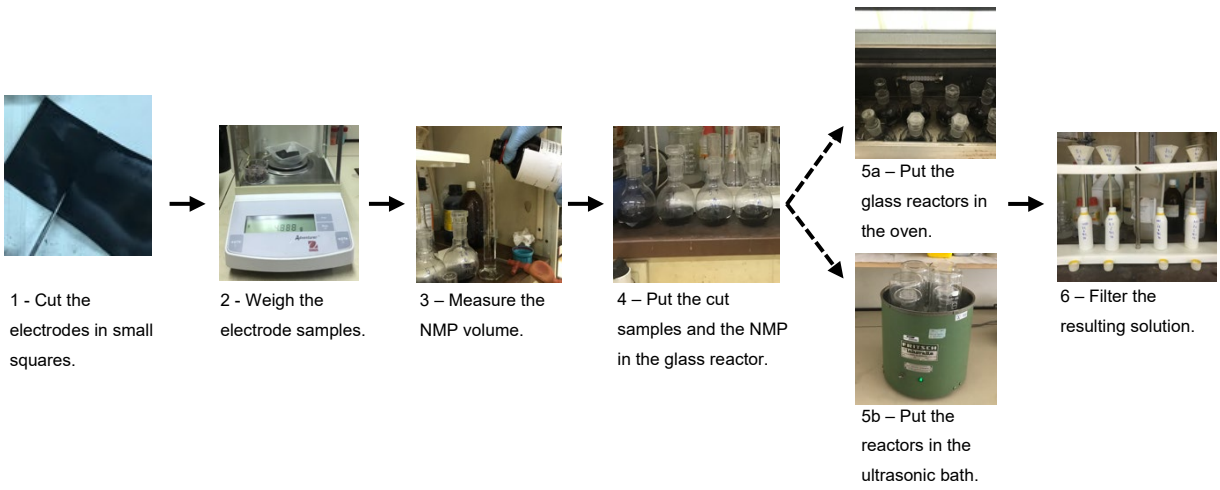

Figure 24 - Schematic representation of the dissolution process.

4.2.3. Mechanical Treatment

After removing the PVDF binder, two different mechanical treatments were done: manual brushing and crushing.

To assess which binder removal process was more efficient, the electrode mass was weighed and manual brushing of each electrode square was done. In the end, the final mass of the separated individual parts (foil and powder) was also documented. Figure 25 illustrates the manual brushing method.

1 - Weigh the electrode samples.

2 – Brush off the electrode powder from the foil.

3 – Weigh the separated individual parts.

Figure 25 - Schematic representation of the manual brushing method.

With the more efficient PVDF removal process determined, a weighed amount of mixed binder-free material (both anode and cathode) was crushed twice in a *Retsch SM2000* cutting mill and sieved through fifteen sieves with a mesh of the standard ISO 3310-1 in a *Retsch* vibratory sieve shaker, for 10 minutes. Simultaneously, to test the significance of the binder removing step, a batch of non-treated electrodes was also crushed and sieved. Each sieve content was registered, individually stored, and analysed to understand where the bulk of the active material was found, i.e. chose the sieve that divides the crushed material into two fractions, the electrode dust reach one and the one with excess scrap metal from the conducting Al and Cu foils. Figure 26 depicts the crushing process. Here, in order to simulate a more accurate industrial process, the crushed electrodes originated from both battery cells.

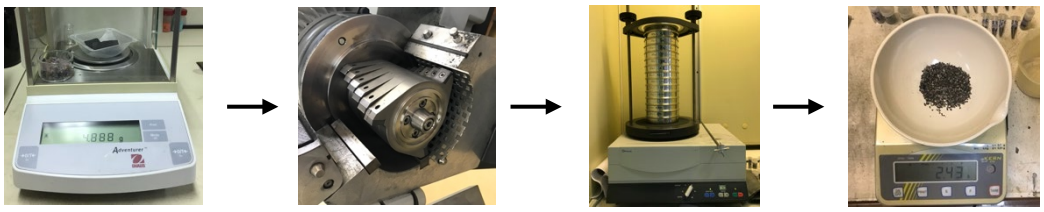

1 – Weigh the electrode samples.

2 – Crush the electrode samples.

3 – Sieve the crushed material.

4 – Weigh the sieved material.

Figure 26 - Schematic representation of the crushing process.

4.3. Characterization

Inductively Coupled Plasma-Atomic Emission Spectometry (ICP) and Atomic Absorption Spectrometry (AAS), using *Thermo Elemental Solar 969*, were employed to determine the metal concentration in the leaching liquor and pre-treated samples. In preparation for this technique, the samples of the pre-treated material were dissolved by digestion in aqua regia (a mixture of hydrochloric acid and nitric acid, in volume ratio 3:1) in a hot plate near boiling for 2 hours. Each sample was diluted and analysed with ICP or AAS, with the resulting measurement used for calculations of metals recovery. Typically, in hydrometallurgical laboratory tests the precision of the results (solution concentrations and solid contents, yields, and efficiencies) can be generally assumed to be 3-5% (relative error), including the uncertainties of metal analysis and other experimental procedures. Errors can be higher due to heterogeneity of solid samples.

Microscopic morphology and chemical composition of surface elements were characterised with Scanning Electron Microscopy (SEM), using *S2400 Hitachi* and *Phenom ProX G6*, and Field Emission Gun Scanning Electron Microscope (FEG-SEM), using *JEOL JSM-7001F*, with Energy Dispersive Spectroscopy (EDS). Before analysing, the samples were coated with Au and Pd.

X-ray diffraction patterns of the powders were acquired with X-Ray Powder Diffraction (XRPD), using *Panalytical X'pert Pro*. Cu Kα radiation was used to identify the phases in the cathodic and anodic powders with a step size of 2Θ=0.033º and an acquisition time of approximately 50 seconds. Phase identification was carried out using *X'Pert HighScore Plus*.

4.4. Acid Leaching

Acid leaching plays a significant role in the metal recovery process. Here, metallic components of the spent active material are dissolved as ions into the leaching solution. Therefore, optimization of acid leaching is of the utmost importance in assuring maximum efficiency in the subsequent metal separation step.

The acid leaching experiments can be divided into three parts. The first one, where the influence of the thermal treatment conditions in the leaching efficiency was studied. A second one, where the reducing behaviour of both electrode foils, was, independently and simultaneously, investigated. And, lastly, a third one, where the variation of four different factors was explored.

The effects of four different factors on Co, Ni, Li, and Mn leaching efficiency were investigated using a Factorial Design Experiment (FDE) methodology. The studied parameters were acid concentration, temperature, time, and liquid/solid ratio. The chosen leaching and reducing agents were H_2SO_4 and $Na_2S_2O_5$, respectively.

For the two first sets of experiments, the cathodic powder was obtained from the manual brushing step. In the last experiment, the cathode powder came from the grinding of the two different cells electrodes. To attain a well-distributed sample, the resulting crushed cathode powder was divided into two fractions using a Jones riffle splitter from *Minerais & Métaux* (Figure 27.1), and then, from each fraction, sixteen samples of 12 g of cathode powder each were obtained using a *Spinning Riffler* from *Microscal Ltd* (Figure 27.2). Figure 27 exemplifies the sample preparation process.

1 – Divide the crushed cathode powder into two fractions.

2 – Divide the fractions into sixteen 12g samples.

Figure 27 - Schematic representation of the sample preparation process.

Experiments were done using round glass reactors that were put in a temperature-controlled oven from *Cassel* with orbital agitation (120 rpm) for a specific amount of time.

For each experiment, the prepared solution was added to the round glass reactors and placed in the pre-heated temperature-controlled oven. After the solution has warmed up to the desired temperature, a weighed amount of cathodic powder was added. For the first two sets of experiments, 3-4 mL samples were taken from the glass reactor after 30 and 120 minutes, centrifuged, and a precise volume of clean leaching liqueur was diluted with water in a 20 mL round flask. To calculate the leaching efficiency, these diluted samples were then analysed with AAS. For the last set of experiments, the samples were taken after 15, 30, 60, and 120 minutes. Figure 28 outlines the complete leaching experiment.

After every experiment, the resulting leaching liqueur was filtered. The obtained residue was dried and, in specific cases, analysed with XRPD.

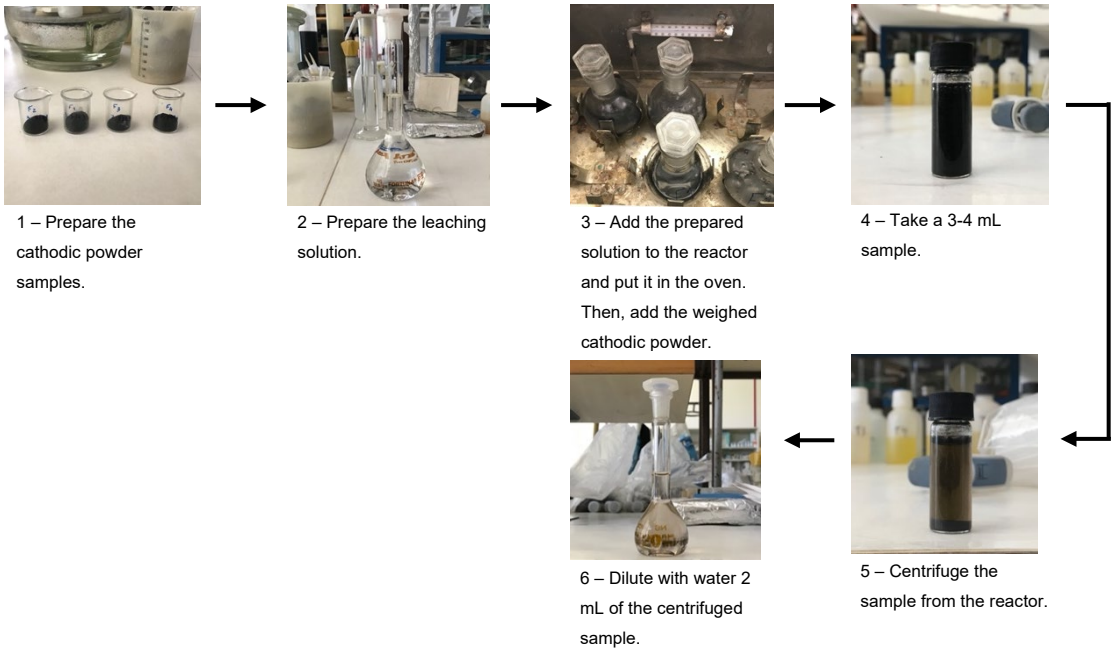

Figure 28 - Schematic representation of the leaching experiment.

4.5. Metal Separation

After leaching, the resultant metal-rich liquor is not only full of the desired metals, i.e. the cathode components, but also with some contaminants, namely Cu and Al. And so, a preliminary purification step is needed. As precipitation depends on the different solubilities of metal components at a certain pH value, and some metals precipitate at close pH values, thus contaminating the resulting precipitate, two techniques were used for this final stage of the metal recovery process: solvent extraction and chemical precipitation.

Solvent extraction was used for separating Cu from the leaching solution. The extractant used was composed of a 20% v/v of ACORGA M5640 (a combination of 5-nonylsalicylaldoxime and 2,4,4-trimethyl-1,3-pentanediol diisobutyrate), the trade name of the organic compound produced by *Solvay*, diluted in ESCAID 102, a commercial diluent with approximately 14% of aromatic content,

according to the solvent's brochure. The process started by mixing the extractant with the feed solution using a separating funnel, at an organic/aqueous volume ratio (O/A) of 1/1, stirred in an orbital shaker for 15 minutes. The phases were allowed to separate and the depleted aqueous solution, i.e. raffinate, was then filtered, so as to assure that no extractant remains in the raffinate, and put aside for the following recovery steps. The Cu was stripped from the organic phase using a solution of 3 M H_2SO_4, with the same procedure used in the extraction step. The resulting aqueous solution, loaded with Cu, was evaporated until crystallization of $CuSO_4$ occurred. The crystallized Cu was then filtered, washed with acetone, and dried in an oven at 55 ºC for 24h. Figure 29 displays the stripping of the Cu from the organic phase.

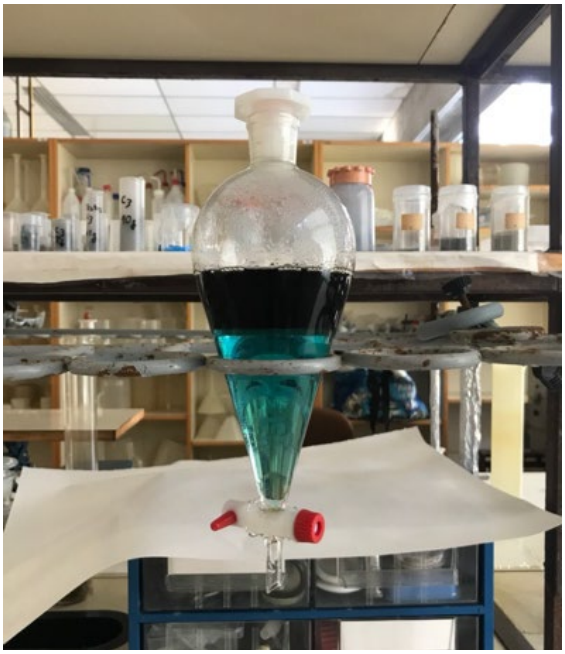

Figure 29 - Stripping of the Cu from the organic phase.

Al, Li, Co, Mn, and Ni were separated using chemical precipitation. To adjust the pH value (measured with a glass combined electrode connected in a pH meter by *Hanna Instruments*) the precipitant used was a solution of 4M of NaOH. The neutralization and precipitation was carried out at room temperature in a glass cylindrical reactor with an overhead stirrer provided with a two-blade impeller, as seen in Figure 30. Al precipitated first and then filtered washed with demineralized water and dried in an oven at 55 ºC for 24h. The purified resulting solution was again neutralized at higher pH values in order to obtain a mixed precipitate of Ni, Co, and Mn. As in the previous precipitation, the obtained precipitate was also filtered, washed with demineralized water, and dried in an oven at 55 ºC for 24 hours. To end, the resulting Li-rich solution was evaporated in a hotplate and then a solution of 2.5 M sodium carbonate (Na_2CO_3) was added to precipitate lithium carbonate. The precipitate attained at this stage was too filtered, washed with a saturated solution of Li_2CO_3 (to avoid the use of water, which would re-dissolve the lithium precipitate), and dried in an oven at 55 ºC for 24h.

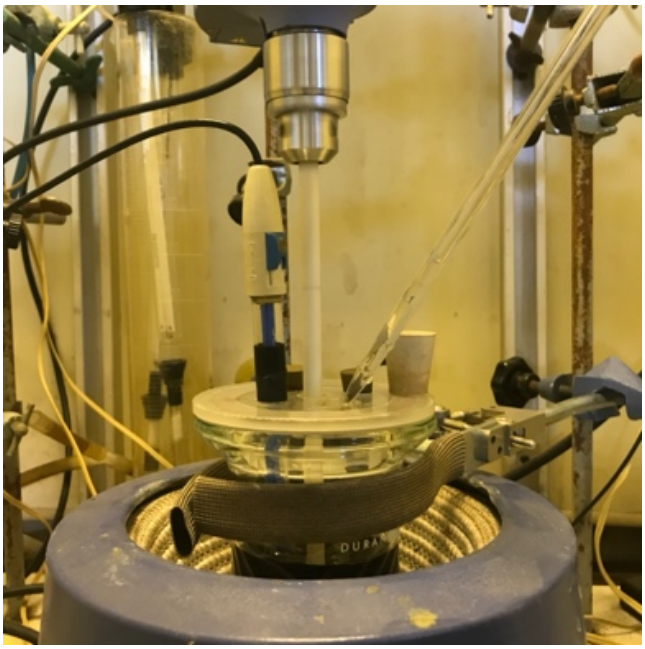

Figure 30 - Precipitation of Ni, Mn, and Co via neutralization of the purified solution with 4M NaOH.

Chapter 5

Results and Discussion

5.1. Pre-Treatment

The elemental chemical analysis of the electrode material (complete foils with powder active material) used in this section, obtained by ICP analysis, is shown in Table 2.

Table 2 - Sample characterization of the spent LIB electrodes from cell 5 and 7 after drying.

	Elemental Composition / wt%					
	Li	Ni	Mn	Co	Al	Cu
Cathode 5	5.0	19.7	15	19.7	6.9	-
Cathode 7	6.0	21.1	17.5	21.1	17.8	-
Anode 5	0.3	-	-	-	-	32.3
Anode 7	0.5	-	-	-	-	29.6

Using equation (4) and the values from Table 2, the molar fractions of each element can be calculated. For cell 5, Ni, Mn, and Co molar proportions were found to be 33,54%, 27,23%, and 30,40%, respectively. For cell 7, Ni, Mn, and Co molar proportions were 35,98%, 31,85% and 33,57%, respectively. These results are in concordance with the theoretic formula for the NMC cell exhibited in equation (5).

$$Molar\ fraction = \left(\frac{wt\%}{Molar\ Mass}\right) \times 100 \quad (4)$$

$$NMC = Li(Ni_{0.3}Mn_{0.3}Co_{0.3})O_2 \quad (5)$$

The variation of the aluminium content seen in Table 2 can be justified by the difference of the foil thickness of the two cells analysed. The Li content in the anode can be related with the content of some electrolyte salt or, alternatively, with some residual Li intercalated in the graphite structure.

5.1.1. Thermal Treatment

During calcination, both electrodes were treated as explained in Chapter 4. Figure 31 summarizes the weight loss throughout the process. It is possible to observe a tendency for an increase in weight loss with the increase in temperature and exposure time. This said, the same is not true for cell 5 and 7 at 400 ºC. One explanation for this phenomenon is that the binder can reach its removal maximum after 1 hour at 400 ºC, thus not showing any weight loss after 5 hours.

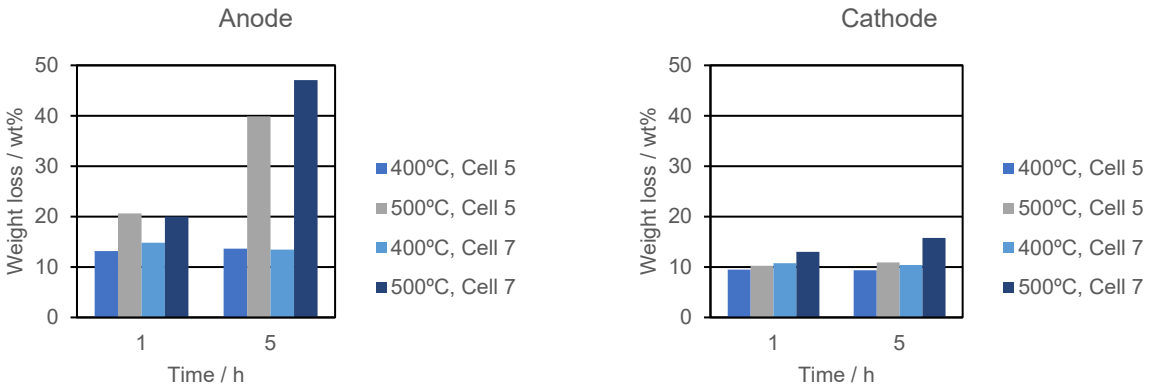

Figure 31 - Weight loss of electrodes over time during calcination.

For both electrodes, 500 ºC for 5 hours registers the highest weight loss, as expected. The high weight losses in the anodes might be linked to the partial decomposition of the graphite.

The anode foils turn extremely brittle after the calcination treatment, as portrayed in Figure 32. This sudden change of behaviour from the material might be justified by the occurrence of Cu oxides on the surface of the electrode material during calcination. As stated by Cástrejon-Sánchez et al. [74], for temperatures above 400 ºC, calcination promotes the growth of a passivating copper oxide layer composed of Melaconite (CuO) and Cuprite (Cu_2O).

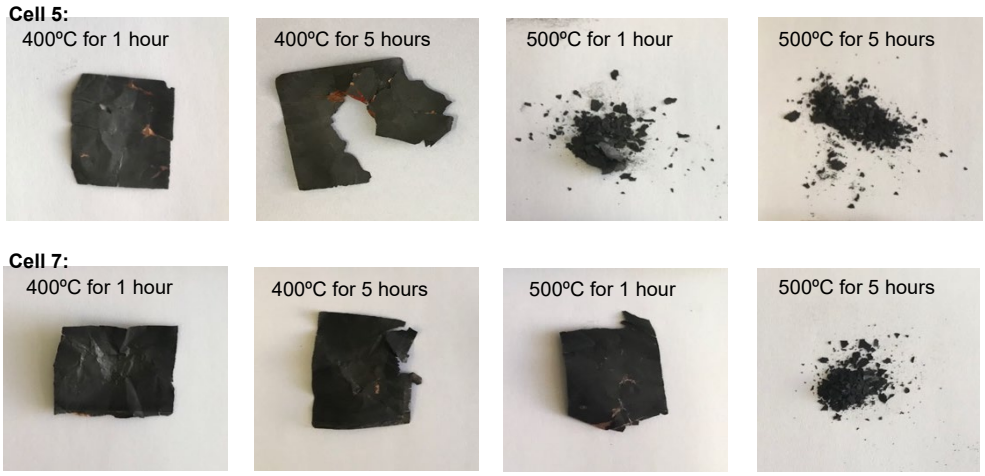

Figure 32 - Anode foils appearance evolution after calcination at 400 ºC and 500 ºC.

To confirm this hypothesis, XRPD was performed in each anode sample to identify the phases present in the anode powder. Four results were selected and are presented in Figure 33, namely

calcination at 400 ºC during 5 hours for both cells and calcination at 500 ºC during 1 and 5 hours for cells 7 and 5, respectively. From the diffractograms, besides de presence of graphite, it is possible to confirm the appearance of Cu oxides between in the higher calcination temperatures. This said, it is important to highlight that identification of the phases is not completely precise due to limitations of the technique.

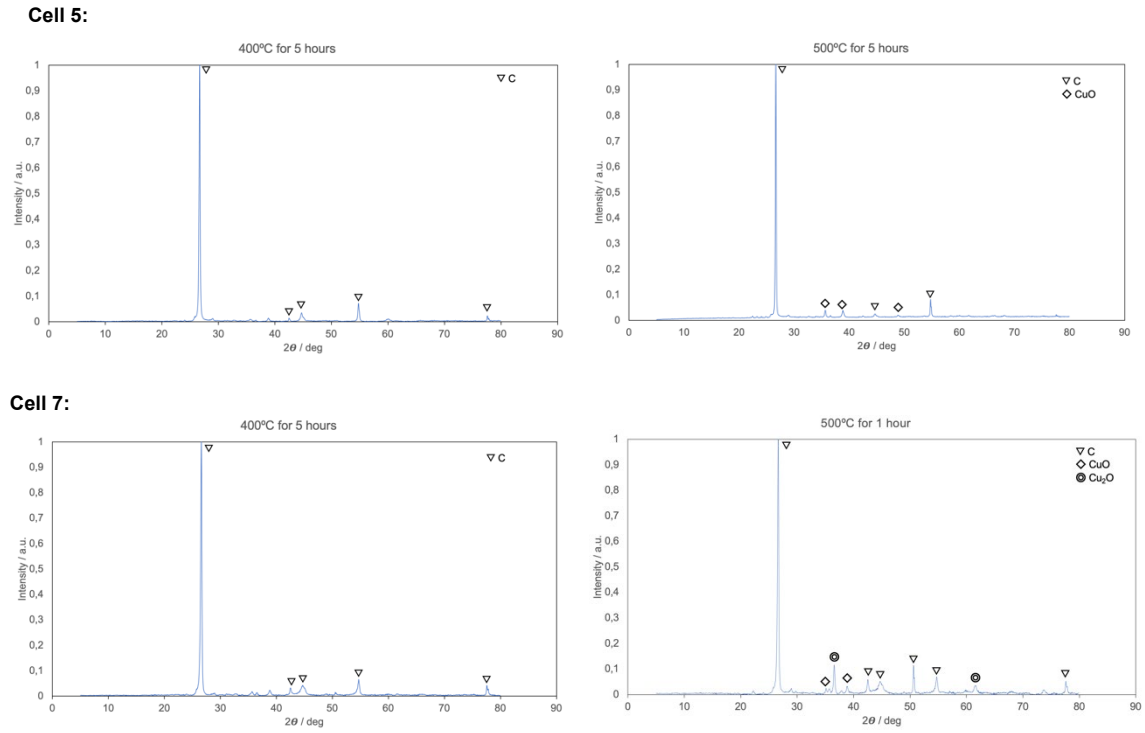

Figure 33 - Resulting diffractograms from the x-ray powder diffraction of the anode powder.

The cathode electrodes were also analysed by XRPD to confirm that no alterations arose during the calcination treatment. The presented results are from the calcination of cells 5 and 7 at 500 ºC for 5 hours. In Figure 34 the peaks identified corresponded to $Li(NiMnCo)O_2$. These results are in concordance with the results of the x-ray diffraction found in [75].

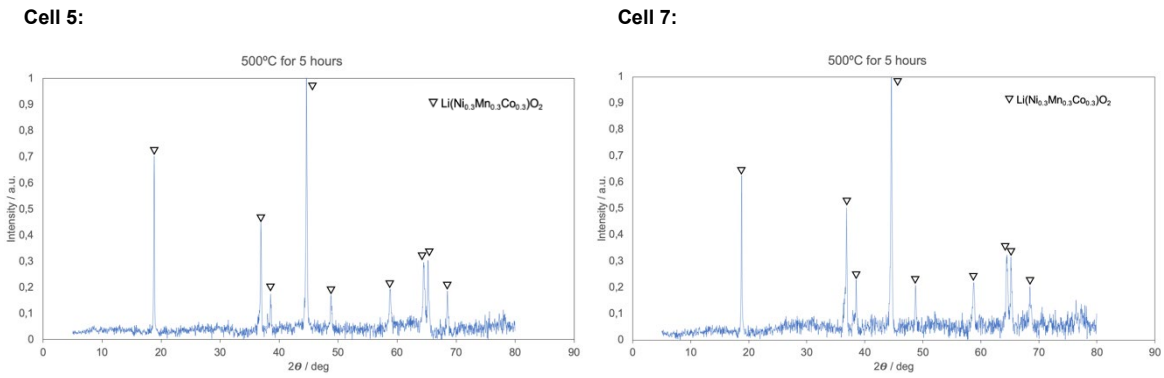

Figure 34 - Resulting diffractograms from the x-ray powder diffraction of the cathode powder.

SEM and EDS analyses were also conducted in the calcinated samples. The EDS results of the anode powder, available in Figure 35, revealed the presence of oxygen. This discovery also supports the claim of possible oxidation of the Cu foil during calcination. The appearance of fluorine in the second spectrum highlights the (even if small) remains of PVDF, maintaining aggregation between particles, or electrolyte salt. Au and Pd are used to convert the sample into a conductive one, and so have nothing to do with the sample itself.

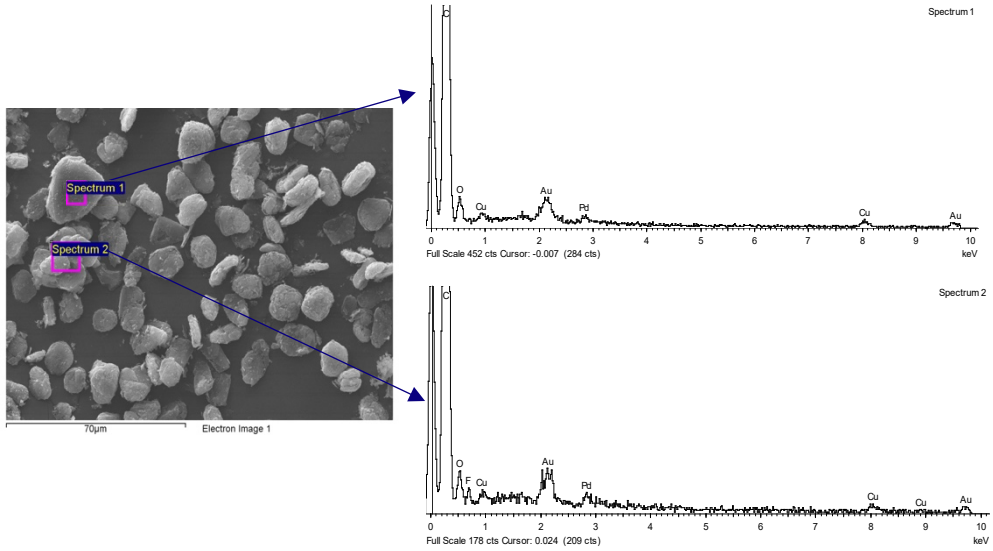

Figure 35 - SEM and EDS analysis of cell 5 anode powder after calcination at 500 ºC for 1 hour.

For the cathode samples, the SEM and EDS analysis, Figure 36, also revealed the presence of oxygen, which can be traced back to either oxidation of Al or $Li(NiMnCo)O_2$. The fluorine presence in the EDS, if real, is masked by the Mn L peak.

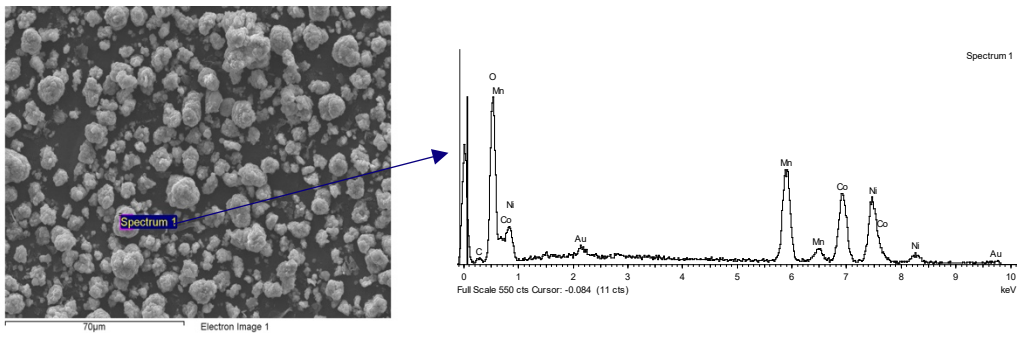

Figure 36 - SEM and EDS analysis of cell 5 cathode powder after calcination at 500 ºC for 1 hour.

SEM analysis of the cathode, Figure 36, displayed a more aggregated sample, with smaller particles, and consequently with non-uniform shapes, whereas for the anode, Figure 35, showed bigger particles, with predominantly rounder shapes, and less agglomerated.

During calcination, the cathode electrodes presented, in most cases, maximum disaggregation in every temperature and exposure time, as disclosed in Figure 37, by manual brushing, revealing an acceptable decomposition of the binder material. The disaggregation of graphite from the anode electrodes was impossible to be studied due to the disaggregation of the supporting copper foils.

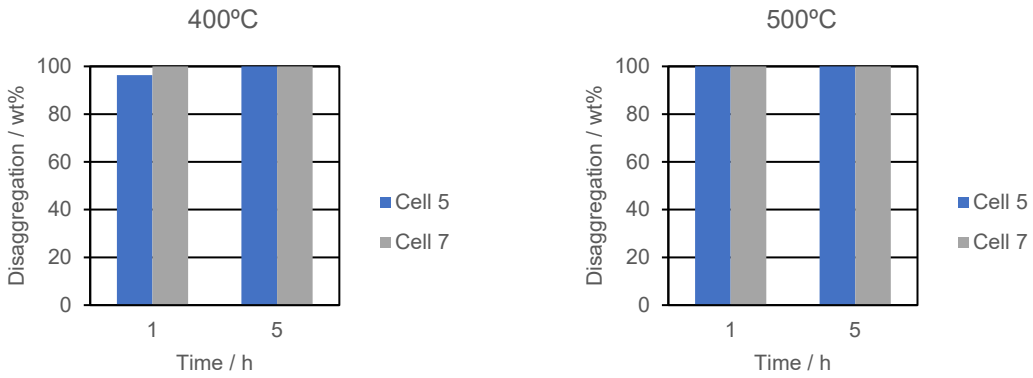

Figure 37 - Percentage of black mass detached from the cathode foil after calcination at two different temperatures.

In this study, a clean electrode foil is considered as presented in Figure 38. Cell 5 after 1h at 400 ºC was the only exception, as can be seen in Figure 38. These results made it possible to determine the percentage of cathode powder and foil for each cell, using equations (6) and (7), respectively. On average, cell 5 is composed of 9.57 ± 0.22 % foil and 90.43 ± 0.22 % powder and cell 7 of 16.65 ± 0.59 % foil and 83.35 ± 0.59 % powder. These results can be compared with the aluminium content determined by chemical analysis of the electrodes (Table 2), assuming that the aluminium present is only coming from the foils. The values are 6.9 and 9.6%, for cell 5, and 17.8 and 16.7% for cell 7, although not being exactly the same, they are in the same order of magnitude.

$$Electrode\ Powder\ \% = \frac{m_{Powder}}{m_{Total}} \times 100 \quad (6)$$

$$Electrode\ foil\ \% = 100 - \left(\frac{m_{Powder}}{m_{Total}} \times 100\right) \quad (7)$$

To further investigate the influence of temperature and exposure time, a leaching test was performed with a sample of each calcination trial (see section 5.2).

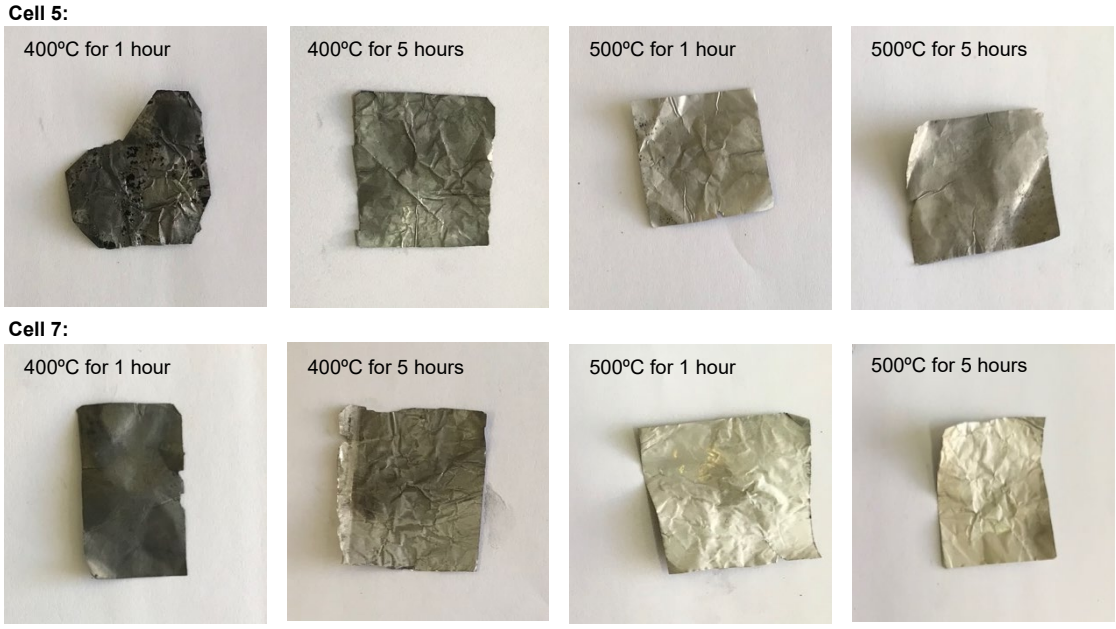

Figure 38 - Calcinated cathodes after manual brushing.

5.1.2. Solvent Dissolution

Here, the PDVF removal process was performed using an organic solvent, NMP, instead of using high temperatures. The results for cathode disaggregation are disclosed in Figure 39 and contemplate the cathode powder released during manual brushing and after filtration of the NMP.

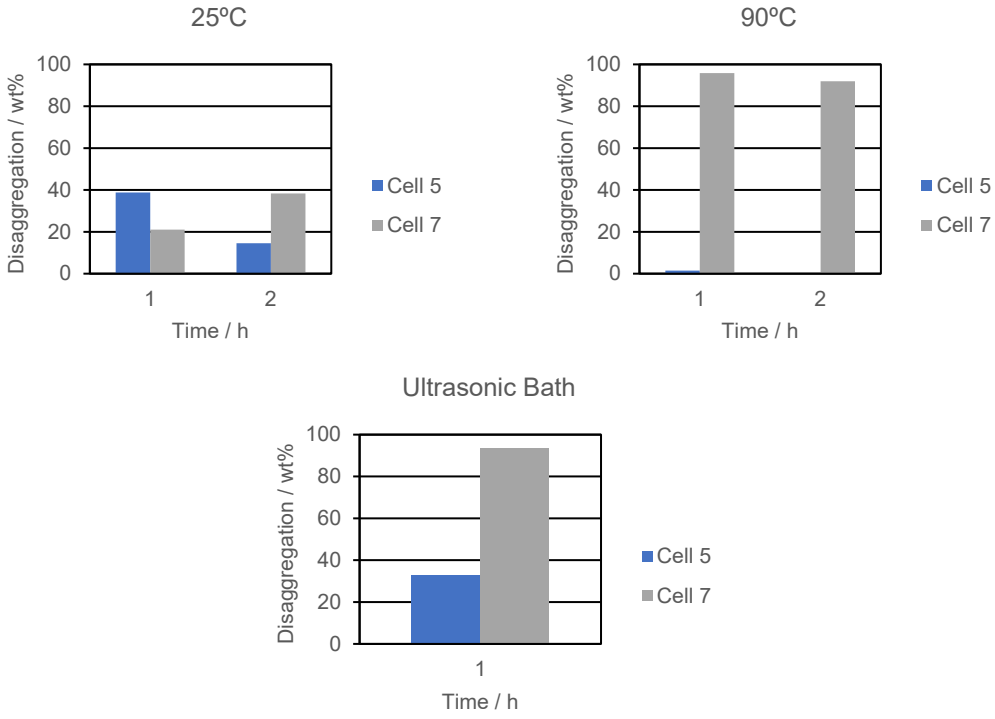

Figure 39 - Percentage of black mass detached from the cathode foils after solvent dissolution.

In the tests varying temperature, cell 7 presents a predictable course, increasing disaggregation with the increase of time and temperature. Cell 5, on the other hand, reveals the opposite, with disaggregation reaching its peak, approximately 39%, at the first stage, 25 ºC after 1 hour.

The results for anode disaggregation are not displayed here, seeing as they were all inferior to 0.5%.

Figure 40 presents the electrode samples after the solvent dissolution process, emphasising the incoherence amongst the results.

Figure 40 - Electrode samples after solvent dissolution and manual brushing.

Some electrodes present signs of degradation. This may be due to some chemical reaction that results in the formation of organic compounds with the NMP. This said, nothing unusual appeared in the XRPD diffractograms.

The majority of the electrode powder detached during solvent dissolution is released into the solvent. As the electrode powder is ultra-fine, the filtration process became difficult and with some losses.

With the intention of understanding if the solvent dissolution process gave rise to any alteration in the electrode material, each sample was submitted to XRPD analysis.

As it can be seen from the results displayed in Figure 41 and Figure 42, the binder removal process didn't affect the composition of the electrode powder, with the results showing very similar diffractograms for cells 5 and 7, presenting graphite for the anode and Li(NMC)O_2 for the cathode. These cathode results are very similar to the calcinated ones and are also in concordance with the results of the x-ray diffraction found in the literature [75]. In both cases, the anode cell underwent solvent dissolution at 90 ºC for 2 hours, whereas the cathode cells process was done in an ultrasonic bath at room temperature for 1 hour. Once again, it is important to highlight that identification of the phases is not completely precise due to limitations of the technique.

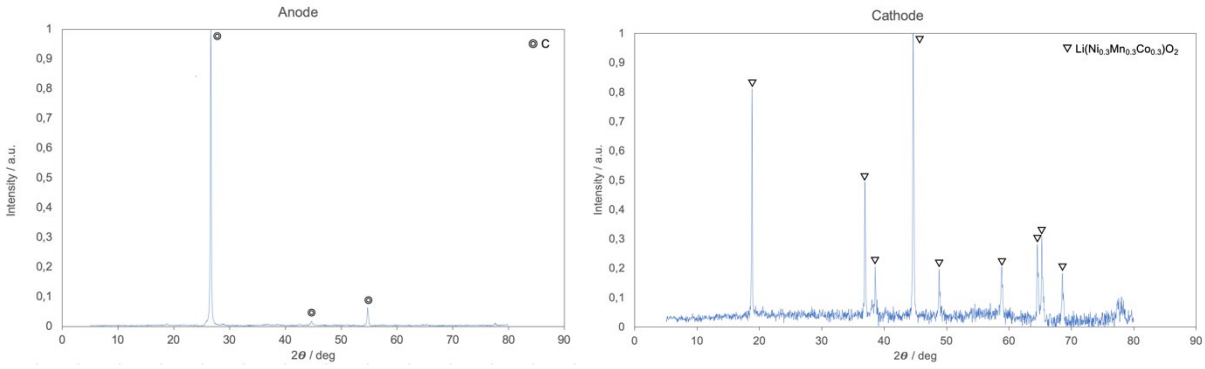

Figure 41 - XRPD diffractogram of cell 5 electrode powders submitted to solvent dissolution with NMP.

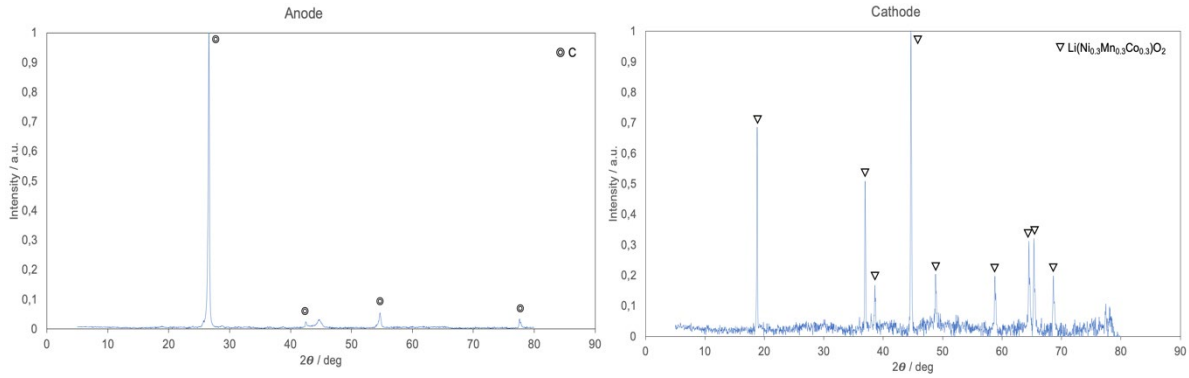

Figure 42 - XRPD diffractogram of cell 7 electrode powders submitted to solvent dissolution with NMP.

The SEM and EDS results for both cells, Figure 43 and Figure 44, showed a poorly dispersed sample, with bigger aggregates when compared with the calcinated samples (see Figure 35 and Figure 36), with traces of phosphorus from the electrolyte ($LiPF_6$) and fluorine from the PVDF binder or the electrolyte. For cell 7, the SEM images portrait a more dispersed sample, as was expected given the disaggregation results presented in Figure 39, and not much difference between particle sizes. In both Figure 43 and 44 the anodes present bigger particle sizes. Each sample in Figure 43 underwent solvent dissolution at 90 ºC for 2 hours, whereas for Figure 44 the parameters used were 25 ºC for 1 hour, seeing as they were one of the few conditions where disaggregation was more efficient.

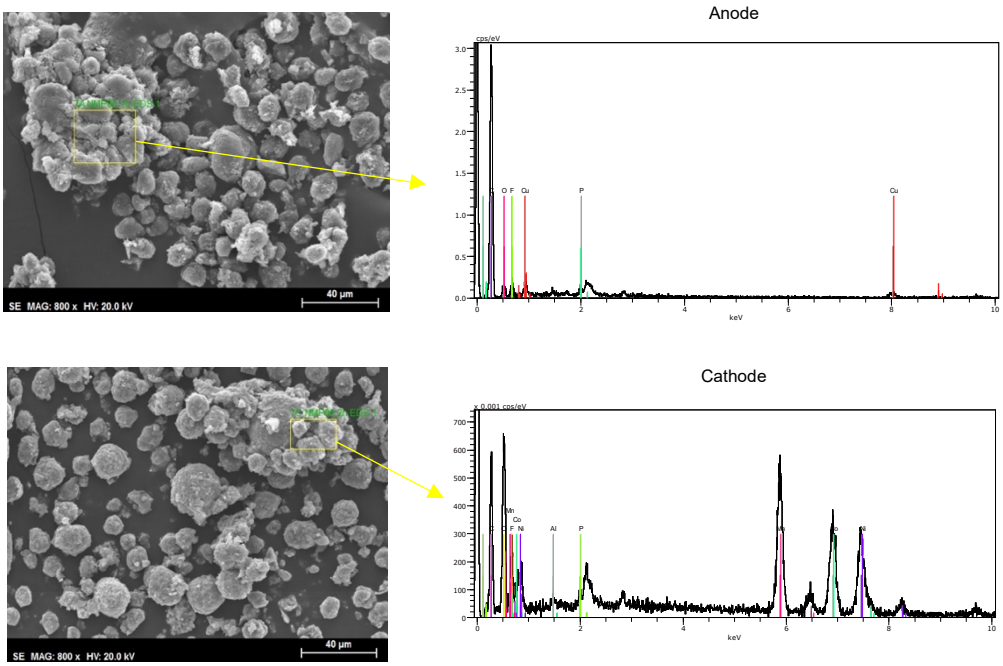

Figure 43 - SEM and EDS analysis of cell 7 electrode powders after solvent dissolution at 90 ºC for 2 hours

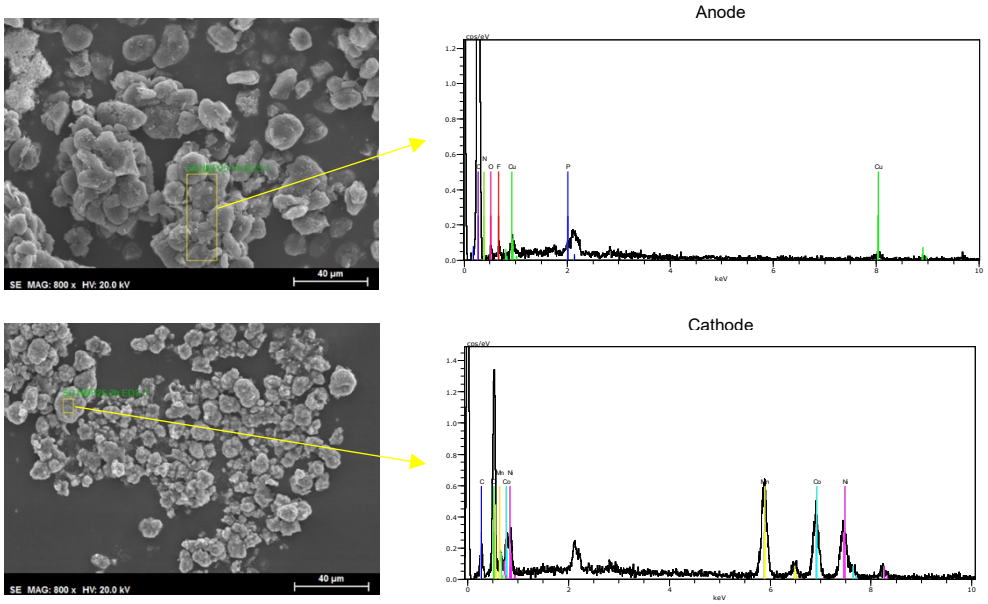

Figure 44 - SEM and EDS analysis of cell 5 electrode powders after solvent dissolution at 25 ºC for 1 hour.

After careful consideration, bearing in mind the disconnection between the poor disaggregation results and the losses during the filtering process, the pre-treatment selected for the subsequent leaching study operation was the thermal treatment.

5.2. Impact of calcination in the leaching behaviour

To study the effect that the calcination conditions have in the leaching behaviour of the metals present in the cathode material, the powder obtained in each thermal treatment, i.e. detached from the foil, was leached with 2M H_2SO_4, 0.25 M $Na_2S_2O_5$, at 60 ºC, 120 rpm, and with a liquid/solid ratio of 5 L/kg, for 2 hours. As explained in the previous chapter, a sample was taken at the first 30 minutes and in the end and analysed with ICP. The ICP analysis enabled the calculation of the leaching yield in percentage using (8):

$$\eta = \left(\frac{C_i \times V}{m \times wt\%}\right) \times 100 \quad (8)$$

where C_i is the metal concentration in the leachate at time i, V is the volume of the solution, m is the initial mass of solid, and *wt%* is the initial mass fraction of the metal in the spent LIB. The results are presented in Figure 45.

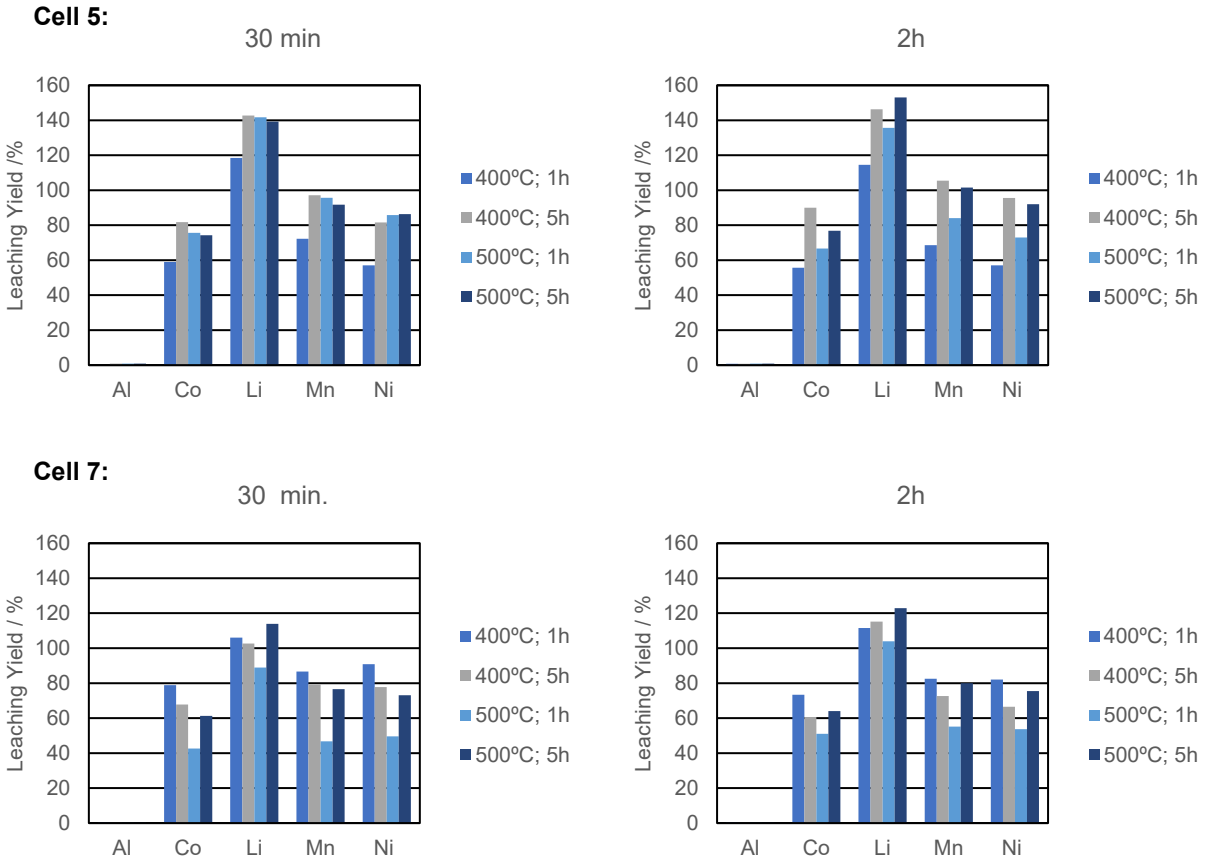

Figure 45 - Leaching yield of each metal from the calcinated cathode powder using 2M H_2SO_4, 0.25 M $Na_2S_2O_5$, at 60 ºC, L/S=5 L/kg, and 120 rpm, during 30 minutes or 2 hours of leaching.

From the results, the first observation is that the reaction is fast and at the time of the first sample, 30 minutes, the results are very close to those obtained at the end of the leaching experiment, with some subtle differences.

As an ion with higher mobility, Li is more easily removed from the solid structure and therefore has the highest leaching yields of all the metals at each time in both cells. Electrolyte salts, if any, might also be contributing to the high leaching yields due to their high solubility. Al, being a contaminant, if present would be at small yields, which is the case (less than 1%).

400 ºC for 1 hour is the condition that presents the worst results for cell 5. 500 ºC for 30 minutes presents the worst leaching yields for cell 7, and for cell 5 the results are also lower than for 5 hours at both temperatures. This, allied to the fact that, as previously stated, at higher temperatures for longer periods the calcinated anode samples start to oxidize, hampering the separation of the powder from the foil and contaminating it with Cu, calcination at 400 ºC for 5 hours was the pre-treatment selected for the subsequent leaching experiments.

The leaching yields higher than 100% are attributed to experimental errors and also to the fact that the yields were calculated using an average initial metal content, and the samples used in each test can have variable contents due to heterogeneity of the materials, despite all the caution taken in sampling procedures. The only value that seems to be outside the reasonable experimental dispersion is the Li yields for Cell 5 at 30 minutes, with leaching yields up to 140%. This phenomenon may be attributed to unexpected sources of lithium in the sample such as lithium salts (remaining in the solids after evaporation of the electrolyte), not accounted in the Li content due to possible segregation to the edges of the foils during the evaporation. Contamination of Li-ions from the anode might also provide additional Li content.

5.3. Impact of the presence of reducer in the leaching behaviour

In this section of the work, the performance of the reducer during the leaching process was evaluated. The reducers tested were $Na_2S_2O_5$, Al foil, and Cu foil. The idea behind these tests was to evaluate if the foils can (or not) have a reductive effect in the leaching of the metals from the cathode. In order to do so, six different leaching tests were done on a detached cathode powder sample after calcination at 400 ºC for 5 hours of each cell. The L/S ratio was set at 5 L/kg, the leaching temperature at 60 ºC, the $Na_2S_2O_5$ concentration at 0.25 M, and the H_2SO_4 concentration at 2M. The amount of added electrode foil (when applicable) was proportional to the quantity of electrode powder, i.e. the foil/powder ratio was 2/8 and 1/9 for cells 7 and 5, respectively. Table 3 resumes the experiments performed with the correspondent parameters.

One of the tested reducing agents was $Na_2S_2O_5$, a white crystalline solid, soluble in water. The general equation that describes the reductive leaching can be written as follows:

$$4LiMO_2(s) + Na_2S_2O_5(aq) + 6H_2SO_4(aq) \leftrightarrow 2Li_2SO_4(aq) + 4MSO_4(aq) + 2NaHSO_4(aq) + 5H_2O(l) \quad (9)$$

where M stands for any of the transition metals present in the electrode powder, i.e. Ni, Mn, or Co.

Table 3 - Leaching parameters for the study on the impact of the presence of reducer in the leaching behaviour. The **X** stands for the presence of the chemical reagent/component as a reducing agent in the leaching process.

	T / ºC	*L/S / L/kg*	*H_2SO_4*	*0.25 M $Na_2S_2O_5$*	*Al foil*	*Cu foil*
Experiment 1	60	5	2 M			
Experiment 2	60	5	2 M		**X**	
Experiment 3	60	5	2 M			**X**
Experiment 4	60	5	2 M		**X**	**X**
Experiment 5	60	5	2 M	**X**	**X**	**X**
Experiment 6	60	5	2 M	**X**		

In addition to $Na_2S_2O_5$, the reducing behaviour of the electrode foils was studied. Equations (10) and (11) describe the reductive leaching for the Al and Cu foils, respectively, where M represents any of the transition metals present in the electrode powder.

$$3LiMO_2(s) + Al(s) + 6H_2SO_4(aq) \leftrightarrow {}^{3}/_{2}\, Li_2SO_4(aq) + 3MSO_4(aq) + {}^{1}/_{2}\, Al_2(SO_4)_3(aq) + 6H_2O(l) \quad (10)$$

$$2LiMO_2(s) + Cu(s) + 4H_2SO_4(aq) \leftrightarrow Li_2SO_4(aq) + 2MSO_4(aq) + CuSO_4(aq) + 4H_2O(l) \quad (11)$$

As in the previous leaching tests, a sample was taken and analysed by ICP, in the first 30 minutes and at the end of leaching. The leaching yield was calculated using equation (8). The results are available in Figure 46.

As in the previous set of experiments, the first sample results show that the reaction is quick, achieving leaching yield values close to the ones obtained at the end of the process. Li continues being the metal with the highest leaching yield, for the same reason as before, being an ion with higher mobility, less bound to the solid structure.

A test using only an acid solution was carried out to evaluate the absence of reducer. Figure 46 reveals that the absence of a reducing agent suppresses the leaching yield results, with the exception of Li, for the same reason given above and because it doesn't change its oxidation state during leaching.

Higher leaching yield values are achieved when using $Na_2S_2O_5$, or a combination of $Na_2S_2O_5$ with the electrode foils. For the second case, the yield increases with time probably because the pulp density increases, due to the presence of the cut electrode foils, and the acid takes more time to take effect.

For cell 5, the worst results were obtained when Cu foil was used as a reducer. Al foil's performance as a reducing agent was more acceptable, revealing increases in the leaching yields, especially in the first 30 minutes, but still inferior to the ones using $Na_2S_2O_5$. This yield gap between Al and Cu wasn't as

pronounced for cell 7. Overall, the difference in results isn't as marked for cell 7 as it is for cell 5. This said, $Na_2S_2O_5$ still maintains its role as a leading reducer.

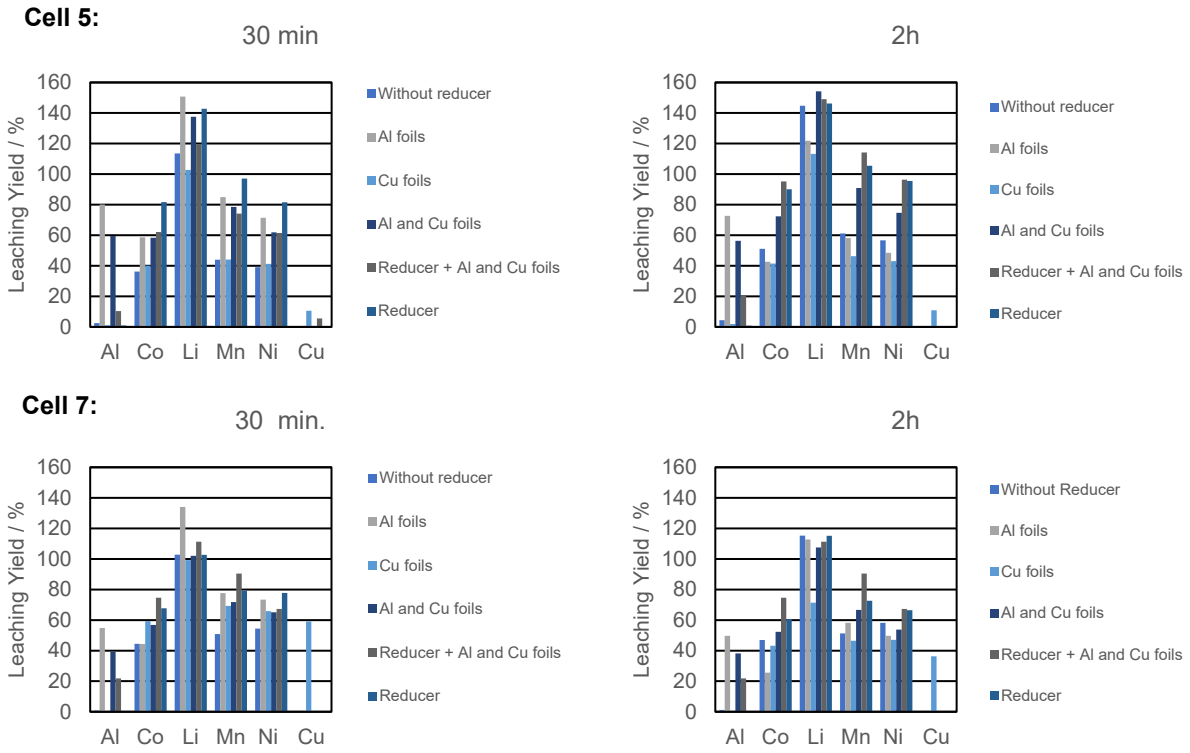

Figure 46 - Leaching yield results of each metal with the different leaching parameters.

5.4. Optimisation of the leaching operation

For the optimisation of the leaching operation, the material used should be as similar as possible to a real fraction of black mass in industrial practice. With the intention of simulating a process of industrial crushing, a mixture of both cells was prepared in the corresponding proportions, i.e. 66.18% of cell 7 and 33.82% of cell 5. These values were obtained using equation (12), where $m_{electrodes\ A}$ and $m_{electrodes\ B}$ are the total mass of the electrodes of cells 5 and 7, respectively. This electrode mixture was used throughout this work.

$$wt\%_{cell\ A} = \frac{m_{electrodes\ A}}{m_{electrodes\ A} + m_{electrodes\ B}} \times 100 \quad (12)$$

5.4.1. Material Preparation

After selecting the more effective pre-treatment, a considerable amount of electrode material was calcinated at 400 ºC for 5 hours and crushed in a cutting mill with a discharge grid of 6 mm. This material

is designated as “pre-treated”. As means of comparing, a weighed amount of non-treated material was also crushed.

Following crushing, the resulted material underwent granulometric distribution using fifteen sieves: 5.66 mm, 4 mm, 2.8 mm, 2 mm, 1.4 mm, 1 mm, 0.71 mm, 0.5 mm, 0.355 mm, 0.25 mm, 0.18 mm, 0.125 mm, 0.09 mm, 0.063 mm, and 0.045 mm.

After crushing the first time, as it is possible to see in Figure 47, the majority of electrode foils that showed signs of disaggregation were cathode foils (aluminium), present in the coarse fractions. By the contrary, the evidence of presence of clean anode foils (copper) was scarce. And so, a second crushing step was introduced for the coarser material, i.e. with a grain size superior to 0.5 mm, in order to increase disaggregation of graphite from the anode foils. In this second step, the same mill was used but with a discharge grid of 2 mm. As in after the first crushing, the resulting material underwent granulometric distribution using the same fifteen meshes.

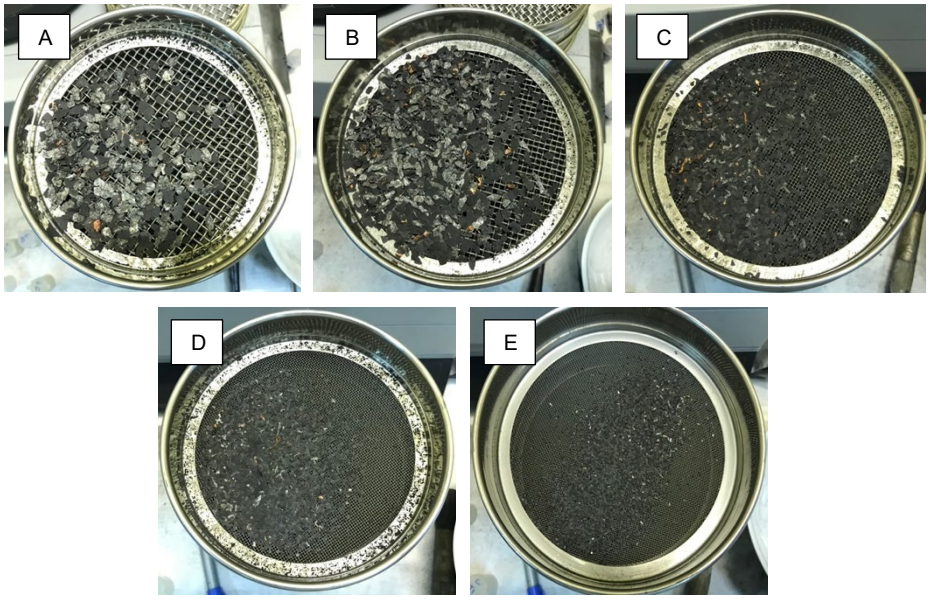

Figure 47 – Pre-treated sieved material after first crushing retained in sieves: a) 2.8 mm; b) 2 mm; c) 1 mm; d) 0.7 mm; e) 0.5 mm.

The resulting cumulative curves for both pre-treated and non-treated samples are displayed in Figure 48. The first conclusion is that the pre-treatment facilitated the disaggregation of the electrode powders, with median percentiles for the pre-treated samples showing that more than 50% of the particles are finer than 0.125 mm and 0.71 mm, for the first and second crushing, respectively. Whereas for the non-treated sample, for the first and second crushing, approximately 50% of the particles were smaller than 0.71 mm and 1.4 mm, respectively. Additionally, it is possible to see that, from the first crushing, more than 20% of the powder is thinner than 0.045 mm, revealing a satisfactory electrode powder release. On the contrary, for the non-treated fraction of material, less than 1% of the powder is thinner than 0.045 mm. Meaning that for the pre-treated sample there is more powder disaggregation, thus emphasizing the importance of the binder removal role in the disaggregation process. Figure 49

also highlights the importance of the binder removal process, revealing poorly disaggregated foils for the non-treated material. There is barely any exposed cathode foil.

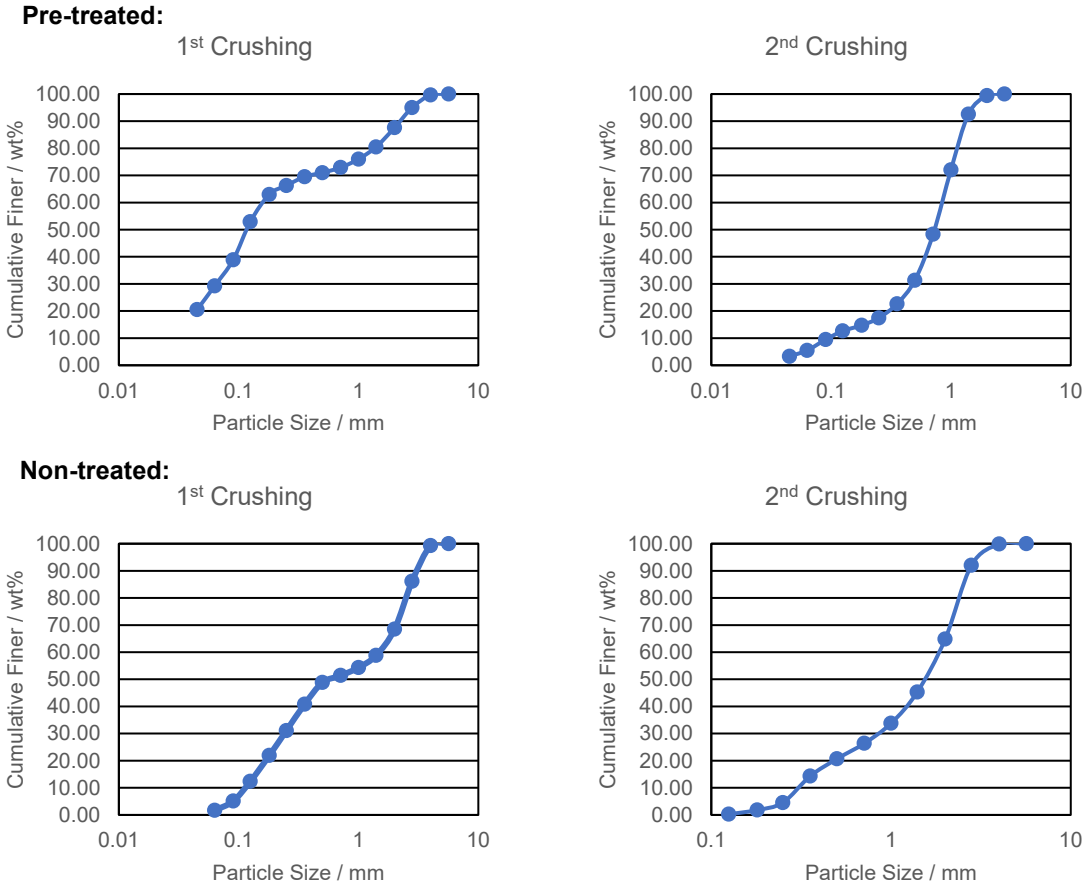

Figure 48 - Cumulative curves for pre-treated and non-treated material after the first and second crushing.

Figure 49 - Sieved non-treated material after first crushing for sieve 2.8 mm.

Getting back to Figure 47, as previously said, the majority of electrode foils that showed signs of disaggregation were cathode foils, and the majority of the covered electrodes were anode foils. This said, one can assume that after the first crushing the powder released is composed of Li, Ni, Mn, and Co. Contrastingly, in the event of a second crushing, the powder released will be predominantly graphite. Taking that into consideration, the larger sieved particles from the first crushing (particle size superior to 0.5 mm) were crushed one more time. 0.5 mm was chosen as the parting sieve because thenceforth, as divulged in Figure 50, little to no aluminium particles were seen in the sieved content. To validate this choice, the sieved content of a selected group of sieved material samples was dissolved with aqua regia and analysed with AAS. The results are available in Figure 51.

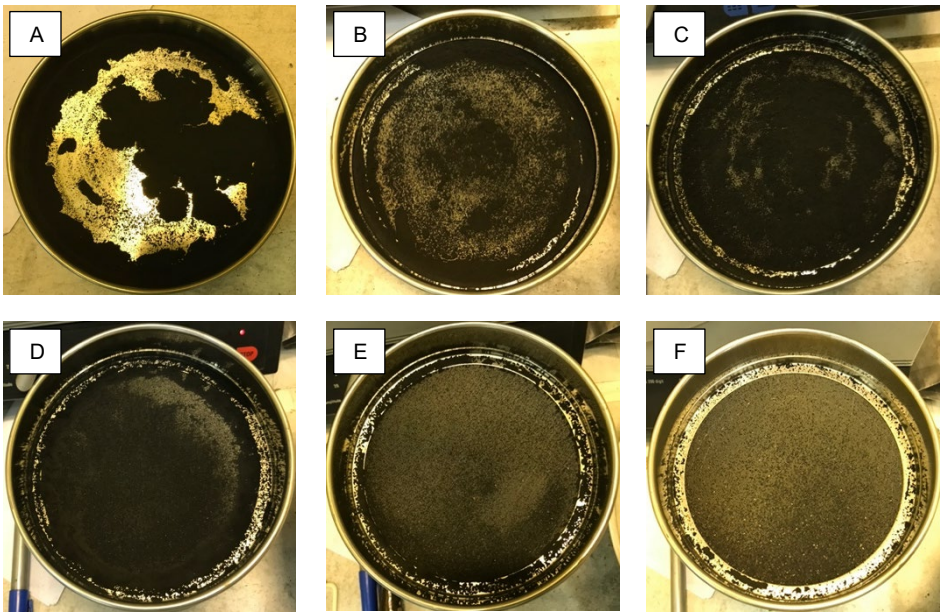

Figure 50 - Sieved pre-treated material after first crushing retained in sieves: a) 0 mm; b) 0.045 mm; c) 0.063 mm; d) 0.125 mm; e) 0.18 mm; f) 0.25 mm.

Just by looking at Figure 52, it is possible to see that more clean Cu foils started to appear on the sieves after the second crushing. It is important to point out that after the second crushing, the covered electrodes remained anode foils. To support this claim, a selected group of sieved material samples was also dissolved with aqua regia and analysed with AAS analysis to understand the elemental content in each sieving step. The results are available in Figure 51 and were obtained using Equation 13.

$$\eta = \left(\frac{C_i \times V}{m}\right) \times 100 \quad (13)$$

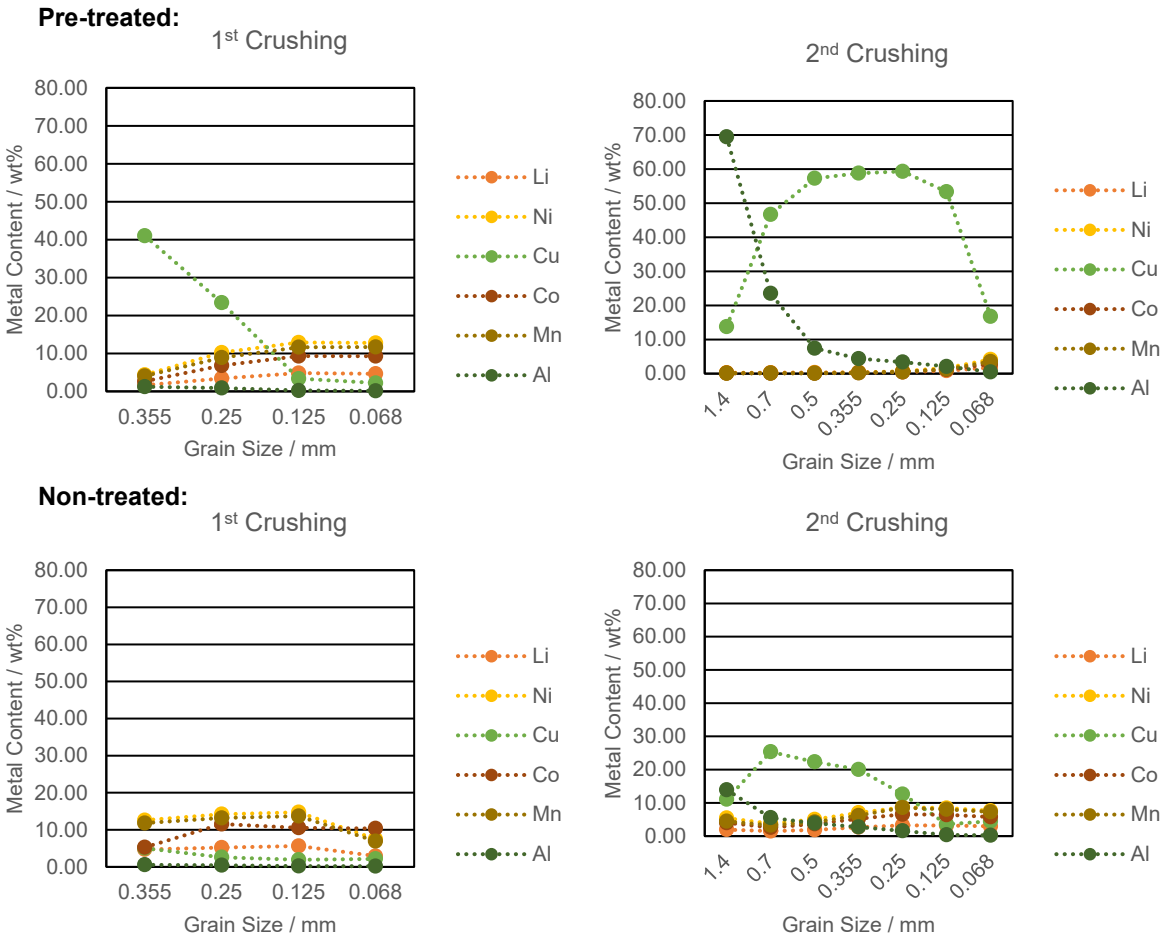

Figure 51 - Metal content in some selected sieved material fractions after first and second crushing, for pre-treated and non-treated material.

Figure 52 - Crushed pre-treated material retained in sieve 1.4 mm after second crushing.

From Figure 51, it is possible to conclude that, for the first crushing, for both pre-treated and non-treated material, Al content is always low (below 1.5%), and it decreases as the mesh size increases, as does the content for Cu. The bulk of the Al is found in the sieves with superior mesh sizes, as seen in the second crushing steps for both materials. On the other hand, Li, Ni, Mn, and Co increase their content as the mesh size decreases. Since the material with grain size inferior to 0.5 mm was crushed a second time, there is no record of their metal content after the first crushing.

For the second crushing of the pre-treated material, Figure 51 displays the Al content decreasing as the grain size decreases, with the bulk of content found in meshes superior to 0.5 mm. That said, Cu assumes a parabolic role, which is perfectly understandable. Seeing as the calcinated anode material tends to have a more brittle behaviour due to partial oxidation, it is normal that the bulk of the material is found in meshes of inferior size. The cathodic elements content is very low, with a slight increase as the mesh grows thinner. This confirms the theory introduced above that the second crushing would allow the disaggregation of the graphite, whereas the cathode powder would be abundant in the material resulting from the first crushing. And so, although some contamination from Cu and Al may occur from the second crushing, it is worth it, seeing as contaminants may be extracted through extraction processes, and another crushing step allows for the disaggregation of graphite and more cathode elements. This cathode elements disaggregation may appear small on a laboratory scale but, on a large scale, it can represent a great deal of material.

In the results for the second crushing of the non-treated material, there is an increase in contamination from the first to the second crushing, even if not as high as the one from the pre-treated material. There is still a considerable amount of cathode material present, which is normal considering that, as seen in Figure 49, there isn't as much disaggregation from the electrode foils.

Finally, regarding the choice of the parting sieve, the results from Figure 51 confirm, for both pre-treated and non-tread materials, the higher concentration of electrode powder material, making 0.5 mm an acceptable choice.

In the end, a large bulk of electrodes was crushed two times, the material was mixed, and samples were prepared for the subsequent leaching tests using FDE methodology, following the procedure explained in the previous chapter (see Chapter 4). Those samples were analysed via ICP to obtain their elemental composition. Table 4 showcases the results.

Table 4 - Sample characterization of the crushed mixed electrode powder.

	Elemental Composition / wt%					
	Li	*Ni*	*Mn*	*Co*	*Al*	*Cu*
Sample 1	5.1	13.5	14.5	14.8	1.4	13.8
Sample 2	4.2	12.6	11.8	13	1.1	13.1
Average	4.7	13.1	13.1	13.9	1.2	13.5

5.4.2. Factorial Design Experiment

To evaluate the significance of the main factors in the leaching yields, an FDE was done. This kind of methodology allows the efficient combination of experimental independent variables, i.e. factors, gathering maximum information with minimum experimental effort, using statistical and mathematical techniques.

A 2^4 design program was applied, involving 4 experimental factors and 2 levels for each factor, low and high, expressed by -1 and +1, respectively, when represented as coded factors. The factors considered for evaluation were temperature (T, ºC), liquid-solid ratio (L/S, L/kg), concentration of leaching agent ([H_2SO_4], M), and reaction time (t, min). The response or dependent variable evaluated was the leaching yield (η, %). The adopted ranges for the parameters were as follows: 60 and 80 ºC for temperature; 5 and 7.5 L/kg for L/S; 2 and 3 M for acid concentration; and 30 and 120 min for time. The other processing conditions were maintained constant, namely the concentration of the reducing agent ([Na_2SO_4] = 0.25 M) and the stirring velocity (v = 120 rpm). Table 5 summarizes the FDE's factors and levels, along with the leaching yield for each individual metal. Tests 1 to 16 correspond to the combination of factors while tests 17 to 20 are replicates at the central point of the programme, through which the experimental error can be estimated.

Table 5 - List of experiments and corresponding responses obtained in the 2^4 factorial design.

Exp.	Factors and levels				Leaching Yield / %					
	L/S	[H_2SO_4]	T	t	Li	Ni	Mn	Co	Al	Cu
	L/kg	*M*	*ºC*	*min*						
1	5	2	60	30	74.2	63.7	70.3	63.9	18.0	70.1
2	7.5	2	60	30	83.8	75.2	77.4	75.6	47.0	62.7
3	5	3	60	30	95.2	86.3	93.9	87.5	78.8	85.6
4	7.5	3	60	30	93.0	87.0	85.9	85.7	89.5	64.9
5	5	2	80	30	88.2	83.2	89.7	87.1	14.7	82.7
6	7.5	2	80	30	84.8	75.9	78.2	79.2	58.0	63.3
7	5	3	80	30	95.0	99.6	100.0	97.6	72.5	100.1
8	7.5	3	80	30	102.4	102.9	101.8	104.4	103.4	78.0
9	5	2	60	120	68.8	65.2	66.9	67.0	19.6	70.4
10	7.5	2	60	120	77.2	69.2	73.4	71.9	47.6	62.5
11	5	3	60	120	97.6	89.6	98.0	93.2	84.7	91.4
12	7.5	3	60	120	93.0	81.6	83.9	82.3	92.2	69.3
13	5	2	80	120	87.9	78.6	88.1	81.4	41.7	79.4
14	7.5	2	80	120	75.5	64.3	67.0	65.8	49.7	62.8
15	5	3	80	120	95.6	92.5	97.0	93.7	75.2	102.5
16	7.5	3	80	120	113.7	104.5	110.0	106.1	112.6	103.4
17	6.25	2.5	70	75	99.6	102.6	110.2	102.3	72.0	76.4
18	6.25	2.5	70	75	106.8	108.0	101.0	86.1	88.0	90.9
19	6.25	2.5	70	75	103.1	93.4	96.1	100.2	79.7	80.5
20	6.25	2.5	70	75	105.7	107.3	103.7	96.9	96.7	82.4

The first observation that can be made from the results displayed in Table 5 is that time does not seem to have a big influence on the outcomes, in the range studied, with the results displaying similar leaching yields for both times.

By applying Fisher's distribution, the quantification of the significance of the effects can be studied through the analysis of the variance. Tables 6 to 11 display the evaluation of the variance of the factors for the leaching of each metal.

In general, the concentration of leaching agent and temperature have a positive and significant effect on the leaching efficiency, i.e. have a p-value inferior to 0.05, with Ni at the limit of significance. Exceptionally, for Li (Table 6) the concentration of the leaching has a very significant effect, i.e. the p-value, in this case, is inferior to 0.01. On average, the leaching yields rise by about 25% and 10% when the concentrations of leaching agent and temperature increase, respectively. For Al temperature has no significant effect.

The L/S ratio seems to not have any significant effect on the leaching efficiency of any metal besides Al and Cu. For Al, the ratio is significant and positive, with the leaching yield increasing by about 24% with the increase of L/S. On the other hand, for Cu the ratio has a negative and significant effect, meaning that the leaching yield decreases by about 14% when the L/S increases. This may be due to the fact that with higher L/S values, there is more volume and more reducer available for the reaction which may hinder the dissolution of Cu but increase the dissolution of Al.

Time has no significant effect on the leaching efficiency of any metal, as do not any interactions.

As a final point, taking into account all the effects described above, experiments 7 and 8 create the optimal conditions for the leaching process. The choice comes down to L/S. Seeing as the yielding results are very similar between experiments, and experiment 8 has a higher ratio, meaning more volume, more wastewaters, bigger reactor, etc., and therefore, a more expensive process, experiment 7 is the chosen one.

Table 6 - Evaluation of variance of effects for the leaching of Li.

Source of Variation	Effect	Sum of Squares	DF	Mean Square	F	p-value
Factors						
Main Factors						
L/S	2.58	26.6	1	26.6	2.60	0.205
$[H_2SO_4]$	18.16	1318.4	1	1318.4	129.21	0.001
T	7.54	227.6	1	227.6	22.30	0.018
t	-0.93	3.5	1	3.5	0.34	0.601
Interactions						
L/S x $[H_2SO_4]$	2.05	16.9	1	16.9	1.65	0.289
L/S x T	-0.18	0.1	1	0.1	0.01	0.917
L/S x t	-0.26	0.3	1	0.3	0.03	0.880
$[H_2SO_4]$ x T	-0.56	1.2	1	1.2	0.12	0.750
$[H_2SO_4]$ x t	4.50	80.8	1	80.8	7.92	0.067
T x t	1.50	9	1	9	0.88	0.416
Residuals		30.61	3	10.20		
Total		1714.97	13	1697.56		

Table 7 - Evaluation of variance of effects for the leaching of Ni.

Source of Variation	Effect	Sum of Squares	DF	Mean Square	F	p-value
Factors						
Main Factors						
L/S	0.21	0.2	1	0.2	0	0.953
$[H_2SO_4]$	21.07	1775.6	1	1775.6	39.18	0.008
T	10.43	435.2	1	435.2	9.60	0.053
t	-3.54	50.2	1	50.2	1.11	0.370
Interactions						
L/S x $[H_2SO_4]$	1.78	12.7	1	12.7	0.28	0.633
L/S x T	-1.83	13.5	1	13.5	0.30	0.624
L/S x t	-1.82	13.3	1	13.3	0.29	0.626
$[H_2SO_4]$ x T	3.29	43.2	1	43.2	0.95	0.401
$[H_2SO_4]$ x t	1.64	10.7	1	10.7	0.24	0.660
T x t	-1.88	14.1	1	14.1	0.31	0.616
Residuals		135.97	3	45.32		
Total		2504.66	13	2414.01		

Table 8 - Evaluation of variance of effects for the leaching of Mn.

Source of Variation	Effect	Sum of Squares	DF	Mean Square	F	p-value
Factors						
Main Factors						
L/S	-3.29	43.3	1	43.3	1.16	0.360
$[H_2SO_4]$	19.96	1593.4	1	1593.4	42.78	0.007
T	10.24	419.3	1	419.3	11.26	0.044
t	-1.59	10.2	1	10.2	0.27	0.638
Interactions						
L/S x $[H_2SO_4]$	1.47	8.7	1	8.7	0.23	0.662
L/S x T	-1.15	5.3	1	5.3	0.14	0.731
L/S x t	-0.64	1.6	1	1.6	0.04	0.848
$[H_2SO_4]$ x T	1.51	9.1	1	9.1	0.24	0.655
$[H_2SO_4]$ x t	3.44	47.4	1	47.4	1.27	0.341
T x t	-0.29	0.3	1	0.3	0.01	0.931
Residuals		111.74	3	37.25		
Total		2250.36	13	2175.87		

Table 9 - Evaluation of variance of effects for the leaching of Co.

Source of Variation	Effect	Sum of Squares	DF	Mean Square	F	p-value
Factors						
Main Factors						
L/S	-0.06	0	1	0	0	0.988
$[H_2SO_4]$	19.82	1570.5	1	1570.5	30.44	0.012
T	11.01	485.1	1	485.1	9.40	0.055
t	-2.44	23.9	1	23.9	0.46	0.545
Interactions						
L/S x $[H_2SO_4]$	1.69	11.4	1	11.4	0.22	0.670
L/S x T	-1.03	4.2	1	4.2	0.08	0.793
L/S x t	-2.24	20	1	20	0.39	0.578
$[H_2SO_4]$ x T	2.23	19.9	1	19.9	0.39	0.579
$[H_2SO_4]$ x t	2.44	23.7	1	23.7	0.46	0.546
T x t	-2.88	33.1	1	33.1	0.64	0.482
Residuals		154.77	3	51.59		
Total		2346.63	13	2243.45		

Table 10 - Evaluation of variance of effects for the leaching of Al.

Source of Variation	Effect	Sum of Squares	DF	Mean Square	F	p-value
Factors						
Main Factors						
L/S	24.36	2373.2	1	2373.2	20.92	0.020
$[H_2SO_4]$	51.57	10638.9	1	10638.9	93.77	0.002
T	6.29	158	1	158	1.39	0.323
t	5.19	107.8	1	107.8	0.95	0.401
Interactions						
L/S x $[H_2SO_4]$	-2.74	29.9	1	29.9	0.26	0.643
L/S x T	5.57	124.2	1	124.2	1.09	0.372
L/S x t	-4.13	68.2	1	68.2	0.60	0.495
$[H_2SO_4]$ x T	-1.66	11.1	1	11.1	0.10	0.775
$[H_2SO_4]$ x t	-0.06	0	1	0	0	0.992
T x t	2.45	24	1	24	0.21	0.677
Residuals		340.36	3	113.46		
Total		13875.65	13	13648.75		

Table 11 - Evaluation of variance of effects for the leaching of Cu.

Source of Variation	Effect	Sum of Squares	DF	Mean Square	F	p-value
Factors						
Main Factors						
L/S	-14.41	830.4	1	830.4	22.38	0.018
$[H_2SO_4]$	17.68	1250.5	1	1250.5	33.70	0.010
T	11.93	568.9	1	568.9	15.33	0.030
t	4.28	73.4	1	73.4	1.98	0.254
Interactions						
L/S x $[H_2SO_4]$	-1.60	10.2	1	10.2	0.27	0.636
L/S x T	0.12	0.1	1	0.1	0	0.970
L/S x t	2.98	35.6	1	35.6	0.96	0.400
$[H_2SO_4]$ x T	6.27	157.4	1	157.4	4.24	0.132
$[H_2SO_4]$ x t	5.23	109.5	1	109.5	2.95	0.184
T x t	1.71	11.6	1	11.6	0.31	0.614
Residuals		111.31	3	37.11		
Total		3158.97	13	3084.76		

To support the leaching yield results for experiment 7 available in Table 5, XRPD was performed in the final leaching residue. The diffractogram in Figure 53 reveals a pronounced presence of graphite with very small peaks of cryolithionite ($Na_3Li_3(AlF_6)_2$), supporting the leaching yield results for experiment 7 that claim yields of approximately 95% for Li, 100% for Ni, 100% for Mn, 98% for Co, 73% for Al, and 100% for Cu. Although Al yield was not complete, that did not significantly affect the composition of the graphite leach residue, since the initial Al content in the material was low (Table 4), due to efficient separation of Al foil resulting from the crushing and sieving procedure applied.

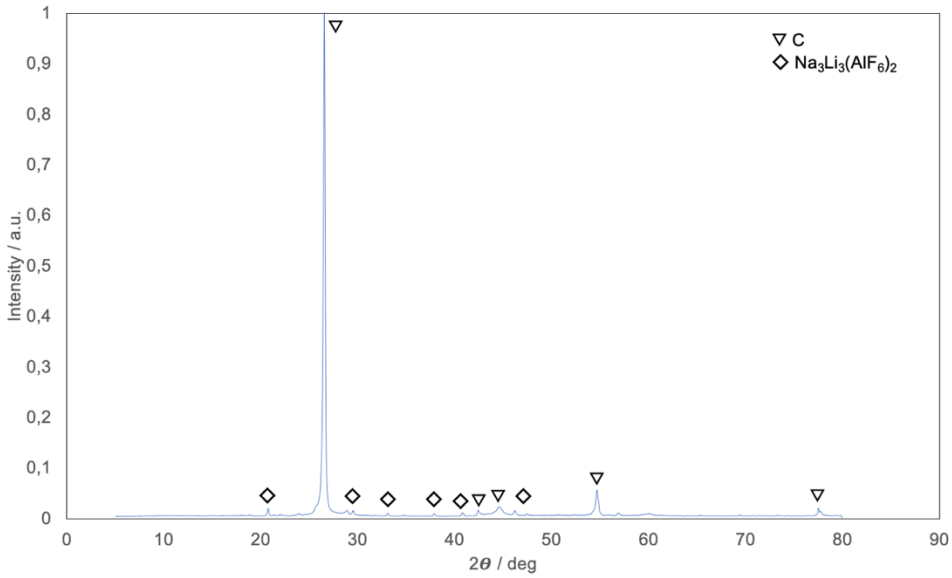

Figure 53 - XRPD diffractogram for the leaching residue of experiment 7.

5.5. Metal Separation

This last section is composed of an exploratory analysis of possible metal separation and recovery routes. Taking into consideration the scale of this work, it wasn't feasible to do an exhaustive analysis but rather give rise to questions to be studied, developed, and analysed in future works.

The work sequence was as follows:

1) Cu separation using solvent extraction.
2) Purification of the solution through Al removal by neutralization of the solution.
3) NiMnCo mixture recovery by precipitation.
4) Lithium Carbonate (Li_2CO_3) production.

The bulk solution used in the following separation processes was a mixture of every leaching liquor resulting from the previous FDE.

5.5.1. Cu Extraction

In the literature, there are several alternatives to extract Cu, e.g. precipitation, solvent extraction, cementation. Solvent extraction seems to be the most effective technique used and it is also less studied and applied regarding Li-ion battery recycling. The conditions selected for these experiments were essentially based on extensive experience in solvent extraction of the LNEG's researchers. [68,71,76,77].

Before starting the extraction process, the pH of the solution was 0.39. As the value was too low, 57 mL of a 4 M NaOH was added to 150 ml of the mixture leaching solution, raising the pH value to 1.59. 150 mL of the pH-corrected solution was used in the subsequent extraction process.

Solvent extraction involves two operations: extraction and stripping. For the first operation, 150 mL of ACORGA M5640 was used since it holds a great affinity for some contaminants, such as Cu, from acidic sulphate solutions at specific low pH values, as is the case. Following extraction, as stated in Chapter 4, the organic phase was stripped of all Cu using 150 mL of a 3M H_2SO_4 solution, to guarantee maximum Cu recovery. A sample of each stripping solution was diluted and analysed with AAS and the extraction yield calculated using (14). The results from the analysis and extraction yield are displayed in Tables 12 and 13.

$$Extraction\ Yield\ \% = \left(\frac{C_i \times V_i - C_f \times V_f}{C_i \times V_i}\right) \times 100 \quad (14)$$

Table 12 - Extraction yield results for the extraction step.

	Al	*Cu*	*Li*	*Ni*	*Mn*	*Co*
Initial aqueous C_i / g/L	0.62	11.67	5.08	13.10	12.62	10.13
Raffinate C_f / g/L	0.56	1.42	5.03	13	12.34	9.98
Extraction Yield / %	9.29	87.87	0.95	0.72	2.24	1.49

Table 13 - Stripping yield results and yield of the complete extraction circuit.

	Al	*Cu*	*Li*	*Ni*	*Mn*	*Co*
Initial loaded organic C_i / g/L	0.06	10.25	0.05	0.09	0.28	0.15
Stripping Solution C_f / g/L	0	9.05	0	0.002	0.001	0.001
Stripping Yield / %	0	88.23	0	2.62	0.3	0.63
Complete Extraction Circuit Yield / % (*)	0	77.5	0	0.02	0.01	0.01

(*) includes the extraction and stripping yields, expressing the overall recovery.

From the results presented in both Tables 12 and 13, it is possible to conclude that a considerable amount of Cu was extracted with barely any manifestation of other elements. Considering an average dispersion of the concentration values between 3 and 5%, usual errors for this kind of analysis, extractions below 5% can be considered as meaningless. The yield for the complete extraction circuit, extraction and stripping, was 77.5% but it can be seen as 88%, since, although the totality of the Cu content was not stripped, it remains in the organic phase and so it can be re-extracted until an almost full efficiency is obtained. Moreover, these experiences were made in single extraction/stripping stages, and in an industrial plant a countercurrent multistage design will be applied. This way, it is believed that more than 99% of Cu could be extracted and recovered.

For the recovery of the copper contained in the strip liquor, the solution was evaporated until crystallization occurred, and the $CuSO_4$ solids obtained were filtered, washed with acetone, dried in an oven for 24 hours, calcinated at 400 ºC for 6 hours, and weighed. The calcinated step was added to remove the excessed acid in the crystallized $CuSO_4$. The weighed amount of extracted $CuSO_4$ was 2.074 g.

To confirm the absence of other elements in the obtained sulphate, XRPD and SEM with EDS analysis were performed.

The XRPD and EDS diffractogram, Figure 54 and 55, respectively, show no sign of other contaminants. The SEM images, Figure 55, reveal a sample with different agglomerate sizes with irregular shapes. The Au and Pd in the EDS spectrum come from the sample preparation. The SEM analysis, as portrayed in Figure 55, reveals a very homogeneous sample.

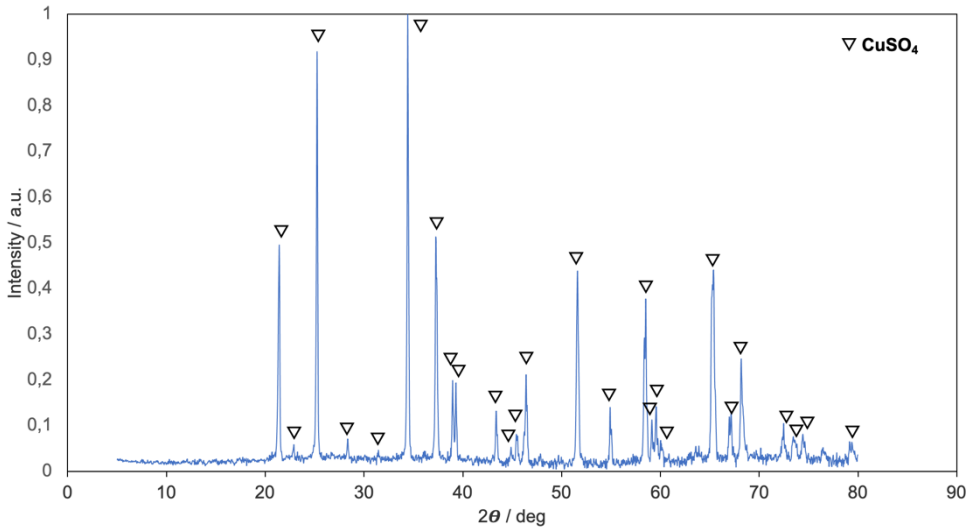

Figure 54 - XRPD analysis results of the crystallized $CuSO_4$.

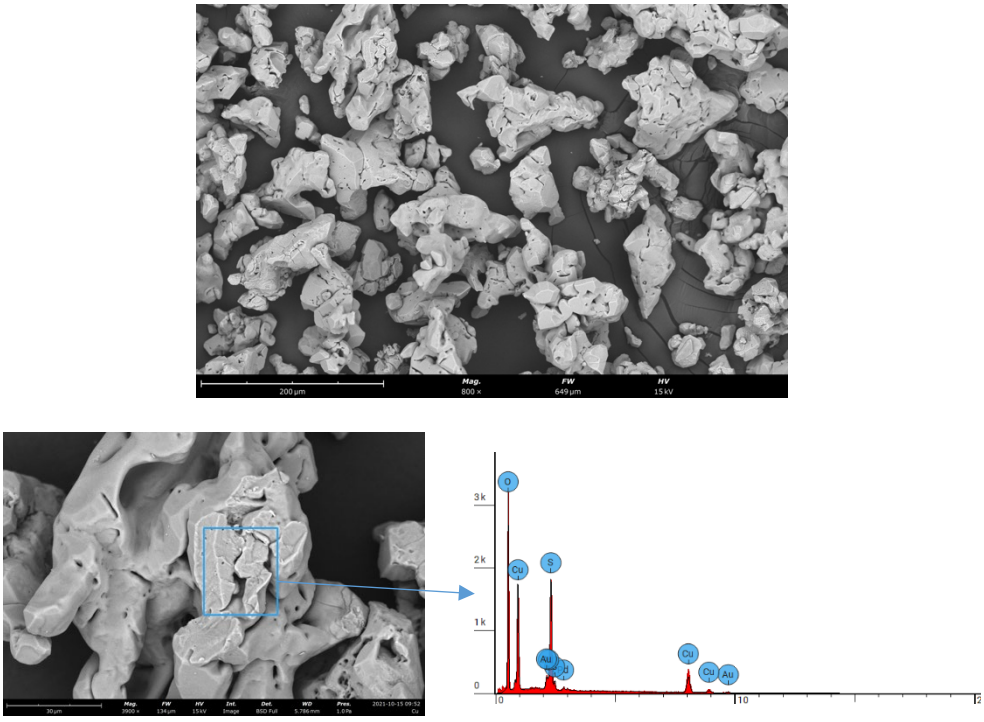

Figure 55 - SEM and EDS results of the crystallized $CuSO_4$.

5.5.2. Al Removal

Due to its much lower solubility product constant, Al can be removed by neutralization in the form of the respective hydroxide. According to Al's Pourbaix diagram, precipitation starts from pH values between 3 and 4 [78].

Before starting the neutralization process, the pH value was 1.37. 15 mL of a 4 M NaOH solution was added to 150 mL of the Cu-free solution, the pH value increased to 4.30, and $Al(OH)_3$ started to precipitate. The Al removal resulted in 0.748 g of precipitate, expectably $Al(OH)_3$.

A sample of the Al-free solution was diluted and analysed with AAS. The metals removed yields were calculated using (14). Both results are available in Table 14.

Table 14 - Extraction yield results for the removal of Al.

	Al	*Cu*	*Li*	*Ni*	*Mn*	*Co*
C_i / g/L	0.56	1.42	5.03	13	12.34	9.38
C_f / g/L	0.24	0.96	3.76	9.65	8.64	7.33
Precipitation Yield / %	53.6	25.05	17.88	18.38	23.01	19.27

The extraction yield values listed in Table 14 reveal 53.6% extraction yield for Al, with considerable contamination coming from the remaining metals.

To support the results given from AAS analysis, XRPD and SEM with EDS analysis were performed in the resultant hydroxide.

Figure 56 reveals a very heterogeneous sample in terms of fraction sizes, with irregular shapes, composed of very small particles agglomerated. EDS analysis, Figure 56, confirms the presence of Li, Ni, Mn, Co, and Cu, in the hydroxide resultant from the precipitation.

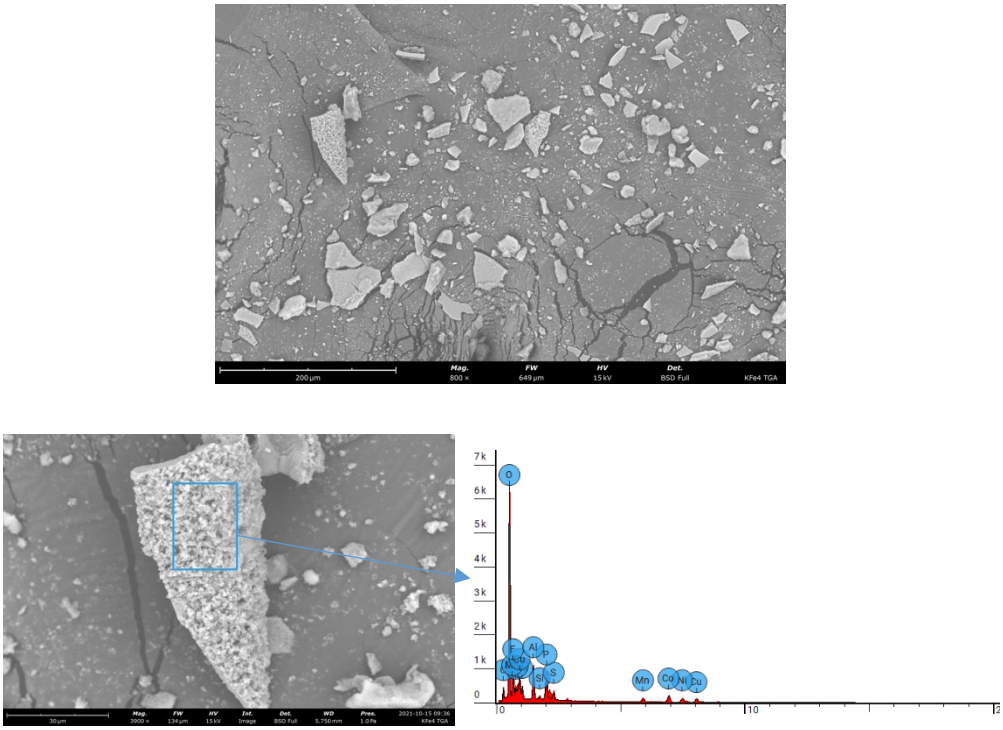

Figure 56 - SEM and EDS results for the precipitated hydroxide.

XRPD reveals an amorphous hydroxide form, very common in products produced by neutralization, not allowing the identification of the phases present. However a small peak was found, attributed to an Al species, as seen in Figure 57, in the form of sodium aluminium hexafluoride (Na_3AlF_6), an inorganic compound extensively used in the industrial production of aluminium metal. The F comes from the binder or the electrolyte. The Na derives from the solution used to increase the pH value. Additionally, the presence of the transition metals can be confirmed by the diffractogram without background removal, Figure 58, due to the fluorescence effect, caused by the transition metals, because the K adsorption edge (K-edge) values for the transition metals are all superior to the Kα radiation peak for Cu. As seen in the literature ([79]), to avoid the fluorescence effect, the wavelength of the Kα radiation peak used should be longer than the K absorption edge (K-edge) of the sample material.

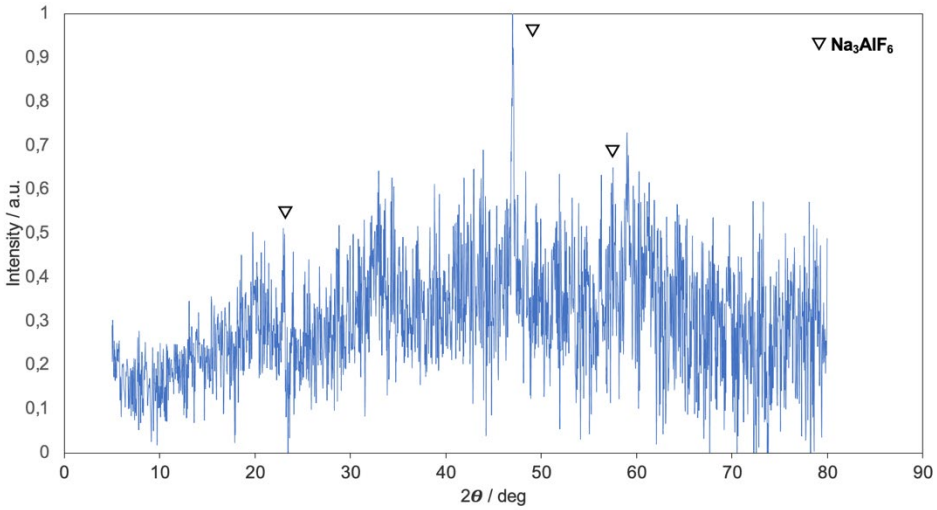

Figure 57 - XRPD diffractogram for the precipitated hydroxide with background removal.

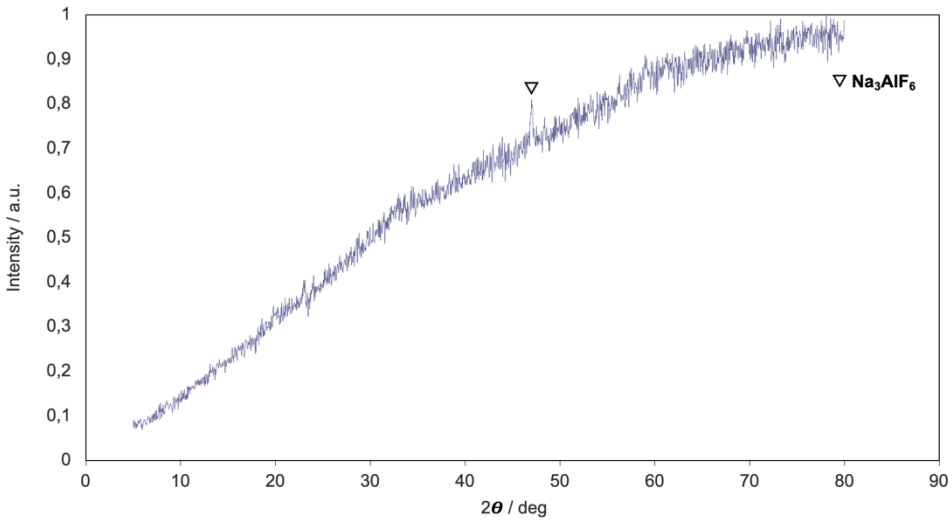

Figure 58 - XRPD diffractogram for the precipitated hydroxide without background removal.

5.5.3. Ni, Mn, and Co Precipitation

According to Ni, Mn, and Co's Pourbaix diagram, the transition metals precipitate around similar pH values, between 7 and 10.5, and so an attempt to precipitate the three metals at the same time was made. This seems an adequate approach since a mixture of the three metals can be a valuable product to be used as raw-material for producing new cathodes [78].

As before, the process started by measuring the pH value of the Al-free solution. Since the pH value reached was 4.49, and Mn only started to precipitate after pH values of 8, 38 ml of the 4 M NaOH solution was added to 165 mL of the Al-free solution, reaching a final pH value of 9.49. The precipitation resulted in 9.486 g of $NiMnCo(OH)_2$.

After precipitation, a sample was taken from the filtrate and analysed with AAS. The AAS results and the extraction yields, calculated using Equation (14), are disclosed in Table 15.

Table 15 - Extraction yield results for the precipitation of Ni, Mn, and Co.

	Al	*Cu*	*Li*	*Ni*	*Mn*	*Co*
C_i / g/L	0.24	0.96	3.76	9.65	8.64	7.33
C_f / g/L	0	0.002	3.45	0.004	0.02	0.001
Precipitation Yield / %	100	99.82	~ 0	99.96	99.73	99.98

The results from Table 15 present approximately 100% extraction for the transition metals. Al and Cu extraction, although showing 100% yield, can't be considered as contaminants since the initial concentration was extremely small, and therefore negligible.

XRPD and SEM were performed on a sample of the hydroxide so as to verify the statements made above. Figure 59 portrays a very heterogeneous sample in terms of agglomerate size distribution, with very small particles aggregated, and irregular shapes, similar to Figure 56. The EDS diffractogram, Figure 59, corroborates with the results presented in Table 15, showing no presence of other elements besides sulphur. Au and Pd in the EDS diffractogram, as mentioned before, come from the sample preparation.

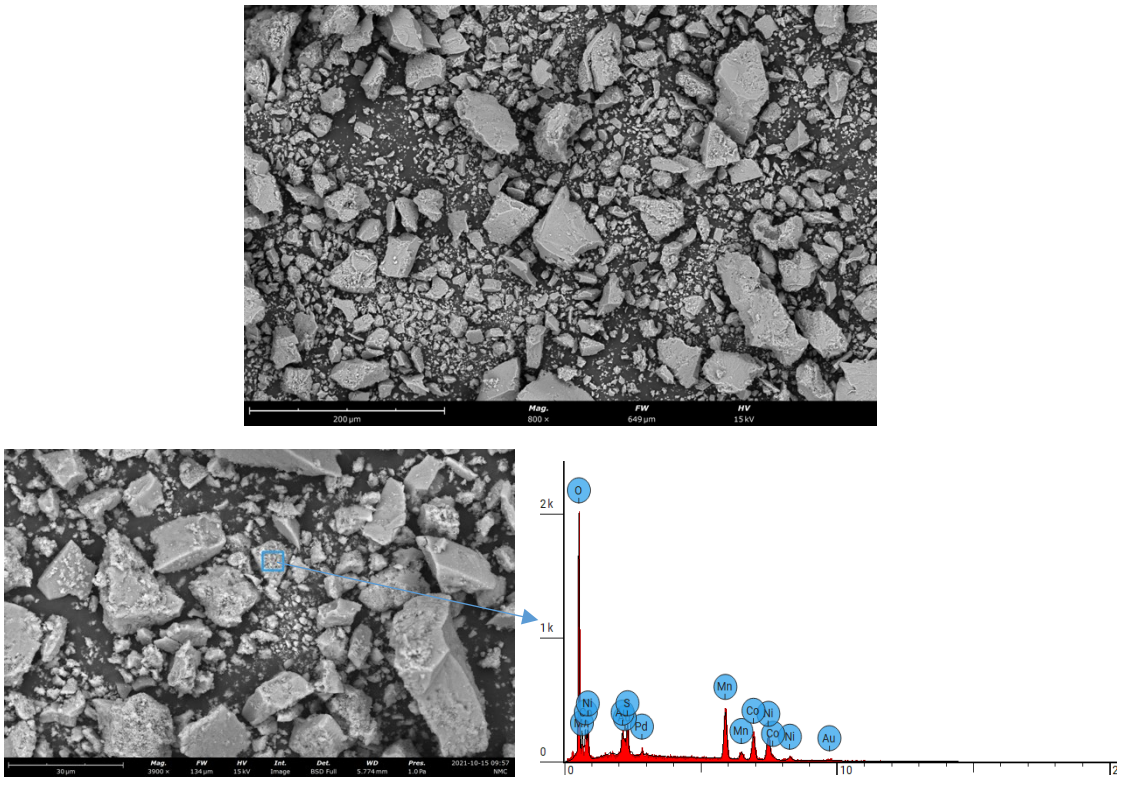

Figure 59 - SEM and EDS results for the precipitated hydroxide of Ni, Co, and Mn.

The XRPD diffractogram, Figure 60, reveals an amorphous sample, with no distinguishable peaks. As in the previous sample, due to the fluorescence effect, the presence of the transition metals, Ni and Co, can be confirmed.

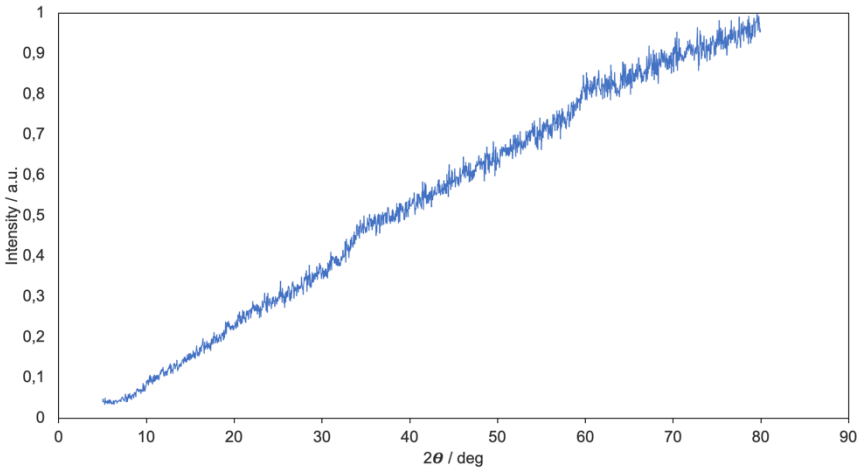

Figure 60 - XRPD diffractogram for the precipitated hydroxide.

5.5.4. Li Precipitation

Closing the metal extraction trials comes precipitation of Li_2CO_3. Seeing as, due to the previous separation trials, the Na content in the solution was already very high, it was decided to evaporate the Li-rich solution to half to facilitate the precipitation of Li_2CO_3 via the addition of 10 mL of a 2.5 M Na_2CO_3 solution to 94 ml of the concentrated Li-rich solution. Na_2CO_3 was chosen over NaOH because with the use of the carbonate, the resulting precipitate would be Li_2CO_3, a cheap (24.8 $/kg [80]), ready-to-use compound in the LIB production. However, precipitation of LiOH would be an option, since it is also a useful commodity for battery electrodes production. This said, LiOH is very soluble, more expensive (30.50 $/kg [81]), and much more difficult to obtain [82].

The precipitated carbonate was washed with a Li_2CO_3 saturated solution, dried, and weighed, resulting in 0.558 g of Li_2CO_3.

To conclude these metal separation trials, a sample of the obtained Li_2CO_3 was analysed with SEM and XRPD. Figure 61 portrays a heterogeneous sample in terms of fraction sizes, as all non-calcinated precipitates obtained throughout this process. The SEM analysis showed two different types of aggregates, one smaller with a more irregular shape and another, bigger, with a more prismatic shape. EDS, Figure 61, revels the presence of Mn in the sample but seeing as the peak is so small it can be disregarded. In addition, it also identifies the big particles as possible sodium sulphates (Na_2SO_4) contaminates, originated from the Na present in solution added to increase the pH value.

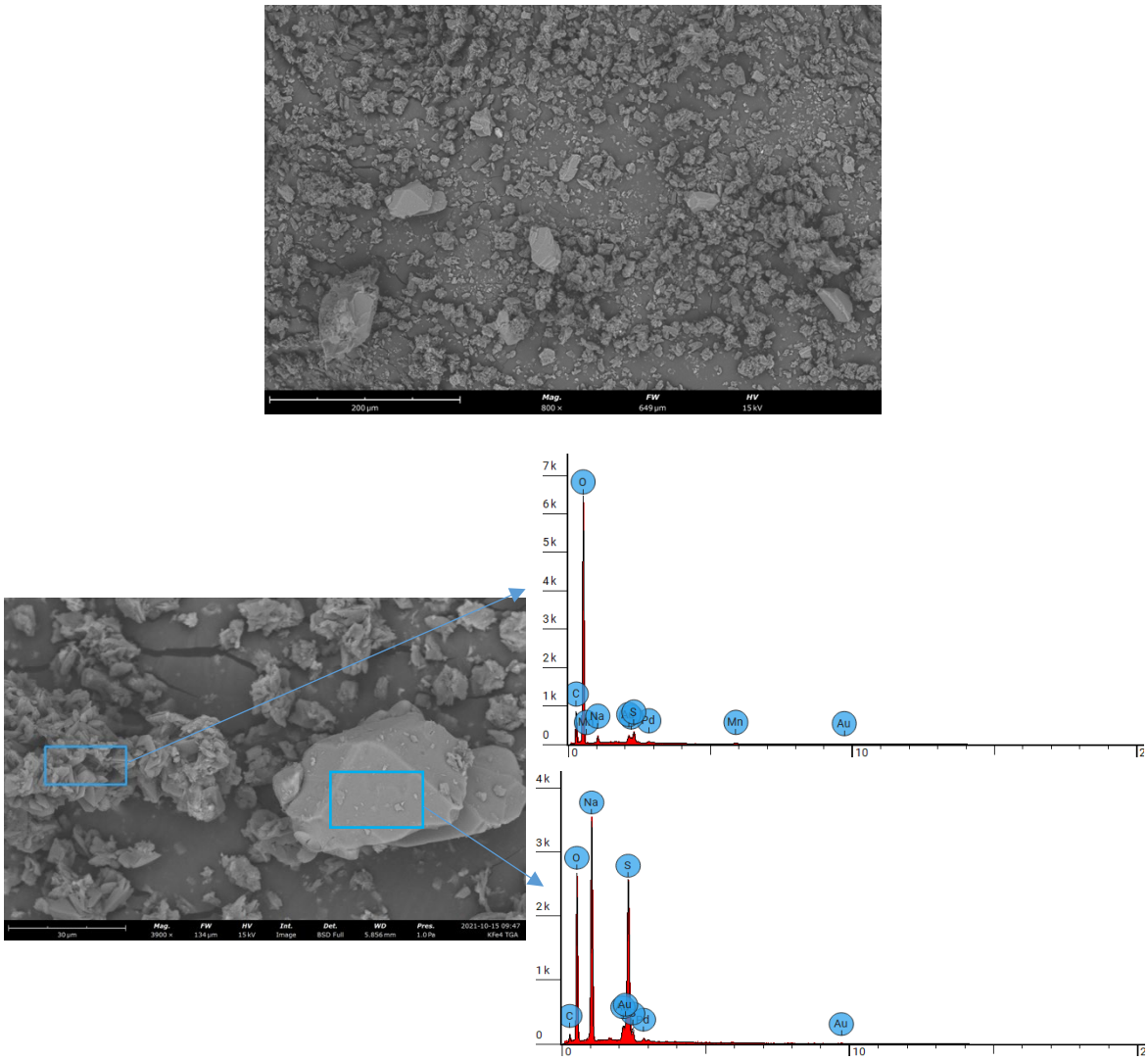

Figure 61 - SEM and EDS results for the precipitate.

The XRPD diffractogram, Figure 62, confirms the formation of Li_2CO_3 and the presence of Na_2SO_4 and reveals no presence of Mn. To tackle this contamination issue, the precipitate should be washed with a saturated Li_2CO_3 solution.

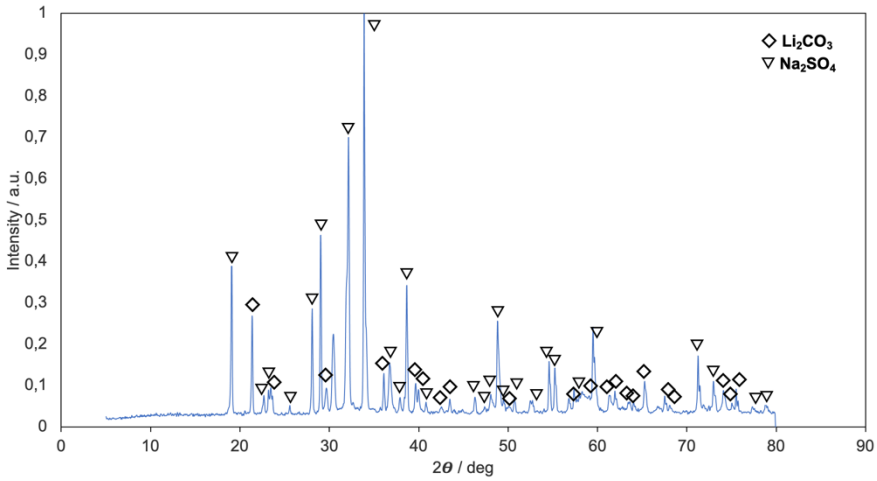

Figure 62 - XRPD diffractogram for the precipitated carbonate.

Chapter 6

Conclusions

6.1. Achievements

This work aimed at the development of a hydrometallurgical recycling process that could potentially be adapted to an industrial scale.

Thermal treatment and solvent dissolution were performed in samples of the electrode materials and only calcination unveiled disaggregation of 100% in almost all cases of the cathode. For the anodes, disaggregation was generally inefficient. The electrode cells were further studied, and the conclusion reached was that the cathode powder represented 90 and 80% of the electrode weight for cells 5 and 7, respectively, the remaining percentage being the Al conductive foils.

The impact of calcination in the leaching behaviour of the cathode metals (Li, Ni, Co, Mn) was also investigated revealing that the thermal treatment at 400 ºC for 5 hours was the optimal condition due to the obtained leaching yields. Additionally, the impact of the reducer, introducing the possibility of electrode foils as reducers, was also considered and revealed that using $Na_2S_2O_5$, or a combination of $Na_2S_2O_5$ with the electrode foils, were the leading alternatives. Nonetheless, the addition of electrode foils does not justify the increase of contaminants in the leaching liquor.

Previous to the final set of leaching experiments, two batches of mixed electrode material, one calcinated and another non-treated, underwent crushing and sieving. After careful consideration of all results, the conclusion reached was that the calcinated crushed material presented better signs of disaggregation. 0.5 mm was chosen as the parting sieve, i.e. the sieve that better separates the powder fractions from the foil fractions.

The leaching of the electrode metal was efficiently achieved, with optimal leaching conditions of 3 M of H_2SO_4 as leaching agent, 0.25 M of $Na_2S_2O_5$ as reducing agent, an L/S ratio of 5 L/kg, temperature of 80 ºC, for 30 minutes, presenting leaching yields for Li, Ni, Mn, Co, Cu, and Al of approximately 95%, 100%, 100%, 98%, 100%, and 73%, respectively. Under the optimized conditions, the leach residue was composed of graphite with good purity.

To end, an introduction to the metal separation processes was developed. $CuSO_4$ was separated and produced after solvent extraction with 20% v/v ACORGA M5640 diluted in ESCAID 102. Purification by neutralization to pH 4.30 allowed the removal of most part of the aluminium, contaminated with some Li, Ni, Mn, Co, and Cu. A mixed hydroxide $NiMnCo(OH)_2$ was precipitated via the addition of NaOH to pH 9.49, where about an average 99.98% of recovery of the three metals was achieved. Finally, Li_2CO_3 was obtained by precipitation with the addition of Na_2CO_3, contaminated with Na_2SO_4, requiring further investigation to optimize precipitation conditions, and washing procedures.

In conclusion, the process presented satisfactory yields in each step and could easily be scaled up to an industrial scale.

6.2. Future Work

Further research on the disaggregation between the anode foils should be conducted to study how to effectively separate the graphite from the copper foil and, consequently, enabling the reuse of these valuable raw materials.

A more thorough study on the effect of the reducing agent should also be carried out, this time fluctuating its concentration, in order to better understand its effect on the main metals and, if possible, reduce its concentration.

Additionally, seeing as the cell content differs from manufacturer to manufacturer, the introduction of more batteries, preferentially with different cathode chemistries, in the recycling process should be encouraged allowing a better understanding of their effect on the leaching yield and separation processes and adjusting the parameters to their challenges, thereby creating a more overarching LIB recycling process.

The metal separation processes require further investigation, especially the precipitation of the Li_2CO_3, which could be held in a continuous system with recirculation of the mother liquor, and therefore allowing a rigorous assessment of the precipitation efficiency of the Li_2CO_3.

Lastly, it is also pertinent to implement a meticulous study on the environmental and economic impacts of this recycling process, taking into account not only the materials and energy consumed but also the output of the collected material and its economic value.

Bibliography

[1] European Commission, Strategic Research Agenda for Batteries 2020, *European Commission*, **2020**.

[2] Kamran, M.;Raugei, M.;Hutchinson, A., A Dynamic Material Flow Analysis of Lithium-Ion Battery Metals for Electric Vehicles and Grid Storage in the UK: Assessing the Impact of Shared Mobility and End-of-Life Strategies, *Resources, Conservation and Recycling*, **2021**, *167*, 105412. doi:*10.1016/j.resconrec.2021.105412*.

[3] Wang, M.;Tian, Y.;Liu, W.;Zhang, R.;Chen, L.;Luo, Y.;Li, X., A Moving Urban Mine: The Spent Batteries of Electric Passenger Vehicles, *Journal of Cleaner Production*, **2020**, *265*, 121769. doi:*10.1016/j.jclepro.2020.121769*.

[4] Arshad, F.;Li, L.;Amin, K.;Fan, E.;Manurkar, N.;Ahmad, A.;Yang, J.;Wu, F.;Chen, R., A Comprehensive Review of the Advancement in Recycling the Anode and Electrolyte from Spent Lithium Ion Batteries, *ACS Sustainable Chemistry and Engineering*, **2020**, *8*, 13527–13554. doi:*10.1021/acssuschemeng.0c04940*.

[5] Bonsu, N.O., Towards a Circular and Low-Carbon Economy: Insights from the Transitioning to Electric Vehicles and Net Zero Economy, *Journal of Cleaner Production*, **2020**, *256*, 120659. doi:*10.1016/j.jclepro.2020.120659*.

[6] Sommerville, R.;Zhu, P.;Rajaeifar, M.A.;Heidrich, O.;Goodship, V.;Kendrick, E., A Qualitative Assessment of Lithium Ion Battery Recycling Processes, *Resources, Conservation and Recycling*, **2021**, *165*, 105219. doi:*10.1016/j.resconrec.2020.105219*.

[7] Xu, L.;Yilmaz, H.Ü.;Wang, Z.;Poganietz, W.R.;Jochem, P., Greenhouse Gas Emissions of Electric Vehicles in Europe Considering Different Charging Strategies, *Transportation Research Part D 87*, **2020**, *87*, 102534. doi:*10.1016/j.trd.2020.102534*.

[8] Colmenar-Santos, A.;Muñoz-Gómez, A.M.;Rosales-Asensio, E.;López-Rey, Á., Electric Vehicle Charging Strategy to Support Renewable Energy Sources in Europe 2050 Low-Carbon Scenario, *Energy*, **2019**, *183*, 61–74. doi:*10.1016/j.energy.2019.06.118*.

[9] Skeete, J.P.;Wells, P.;Dong, X.;Heidrich, O.;Harper, G., Beyond the EVent Horizon: Battery Waste, Recycling, and Sustainability in the United Kingdom Electric Vehicle Transition, *Energy Research and Social Science*, **2020**, *69*, 101581. doi:*10.1016/j.erss.2020.101581*.

[10] European Union, L 197, *Official Journal of the European Union*, **2012**, *55*, 38–71.

[11] LE, P.A., The Recyclability of Lithium-Ion Battery Materials, *University of Queensland - Faculty of Engineering, Architecture and Information Technology*, **2019**.

[12] Doose, S.;Mayer, J.K.;Michalowski, P.;Kwade, A., Challenges in Ecofriendly Battery Recycling and Closed Material Cycles: A Perspective on Future Lithium Battery Generations, *Metals*, **2021**, *11*, 1–17. doi:*10.3390/met11020291*.

[13] European Commission, Regulation of the European Parliament and of the Council Amending Regulation (EC) No 539/2001, **2016**, 1–8.

[14] Velázquez-Martínez, O.;Valio, J.;Santasalo-Aarnio, A.;Reuter, M.;Serna-Guerrero, R., A Critical Review of Lithium-Ion Battery Recycling Processes from a Circular Economy Perspective, *Batteries*, **2019**, *5*, 5–7. doi:*10.3390/batteries5040068*.

[15] Manthiram, A., A Reflection on Lithium-Ion Battery Cathode Chemistry, *Nature Communications*, **2020**, *11*, 1–9. doi:*10.1038/s41467-020-15355-0*.

[16] Reddy, T.B., Lithium Primary Batteries, *McGraw-Hill*, **2015**, *4th Editio*, ISBN:9788578110796.

[17] Wang, S.;Tian, Y.;Zhang, X.;Yang, B.;Wang, F.;Xu, B.;Liang, D.;Wang, L., A Review of Processes and Technologies for the Recycling of Spent Lithium-Ion Batteries, *IOP Conference Series: Materials Science and Engineering*, **2020**, *782*, 022025. doi:*10.1088/1757-899X/782/2/022025*.

[18] Armand, M.;Axmann, P.;Bresser, D.;Copley, M.;Edström, K.;Ekberg, C.;Guyomard, D.;Lestriez, B.;Novák, P.;Petranikova, M.;Porcher, W.;Trabesinger, S.;Wohlfahrt-Mehrens, M.;Zhang, H., Lithium-Ion Batteries – Current State of the Art and Anticipated Developments, *Journal of Power Sources*, **2020**, *479*, 228708. doi:*10.1016/j.jpowsour.2020.228708*.

[19] Werner, D.;Peuker, U.A.;Mütze, T., Recycling Chain for Spent Lithium-ion Batteries, *Metals*, **2020**, *10*, 316. doi:*10.3390/met10030316*.

[20] Elwert, T.;Goldmann, D.;Römer, F.;Buchert, M.;Merz, C.;Schueler, D.;Sutter, J., Current Developments and Challenges in the Recycling of Key Components of (Hybrid) Electric Vehicles, *Recycling*, **2016**, *1*, 25–60. doi:*10.3390/recycling1010025*.

[21] Winslow, K.M.;Laux, S.J.;Townsend, T.G., A Review on the Growing Concern and Potential Management Strategies of Waste Lithium-Ion Batteries, *Resources, Conservation and Recycling*, **2018**, *129*, 263–277. doi:*10.1016/j.resconrec.2017.11.001*.

[22] Duarte Castro, F.;Vaccari, M.;Cutaia, L., Valorization of Resources from End-of-Life Lithium-Ion Batteries: A Review, *Critical Reviews in Environmental Science and Technology*, **2021**, 1–44. doi:*10.1080/10643389.2021.1874854*.

[23] Asadi Dalini, E.;Karimi, G.;Zandevakili, S.;Goodarzi, M., A Review on Environmental, Economic and Hydrometallurgical Processes of Recycling Spent Lithium-Ion Batteries, *Mineral Processing and Extractive Metallurgy Review*, **2020**, *42*, 451–472. doi:*10.1080/08827508.2020.1781628*.

[24] Warner, J., Chapter 7: Lithium-ion and other cell chemistries, *Elsevier*, **2015**, ISBN:9780128014561doi:*10.1016/C2013-0-23144-5*.

[25] Lino dos Santos, C.A., Baterias de Íons Lítio Para Veículos Elétricos, *Revista IPT Tecnologia e Inovação*, **2018**, *2*, 62–82. doi:*10.34033/2526-5830-v2n9-4*.

[26] Sharma, A.S.;Prasath, A.;Duraisamy, E.;Maiyalagan, T.;Elumalai, P., Fundamental principles of lithium ion batteries, **2020**. doi:*10.1201/9781351052702*.

[27] Andrea, D., Lithium-Ion Batteries and Applications, *Artech House*, **2020**, ISBN:9781630817671.

[28] Kim, H.J.;Krishna, T.N.V.;Zeb, K.;Rajangam, V.;Muralee Gopi, C.V.V.;Sambasivam, S.;Raghavendra, K.V.G.;Obaidat, I.M., A comprehensive review of li-ion battery materials and their recycling techniques, **2020**, ISBN:8251510236doi:*10.3390/electronics9071161*.

[29] Li, P.;Kim, H.;Myung, S.T.;Sun, Y.K., Diverting Exploration of Silicon Anode into Practical Way: A Review Focused on Silicon-Graphite Composite for Lithium Ion Batteries, *Energy Storage Materials*, **2021**, *35*, 550–576. doi:*10.1016/j.ensm.2020.11.028*.

[30] Fan, E.;Yang, J.;Huang, Y.;Lin, J.;Arshad, F.;Wu, F.;Li, L.;Chen, R., Leaching Mechanisms of Recycling Valuable Metals from Spent Lithium-Ion Batteries by a Malonic Acid-Based Leaching

System, *ACS Applied Energy Materials*, **2020**, *3*, 8532–8542. doi:*10.1021/acsaem.0c01166*.

[31] Jones, B.;Elliott, R.J.R.;Nguyen-Tien, V., The EV Revolution: The Road Ahead for Critical Raw Materials Demand, *Applied Energy*, **2020**, *280*, 115072. doi:*10.1016/j.apenergy.2020.115072*.

[32] Godoy León, M.F.;Dewulf, J., Data Quality Assessment Framework for Critical Raw Materials. The Case of Cobalt, *Resources, Conservation and Recycling*, **2020**, *157*, 104564. doi:*10.1016/j.resconrec.2019.104564*.

[33] Schmid, M., Challenges to the European Automotive Industry in Securing Critical Raw Materials for Electric Mobility: The Case of Rare Earths, *Mineralogical Magazine*, **2020**, *84*, 5–17. doi:*10.1180/mgm.2020.9*.

[34] Irle, R., Global plug-in vehicle sales reached over 3.2 million in 2020, *EV volumes*, **2020** [Accessed 3rd March 2021] Available on the internet: *https://www.ev-volumes.com*.

[35] European Commission, Study on the EU's List of Critical Raw Materials (2020), Factsheets on Critical Raw Materials, **2020**. doi:*10.2873/11619*.

[36] European Commission, Non-Critical Raw Materials Factsheets, *Study on the EU's list of critical raw materials*, **2020**. doi:*10.2873/867993*.

[37] European Commission, Critical Raw Materials Factsheets, *Study on the EU's list of critical raw materials*, **2020**. doi:*10.2873/92480*.

[38] Copper, *London Exchange Metal*, **2021** [Accessed 9th March 2021] Available on the internet: *https://www.lme.com/en-GB/Metals/Minor-metals/Cobalt#tabIndex=2*.

[39] Lithium, *Trading Economics*, **2021** [Accessed 14th March 2021] Available on the internet: *https://tradingeconomics.com/commodity/lithium*.

[40] Basia, A.;Simeu-Abazi, Z.;Gascard, E.;Zwolinski, P., Review on State of Health Estimation Methodologies for Lithium-Ion Batteries in the Context of Circular Economy, *CIRP Journal of Manufacturing Science and Technology*, **2021**, *32*, 517–528. doi:*10.1016/j.cirpj.2021.02.004*.

[41] Baars, J.;Domenech, T.;Bleischwitz, R.;Melin, H.E.;Heidrich, O., Circular Economy Strategies for Electric Vehicle Batteries Reduce Reliance on Raw Materials, *Nature Sustainability*, **2021**, *4*, 71–79. doi:*10.1038/s41893-020-00607-0*.

[42] Mossali, E.;Picone, N.;Gentilini, L.;Rodrìguez, O.;Pérez, J.M.;Colledani, M., Lithium-Ion Batteries towards Circular Economy: A Literature Review of Opportunities and Issues of Recycling Treatments, *Journal of Environmental Management*, **2020**, *264*, 110500. doi:*10.1016/j.jenvman.2020.110500*.

[43] Bai, Y.;Muralidharan, N.;Sun, Y.K.;Passerini, S.;Stanley Whittingham, M.;Belharouak, I., Energy and Environmental Aspects in Recycling Lithium-Ion Batteries: Concept of Battery Identity Global Passport, *Materials Today*, **2020**, *41*, 304–315. doi:*10.1016/j.mattod.2020.09.001*.

[44] Yang, Y.;Okonkwo, E.G.;Huang, G.;Xu, S.;Sun, W.;He, Y., On the Sustainability of Lithium Ion Battery Industry – A Review and Perspective, *Energy Storage Materials*, **2021**, *36*, 186–212. doi:*10.1016/j.ensm.2020.12.019*.

[45] Harper, G.;Sommerville, R.;Kendrick, E.;Driscoll, L.;Slater, P.;Stolkin, R.;Walton, A.;Christensen, P.;Heidrich, O.;Lambert, S.;Abbott, A.;Ryder, K.;Gaines, L.;Anderson, P., Recycling Lithium-Ion Batteries from Electric Vehicles, *Nature*, **2019**, *575*, 75–86.

doi:*10.1038/s41586-019-1682-5*.

[46] Garrido-Hidalgo, C.;Ramirez, F.J.;Olivares, T.;Roda-Sanchez, L., The Adoption of Internet of Thing in a Circular Supply Chain Framework for the Recovery of WEEE: The Case of Lithium-Ion Electric Vehicle Battery Packs, *Waste Management*, **2020**, *103*, 32–44. doi:*10.1016/j.wasman.2019.09.045*.

[47] Ryu, H.-H.;Sun, H.H.;Myung, S.-T.;Yoon, C.S.;Sun, Y.-K., Reducing Cobalt from Lithium-Ion Batteries for the Electric Vehicle Era, *Energy & Environmental Science*, **2021**, *2*, 844–852. doi:*10.1039/d0ee03581e*.

[48] LFP to overtake NMC as dominant stationary storage chemistry by 2030, *Wood Mackenzie*, **2020** [Accessed 18th March 2021] Available on the internet: *https://www.woodmac.com/press-releases/lfp-to-overtake-nmc-as-dominant-stationary-storage-chemistry-by-2030/*.

[49] Yadav, P.;Jie, C.J.;Tan, S.;Srinivasan, M., Recycling of Cathode from Spent Lithium Iron Phosphate Batteries, *Journal of Hazardous Materials*, **2020**, *399*, 123068. doi:*10.1016/j.jhazmat.2020.123068*.

[50] Schiavi, P.G.;Carla, F.;Padoan, M.;Altimari, P., Process for Recycling Li-MnO 2 Primary Batteries with the Direct Production of LiMnPO 4 Nanoparticles, *Energies*, **2020**, *13*, 4004. doi:*10.3390/en13154004*.

[51] Bi, H.;Zhu, H.;Zu, L.;Gao, Y.;Gao, S.;Peng, J.;Li, H., Low-Temperature Thermal Pretreatment Process for Recycling Inner Core of Spent Lithium Iron Phosphate Batteries, *Waste Management and Research*, **2021**, *39*, 146–155. doi:*10.1177/0734242X20957403*.

[52] Yan, S.;Sun, C.;Zhou, T.;Gao, R.;Xie, H., Ultrasonic-Assisted Leaching of Valuable Metals from Spent Lithium-Ion Batteries Using Organic Additives, *Separation and Purification Technology*, **2021**, *257*, 117930. doi:*10.1016/j.seppur.2020.117930*.

[53] Chen, X.;Li, J.;Kang, D.;Zhou, T.;Ma, H., A Novel Closed-Loop Process for the Simultaneous Recovery of Valuable Metals and Iron from a Mixed Type of Spent Lithium-Ion Batteries, *Green Chemistry*, **2019**, *21*, 6342–6352. doi:*10.1039/c9gc02844g*.

[54] Diaz, L.A.;Strauss, M.L.;Adhikari, B.;Klaehn, J.R.;McNally, J.S.;Lister, T.E., Electrochemical-Assisted Leaching of Active Materials from Lithium Ion Batteries, *Resources, Conservation and Recycling*, **2020**, *161*, 104900. doi:*10.1016/j.resconrec.2020.104900*.

[55] Larouche, F.;Tedjar, F.;Amouzegar, K.;Houlachi, G.;Bouchard, P.;Demopoulos, G.P.;Zaghib, K., Progress and Status of Hydrometallurgical and Direct Recycling of Li-Ion Batteries and Beyond, *Materials*, **2020**, *13*, 801. doi:*10.3390/ma13030801*.

[56] Smith, W.N.;Swoffer, S., Process for Recovering and Regenerating Lithium Cathode Material from Lithium-Ion Batteries, *US8882007B1*, **2014**.

[57] Makuza, B.;Tian, Q.;Guo, X.;Chattopadhyay, K.;Yu, D., Pyrometallurgical Options for Recycling Spent Lithium-Ion Batteries: A Comprehensive Review, *Journal of Power Sources*, **2021**, *491*, 229622. doi:*10.1016/j.jpowsour.2021.229622*.

[58] Liu, T.;Chen, J.;Li, H.;Li, K., An Integrated Process for the Separation and Recovery of Valuable Metals from the Spent LiNi0.5Co0.2Mn0.3O2 Cathode Materials, *Separation and Purification Technology*, **2020**, *245*, 116869. doi:*10.1016/j.seppur.2020.116869*.

[59] Yu, J.;Tan, Q.;Li, J., Exploring a Green Route for Recycling Spent Lithium-Ion Batteries: Revealing and Solving Deep Screening Problem, *Journal of Cleaner Production*, **2020**, *255*, 120269. doi:*10.1016/j.jclepro.2020.120269*.

[60] Zhao, J.;Zhang, B.;Xie, H.;Qu, J.;Qu, X.;Xing, P.;Yin, H., Hydrometallurgical Recovery of Spent Cobalt-Based Lithium-Ion Battery Cathodes Using Ethanol as the Reducing Agent, *Environmental Research*, **2020**, *181*, 108803. doi:*10.1016/j.envres.2019.108803*.

[61] Liu, T.;Chen, J.;Shen, X.;Li, H., Regulating and Regenerating the Valuable Metals from the Cathode Materials in Lithium-Ion Batteries by Nickel-Cobalt-Manganese Co-Extraction, *Separation and Purification Technology*, **2021**, *259*, 118088. doi:*10.1016/j.seppur.2020.118088*.

[62] Yang, X.;Dong, P.;Hao, T.;Zhang, Y.;Meng, Q.;Li, Q.;Zhou, S., A Combined Method of Leaching and Co-Precipitation for Recycling Spent Lini0.6Co0.2Mn0.2O2 Cathode Materials: Process Optimization and Performance Aspects, *Journal of Metals*, **2020**, *72*, 3843–3852. doi:*10.1007/s11837-020-04263-9*.

[63] Vieceli, N.;Nogueira, C.A.;Guimarães, C.;Pereira, M.F.C.;Durão, F.O.;Margarido, F., Hydrometallurgical Recycling of Lithium-Ion Batteries by Reductive Leaching with Sodium Metabisulphite, *Waste Management*, **2018**, *71*, 350–361. doi:*10.1016/j.wasman.2017.09.032*.

[64] Vieceli, N.;Casasola, R.;Lombardo, G.;Ebin, B.;Petranikova, M., Hydrometallurgical Recycling of EV Lithium-Ion Batteries: Effects of Incineration on the Leaching Efficiency of Metals Using Sulfuric Acid, *Waste Management*, **2021**, *125*, 192–203. doi:*10.1016/j.wasman.2021.02.039*.

[65] Chen, X.;Li, J.;Kang, D.;Zhou, T.;Ma, H., Novel Closed-Loop Process for the Simultaneous Recovery of Valuable Metals and Iron from a Mixed Type of Spent Lithium-Ion Batteries, *Green Chemistry*, **2019**, *21*, 6342–6352. doi:*10.1039/c9gc02844g*.

[66] Xiao, J.;Li, J.;Xu, Z., Challenges to Future Development of Spent Lithium Ion Batteries Recovery from Environmental and Technological Perspectives, *Environmental Science and Technology*, **2020**, *54*, 9–25. doi:*10.1021/acs.est.9b03725*.

[67] Lv, W.;Wang, Z.;Cao, H.;Sun, Y.;Zhang, Y.;Sun, Z.H.I., A Critical Review and Analysis on the Recycling of Spent Lithium-Ion Batteries, *ACS Sustainable Chemistry and Engineering*, **2018**, *6*, 1504–1521. doi:*10.1021/acssuschemeng.7b03811*.

[68] Chen, X.;Cao, L.;Kang, D.;Li, J.;Li, S.;Wu, X., Hydrometallurgical processes for valuable metals recycling from spent lithium-ion batteries, *Springer*, **2019**, ISBN:9783030318345doi:*10.1007/978-3-030-31834-5*.

[69] Chen, X.;Cao, L.;Kang, D.;Li, J.;Li, S.;Wu, X., Hydrometallurgical processes for valuable metals recycling from spent lithium-ion batteries, **2019**, ISBN:9783030318345doi:*10.1007/978-3-030-31834-5*.

[70] Diekmann, J.;Hanisch, C.;Froböse, L.;Schälicke, G.;Loellhoeffel, T.;Fölster, A.-S.;Kwade, A., Ecological Recycling of Lithium-Ion Batteries from Electric Vehicles with Focus on Mechanical Processes, *Journal of The Electrochemical Society*, **2017**, *164*, A6184–A6191. doi:*10.1149/2.0271701jes*.

[71] Hanisch, C.;Westphal, B.;Haselrieder, W.;Schoenitz, M., Verfahren Zum Behandeln Gebrauchter Batterien, Insbesondere Wieder Aufladbarer Batterien Und Batterie-

Verarbeitungsanlage, *DE102018102026A1*, **2016**.

[72] Bae, H.;Kim, Y., Technologies of Lithium Recycling from Waste Lithium Ion Batteries: A Review, *Materials Advances*, **2021**, *2*, 3234–3250. doi:*10.1039/d1ma00216c*.

[73] He, L.-P.;Sun, S.-Y.;Song, X.-F.;Yu, J.-G., Recovery of Cathode Materials and Al from Spent Lithium-Ion Batteries by Ultrasonic Cleaning, *Waste Management*, **2015**, *46*, 523–528. doi:*10.1016/j.wasman.2015.08.035*.

[74] Castrejón-Sánchez, V.H.;Solis, A.C.;López, R.;Encarnación-Gomez, C.;Morales, F.M.;Vargas, O.S.;Mastache-Mastache, J.E.;Sánchez, G.V., Thermal Oxidation of Copper over a Broad Temperature Range: Towards the Formation of Cupric Oxide (CuO), *Materials Research Express*, **2019**, *6*,doi:*10.1088/2053-1591/ab1662*.

[75] Jian, Y.;Yanqing, L.;Fangyang, L.;Ming, J.;Liangxing, J., Countercurrent Leaching of Ni, Co, Mn, and Li from Spent Lithium-Ion Batteries, *Waste Management and Research*, **2020**, *38*, 1358–1366. doi:*10.1177/0734242X20944498*.

[76] Nayl, A.A.;Hamed, M.M.;Rizk, S.E., Selective Extraction and Separation of Metal Values from Leach Liquor of Mixed Spent Li-Ion Batteries, *Journal of the Taiwan Institute of Chemical Engineers*, **2015**, *55*, 119–125. doi:*10.1016/j.jtice.2015.04.006*.

[77] Sodha, A.B.;Tipre, D.R.;Dave, S.R., Optimization and Kinetics of Copper Cementation from Bio-Leachate Generated during the Waste Printed Circuit Board (E-Waste) Processing, *Environmental Sustainability*, **2019**, *2*, 391–399. doi:*10.1007/s42398-019-00084-y*.

[78] Pourbaix, M., Atlas of electrochemical equilibria in aqueous solutions, *National Association of Corrosion Engineers*, **1974**, *2nd Edition*, ISBN:9780915567980.

[79] Mos, Y.M.;Vermeulen, A.C.;Buisman, C.J.N.;Weijma, J., X-Ray Diffraction of Iron Containing Samples: The Importance of a Suitable Configuration, *Geomicrobiology Journal*, **2018**, *35*, 511–517. doi:*10.1080/01490451.2017.1401183*.

[80] Benchmark: Lithium carbonate prices reach record high, *Green Car Congress*, **2021** [Accessed 29th November 2021] Available on the internet: *https://www.greencarcongress.com/2021/10/20211009-benchmarklithium.html*.

[81] Lithium at the LME, *London Metal Exchange*, **2021** [Accessed 29th November 2021] Available on the internet: *https://www.lme.com/Metals/EV/Lithium-prices*.

[82] Ma, Y.;Svärd, M.;Xiao, X.;Gardner, J.M.;Olsson, R.T.;Forsberg, K., Precipitation and Crystallization Used in the Production of Metal Salts for Li-Ion Battery Materials: A Review, *Metals*, **2020**, *10*, 1–16. doi:*10.3390/met10121609*.